APTASENSOR BASED APPROACH FOR REAL-TIME MONITORING OF *LISTERIA INNOCUA* AND *LISTERIA MONOCYTOGENES*

A Thesis

by

KATHERINE DENISE HILLS

Submitted to the Office of Graduate and Professional Studies of
Texas A&M University
in partial fulfillment of the requirements for the degree of

MASTER OF SCIENCE

Chair of Committee,	Carmen Gomes
Committee Members,	Elena Castell-Perez
	Alejandro Castillo
Head of Department,	Steve Searcy

May 2016

Major Subject: Biological and Agricultural Engineering

ABSTRACT

Listeria monocytogenes is one of the most common causes of food illness deaths in the world, with multiple outbreaks in the United States alone. The goal of this study was to design biosensors using aptamers with the capability of rapid detection of this potentially deadly pathogen. The biosensor design process involved the use a nano-metallic hydrid platform consisting of a platinum/graphene/platinum (PGP) and PGP+chitosan nanobrush platforms functionalized with aptamers. Polyclonal goat based anti-*Listeria* antibodies were also attached to both platforms to test their capabilities as a biosensor and to compare aptamer specificity. The PGP+chitosan sensors were controlled by the pH sensitivity of the chitosan (CHT) brushes. The detection of the target bacteria relied on the sensors' electrochemical response based on impedance changes caused by the *L. innocua* or *L. monocytogenes* attachment onto the bio-recognition agents. Each sensor tested had a detection time of approximately 17 min including 15 min for bacteria capture and approximately 2 min to run EIS test. Capture efficiency tests were performed on the PGP+CHT platform based on brushes actuation with pH to determine the optimum testing conditions. The best testing condition was observed when the electrode was first placed in a pH 5 suspension with bacteria and then tested at pH 7 in PBS. For the PGP platform, the highest ESA value (0.0718 ± 0.029 cm^2) found was for the PGP+400 nM thiol aptamer sensor and when impedance testing with bacteria was conducted the highest sensitivity (12.14 ± 1.79 1/log(CFU/mL) and lowest limit of detection (LOD) (11.2 ± 0.79 CFU/mL) value. For the PGP+CHT platform, the best results were found for the PGP+CHT+100 nM aptamer sensor in the

presence of *L. innocua* with a sensitivity of 12.14 ± 1.79 1/log(CFU/mL) and a LOD of 9.1 ± 1.1 CFU/mL. Furthermore, this sensor was able to detect bacteria over a wide range from $10 – 10^7$ CFU/mL. The sensitivity of the PGP+CHT+100 nM aptamer sensor was also measured in the presence of *L. innocua* and *S. aureus* suspensions containing equally increasing concentrations and had a sensitivity value of 14.25 ± 1.69 1/log(CFU/mL) and a LOD of 9.4 ± 0.11 CFU/mL. This means that this sensor will be very selective towards *Listeria spp.* and should only detect these bacteria when in a medium that contains other pathogens. Furthermore, PGP+CHT+bio-recognition agent biosensors were also tested in vegetable broth. The LOD for the PGP+CHT+100 nM aptamer was 31.12 ± 0.64 CFU/mL and the PGP+CHT+200 nM antibody was 23.9 ± 0.96 CFU/mL. The aptamers had a sensitivity of 3.76 ± 0.34 1/log(CFU/mL) and the antibodies had a value of 4.9 ± 0.4 1/log(CFU/mL) which were not statistically significant, implying that other bio-recognition agents could be attached to the PGP+CHT platform and have similar detection capabilities. Both PGP and PGP+CHT sensor platforms were comparable to each other in terms of LOD, sensitivity, and linear range of detection with best results observed for the PGP + 400 nM thiol aptamer and PGP + CHT + 100 nM aptamer and PGP + CHT + 200 nM antibody sensors. The biosensors created in this study are easy to follow impedance test procedure, low LOD and a short response time allowing these biosensors to have the potential to replace the detection standard methods that are currently being used by the food industry.

DEDICATION

For all the little bubble gum makers

ACKNOWLEDGEMENTS

I would like to thank my committee chair, Dr. Gomes, and my committee members, Dr. Castell and Dr. Castillo, for their guidance and support throughout the course of this research. I would also like to thank Dr. McLamore's research group at University of Florida for being so helpful throughout this project.

My gratitude also goes to the department faculty and staff for making my time at Texas A&M wonderful. I would especially like to thank Cassie for being a constant comrade in arms. We faced many failures and triumphs together over these three years and you kept me laughing and sane through it all.

This journey has been quite a roller coaster and I would not have made it through without your love and support Doug. Thank you for sitting with me for hours on end at the coffee shop while I wrote, for always listening to my work rants and for all the first half of movies you watched because I fell asleep before the second half.

To end, I would like to thank my brother for all the entertainment on the long family car trips, for always having reliable suggestions on TV shows and movies and for keeping that goofy sense of humor that I love so much. I can't thank my parents enough for all of the love, laughter, support and guidance they have given me over the years. You always said I could be anything I wanted to be and were smart enough to let me make my own mistakes. A kid couldn't ask for better parents.

NOMENCLATURE

BPW	Buffered Peptone Water
CHT	Chitosan
ESA	Electroactive Surface Area
EIS	Electrical Impedance Spectroscopy
CV	Cyclic Voltammetry
ELISA	Enzyme-linked Immunosorbent Assay
PCR	Polymerase Chain Reaction
PGP	Platinum/Graphene/Platinum
TPB	Tryptose Phosphate Broth
TSB	Tryptic Soy Broth
SAM	Self-assembled Monolayer
PBS	Phosphate Buffer Solution
GO	Graphene Oxide
EDC	1-Ethyl-3-(3-dimethylaminopropyl)carbodiimide
NHS	N-Hydroxysuccinimide

TABLE OF CONTENTS

Page

LIST OF FIGURES

Page

LIST OF TABLES

Page

CHAPTER I

INTRODUCTION

While *Listeria monocytogenes* may not be a leading source of foodborne illness, it is one of the top 3 causes of death from foodborne illness in the world. From as early as the 1980s cases of *Listeria monocytogenes* resulting illnesses have plagued specifically the United States, with the most common food sources of infection being cheeses and processed meats (CDC, 2015; USDA, 2012). However, a few cases have been reported in cantaloupes and dairy products such as raw milk. The Listeriosis' reside in water and soil and are passed onto humans when the contaminated soil or water comes in contact, whether directly or indirectly, with food meant for human consumption (USDA, 2012). The food then becomes contaminated and human illness can occur as a result. *Listeria innocua* is similar to *L. monocytogenes* with many of the same ecological, biochemical and genetic characteristics with the exception that *L. innocua* is non-pathogenic (Liu, Puri, & Demirci, 2009). This makes it an ideal surrogate organism for *L. monocytogenes* testing.

A biosensor is a diagnostic device that changes the response from a biological organism into an electrical output that can be analyzed (Lee, Niederer, & Reilly, 2010; Song, Wang, Li, Fan, & Zhao, 2008). This basically means that the sensor can be broken down into two main components, a biological part that senses the material that is trying to be detected and a transducer element that converts what the biological part is sensing into a quantifiable number. The biological component can use anything from enzymes

to antigens and the transducer can use electrical current to viscosity to detect the material that is trying to be sensed (Lee et al., 2010).

Aptamers are one of the biological components that can be attached to a biosensor to function as the recognition biomolecule; when the two are combined they can be called an aptasensor. Aptamers are composed of RNA or DNA molecules that are capable of forming secondary and tertiary structures with the ability to specifically bind to proteins or other cellular components in an organism. Essentially they can be viewed as having the same chemical equivalence as antibodies. However, aptamers have superiority of antibodies because of their small size, high specificity to detect certain strains, shelf-life stability, robustness, and non-immunogenic properties (Ni, Castanares, Mukherjee, & Lupold, 2011).

Nanomaterials such as graphene and platinum have been used in biosensors as a means to improve the sensitivity, selectivity and speed at which the sensors will detect microbes (Sanvicens, Pastells, Pascual, & Marco, 2009). These enhancements come from the nanomaterials electrical properties and their surfaces, which can be easily functionalized to significantly improve the electron transfer on the surface of the electrode (Wang, 2005). These surfaces also allow for easy attachment of bio-recognition agents, as well as other materials like biopolymers including chitosan.

Chitosan, a derivative of chitin, is a material usually derived from shellfish that can be made into a hydrogel. Chitosan nanobrushes are synthesized from this hydrogel in order to take advantage of chitosan's unique properties such as pH-responsiveness, biocompatibility and biodegradability to immobilize aptamers using covalent cross-

linking onto the surface of the polymer. Because aptamers have thus far been found to have only a small number of functional groups (amine, thiol, and biotin) available for chemical reactions, it can be difficult to find a metal or polymer base that will allow for crosslinking (Balamurugan, Obubuafo, Soper, & Spivak, 2008). Since chitosan's isoelectric point is at pH 6.5, it can expand at pH 5 and contract at pH 7 based on which pH the sensor is exposed to, which can be useful on controlling capture of the target microorganism (López-León, Carvalho, Seijo, Ortega-Vinuesa, & Bastos-González, 2005). It also has the capability to increase the total amount of aptamers that can be loaded on to the biosensors surface based on polymer length. In addition, chitosan is a very porous material (Khoushab & Yamabhai, 2010), this means that it may be able to improve the electron transfer in the system and potentially increase the sensitivity of the biosensor.

CHAPTER II

OBJECTIVES AND HYPOTHESIS

2.1. Objective

The main goal for this study was to design a biosensor for detection of *Listeria innocua* and *Listeria monocytogenes* based on aptamers functionalized onto a chitosan hybrid nano-metallic platform with enhanced sensitivity, range and lower limit of detection.

2.2. Hypothesis

The design of a biosensor based on chitosan hybrid nano-metallic platform functionalized with aptamers will provide a better detection performance than conventional methods and currently available biosensors.

2.3. Specific Objectives

1) Design a hybrid nano-metallic structure composed of platinum/reduced graphene/platinum (PGP) coating for the biosensor platform.
2) Optimize the loading capacity of aptamers selective to *Listeria* (*Listeria*-aptamers) on the surface of the Pt/reduced graphene/Pt (PGP) biosensor platform for in order to design aptasensor for *Listeria* detection.
3) Determine the limit of detection, range and sensitivity of PGP-aptamer biosensor (PGP-aptasensor) for *L. innocua* detection
4) Compare PGP aptasensor performance with antibodies attached to the same biosensor platform (PGP immunosensor).
5) Design a PGP-chitosan (CHT) nanobrush for biosensor applications.

6) Optimize the loading capacity of aptamers onto PGP-CHT platform in order to design aptasensor for *Listeria* detection.
7) Determine the limit of detection, range, sensitivity and selectivity of PGP-CHT-aptamer biosensor for *L. innocua* detection
8) Compare PGP-CHT aptasensor performance with antibodies attached to the same biosensor platform (PGP-CHT immunosensor).

2.4. Significance and Rationale

Food safety is a complex issue that impacts all segments of society and unsafe foods in consumer products can lead to human illness and public unrest. The Centers for Disease Control and Prevention (CDC) estimated that 1600 illnesses and 260 deaths each year in the United States are caused by *Listeria monocytogenes* (CDC, 2015). Thus, we need to find ways to detect *Listeria* and other food pathogens in food products to ensure food safety and consumer health.

Methods of pathogen detection that are easy to use, fast and inexpensive are especially in demand for non-laboratory settings such as food production lines where products can be sent to retailers in as little as a day after processing and standard detection techniques like plate counting are time consuming and require trained workers to perform the test (Abubakar et al., 2007). But to date, there has been very few methods tested in the field that can give fast and quantitative results for pathogens in food products. Aptamers are isolated oligonucleotide sequences that can be used to detect almost any kind of molecule and are currently very popular in biosensor research because of their bio-recognition properties which are comparable to another commonly

used bio-recognition agent, antibodies. Some of these properties include being non-immunogenic, easy to produce, small size, high specificity (similar to antibodies), and a long shelf life (Jayasena, 1999).

Hybrid metallic nanoparticles offer opportunities for creating powerful electrochemical biosensors because these nanocomposites can improve the response time, sensitivity and detection limit (Wang, 2007). For instance, reduced graphene and platinum nanoparticles have shown to have high electrical conductivity which improves the transportation of electrons when deposited on the electrode's surface and in turn these nanocomposites improve the electroactive surface area of the sensor (Claussen et al., 2010; Luedtke, 2015). However, using nanomaterials does pose the challenge of finding ways to adhere recognition agents that will get the best results. This research also seeks to explore different methods of biorecognition agents attachment and determine if one is superior.

Biopolymers are biodegradable polymers made from both renewable resources and also from fossil-based sources, and there are several advantages to using them in biosensor applications (Niaounakis, 2015). First, they can hold a lot more bio-recognition agents because of their tridimensional shape. Secondly, biopolymers when used as part of a biosensor platform, like chitosan, can be dried and stored for longer periods of time than their non-polymer biosensor counterparts. Third, the matrix that comprises the biopolymer can be used to attach and protect bio-recognition agents like aptamers (Liu, 2011). Lastly, stimuli-responsive biopolymers, like chitosan which changes its conformation from swollen to shrunken based on pH changes, when used in

biosensors these biopolymers can be modified to improve the sensors performance such as detection limit and sensitivity by increasing the electroactive surface area when the chitosan is shrunk and increasing bacteria capture due to exposure of bio-recognition agents when it is swollen.

The information from this study will increase our understanding on interactions between aptamers and the biopolymer chitosan and its actuation properties for biosensor applications. Furthermore, it will improve knowledge on biopolymer structures and how they can be used to improve biosensor performance by exploring its actuation properties. Additionally, it will provide a better understanding of the use of graphene and platinum hybrid nanostructures combination with aptamers and chitosan structures and their effect on enhancing electrochemical performance of the biosensor. In regards to application opportunities, by increasing the pathogen detection capabilities of biosensors such as response time, sensitivity, linear range of detection, durability and detection limit, there will be a large impact on how we monitor our food supplies and reduce occurrences of foodborne outbreaks, and in turn, ensure food safety and the health of consumers. Biosensors have the potential to improve how quickly and reliably bacteria contamination information is gathered and this sensor in particular has the possibility to improve upon other published biosensors in its shelf life, biopolymer actuation capabilities, and detection limit.

CHAPTER III

LITERATURE REVIEW

3.1. Biosensors

3.1.1. Background

Food is essential to human growth and survival; therefore, it is important to keep our food safe from outside contamination so as to prevent illness from spreading into the human population. This is especially important in fresh produce where products usually undergo very little to no thermal processing to kill bacteria and can be in store shelves in as few as a day or two. So, it is becoming increasingly important to find methods that are quickly able to detect small amounts of pathogens that may cause illnesses for real-time monitoring. *Listeria monocytogenes* has been estimated to have as an effective dose as small as 1,000 cells (USDA, 2012) and many conventional methods either take too long to get results or are very complicated to employ (Sanvicens et al., 2009).

Biosensors are an emerging method of foodborne pathogen detection in the food industry with research being conducted to detect pathogens like, *Staphylococcus aureus* (Bai et al., 2010), *Salmonella Typhimurium* (Singh et al., 2012), *Escherichia coli* O157:H7 (Wang, Ye, & Ying, 2014) and *Campylobacter jejuni* (Huang et al., 2010). However, there is much literature on the topic for the medical industry, since it has been used for many years in the detection of glucose in blood for patients with diabetes, for example (Bai et al., 2010; Lin, He, Zhao, & Zhang, 2009; Ren, Shi, Li, & Ma, 2012; Shi et al., 2012; Tsai, Chen, & Liaw, 2007). Most of the biosensors created for this purpose are not all composed of the same materials (Du, Luo, Xu, & Chen, 2007; Lin et al.,

2009). For instance, Bai et al. (2010) constructed a biosensor to detect glucose that had a palladium nanoparticle/chitosan-grafted graphene nano-composite base. They showed that the chitosan was able to prevent the graphene from oxidizing by coating the sheets; this allowed for the graphene to maintain its electro conductivity properties and in turn, increased the sensitivity of the sensor to glucose.

A previous study used a sensor composed of just graphene oxide and platinum black as a base to attach the glucose oxidase enzymes (Shi et al., 2012). Their work also showed a marked increase in sensitivity for detection of the glucose when both were used together as opposed to when graphene oxide or platinum black was just used alone. However, biosensors are not just limited to glucose detection, many studies (Hernández et al., 2014; Sanvicens et al., 2009; Zelada-Guillén, Bhosale, Riu, & Rius, 2010) have designed biosensors with the intent to detect bacteria in samples.

3.1.2. Types of Transducers

Biosensors use many different ways to detect its target material. This is largely accomplished based on the type of transducer that is used in the biosensor platform. The main types of transducer that have been used for biosensors are, thermal, mass, optical and electrochemical (Wagner & Guilbault, 1994). Thermal transducers usually operate off of some kind of reaction that leads to a measureable change in temperature. These types of reactions tend to be either enzyme catalyzed or due to some kind of gas combustion. Mass transducers use a piezoelectric crystal that changes its vibration based on its overall mass as acoustic waves come in contact with it. Optical transducers use electromagnetic, visible and infrared electromagnetic radiation to detect their target

material. The sensing element in the transducer exams either light emitted or adsorbed by the sample. The samples can naturally emit or absorb light or they can be tagged with a compound to detect the presence and where any target material may be (Banica, 2012).

Lastly, electrochemical transducers can be used to detect the target material; this type of transducer deals with the electron transfer where the solution comes into contact with a solid state conductor like an electrode. Electrochemical transducers can even be classified further into potentiometric, amperometric and impedimetric transducers. Potentiometric transducers use a membrane placed between two different solutions, one is the sample and the other is a solution with an analyte ion (Banica, 2012). As ions are exchanged at the membrane's surface a measurable potential difference begins to occur between the two solutions. Amperometric sensors have a potential set to a value so the analyte in the system creates a current. The applied potential then serves to force an electron transfer reaction, and the current that is produced can be used as a direct measurement of the rate that the electron transfer is occurring (Velusamy, Arshak, Korostynska, Oliwa, & Adley, 2010). Finally, electrochemical transducers can be based on impedance measurements. This type of testing can give information about the physicochemical processes that are taking place inside the electrochemical system (Banica, 2012) and are discussed further in the following paragraphs. In comparison, to the other sensing methods mentioned above electrochemical sensors have the advantages of being able to be label-free, ability to work in turbid media, only a small sample amount is needed, they are relatively cheap to produce, a fast detection time and have

simple procedures to follow (Arora, Sindhu, Dilbaghi, & Chaudhury, 2011; Velusamy et al., 2010).

3.1.3. Impedance Biosensors

The type of biosensor that was employed in this research uses impedance as a means to determine the sensitivity, limit of detection, range of detection and selectivity of the sensor. Impedance is a form of complex resistance that occurs when either an (alternating current) AC or DC (direct current) current flows through an electrical circuit comprised of many different capacitors, resistors and inductors (Lvovich, 2012). Impedance is similar to resistance in that it is the ratio of voltage to current. However, impedance takes into account how a circuit can resist the flow of current, known as "real impedance" and how well a circuit can retain electrical energy, known as "imaginary impedance" (Barsoukov & Macdonald, 2005).

The cell membrane of a bacterium is composed of a lipid bilayer that has capacitance and resistance that will hinder the electrodes ability to conduct current. So as the bacteria become attached to the bioreceptors that are immobilized on the surface of the electrode, a change in the impedance is used to determine the characteristics of the sensor (Wang, Ye, & Ying, 2012). Impedance biosensors can use a wide range of bio-recognition agents to detect bacteria, such as, antibodies, bacteriophages, lectins and aptamers (Daniels & Pourmand, 2007). In particular, this research focused on antibodies and aptamers.

It is vital in impedance biosensors, for either of these bio-recognition agents to understand the method with which they were attached to the electrode surface since it

can greatly impact the performance of the biosensor. The most common methods used for immobilization are covalent binding, physical adsorption and creating a self-assembled monolayer (SAM). Physical adsorption takes advantage of the non-specific interactions that occur between the bacteria attachment mechanism and the electrode, like ionic bonds, van der Waals forces and hydrophobic interactions (Wang et al., 2012). An example would be of the biosensor developed by Yang et al.(Yang & Li, 2005) that used physical adsorption to attach anti-*Escherichia coli* antibodies onto an interdigitated array microelectrode to detect *E. coli* O157:H7. The sensor had a limit of detection at 10^6 CFU/mL and a range of detection from 4.3×10^5 to 4.36×10^8 CFU/mL. Physical adsorption is less commonly used; however, because it only does a random placement of the antibodies and aptamers and tends to have a low stability. Both of which equate to the biosensors being produced from this method having a difficult time attaching bacteria, which in turn makes the biosensor less sensitive.

SAMs on the other hand have proven to be a very easy way to create very thin films out of biological materials on the surface of the electrode. Each of these films contains groups of free end groups like amines, thiols or carboxyl groups that the antibodies and aptamers can then be attached to (Wang et al., 2012). Braiek et al. (2012) used 3-mercaptoacetic acid to form a SAM for immobilizing anti-*Staphylococcus aureus* antibodies on an gold electrode. The immobilization of antibodies was executed using an intermediate linker generated by 1-ethyl-3-(3-dimethylaminopropyl)carbodiimide (EDC) and N-hydroxysuccinimide (NHS), which allowed the antibodies to covalently bind onto the SAM and improve the sensitivity of the biosensor. The sensor had a limit of

detection of 10 CFU/mL and showed linear relationship between the changes in electron transfer resistance and the logarithmic value of *S. aureus* bacteria concentrations that ranged from 10 to 10^6 CFU/mL. The SAM produces a noticeably more sensitive biosensor than the physical adsorption method. However, the SAM immobilization method does not come without some downsides such as desorption of the monolayer when the biosensor comes in contact with an electric field or heat and adsorption of other materials onto the surface because its surface energy has been increased (Wang et al., 2012).

Lastly, covalent attachment is a well-known approach to the attachment of materials like proteins to reaction layers (i.e., surfaces and substrates). Proteins are usually bound to the surfaces using amino, carboxyl or sulfhydryl groups using coupling reagents that are specifically designed for each group. When things like metals and small organic material undergo these surface modifications they may have to be altered to allow for functional groups to be attached. Covalent binding has been criticized for being a more laborious process than some of the other immobilization techniques; however, covalent binding does have some advantages, which make it a better option than the previously discussed attachment methods. Firstly, materials that have been covalently attached tend to have more durable surface after modification, which allow them to have greater stability when put through rigorous testing. Secondly, compared to other techniques like adsorption, covalent binding has been shown to deliver a better surface structure that allows for more binding sites and more controlled attachment (Cunningham, 1998).

Impedance biosensors have been praised as the best method for bacteria detection in comparison to the other biosensors (Arora et al., 2011). The association of Analytical Communities international (AOAC) has even acknowledged impedance biosensors as the best technique for the detection of *Salmonella* in food samples (Gibson, Coombs, & Pimbley, 1992).

3.1.4. Electrochemical Impedance Spectroscopy (EIS)

The idea of electrical impedance has been around since the 1880s when Oliver Heaviside first introduced the concept and was further developed by A.E. Kennedy and C.P. Steinmetz to use complex numbers and vector diagrams to represent it (Lvovich, 2012). Impedance values are determined from four electrical parameters, resistance, capacitance, inductance, and frequency. An impedance vector is usually comprised of a real component, resistance, and an imaginary component, the reactance. The real component is not dependent upon frequency and the imaginary component is dependent upon frequency. The imaginary component is made up of the capacitance and inductance parts of impedance. As the measurement frequency decreases the capacitance parameter should increase resulting in a measurable phase angle shift (Lum, 2014).

These measurements can be displayed as diagrams, which are often represented in two forms, a Nyquist or a Bode plot. Nyquist plots are most commonly employed when using a redox probe to measure Faradic impedance and show the real impedance (Z_{REAL}) data (X-axis) versus the imaginary impedance (Z_{IM}) data (Y-axis) as seen in Figure 3.2. Nyquist plots are usually analyzed by fitting the data to equivalent circuit

model, like the Randles circuit seen in Figure 3.1. This circuit consists of a solution resistance (R_s) in Ohms, that relates the movement of charge through the testing solution, a double-layer capacitance (Q) in Farads, that mocks up the double-layer formation that occurs at the electrode surface, a charge-transfer resistance (R) that models the charge transfer reaction in Ohms at the electrode surface, and lastly a Warburg impedance (W) which relates the impedance for the diffusion layer when the layer has infinite thickness, it has units of Ohms per square root second (MacDonald & Andreas, 2014).

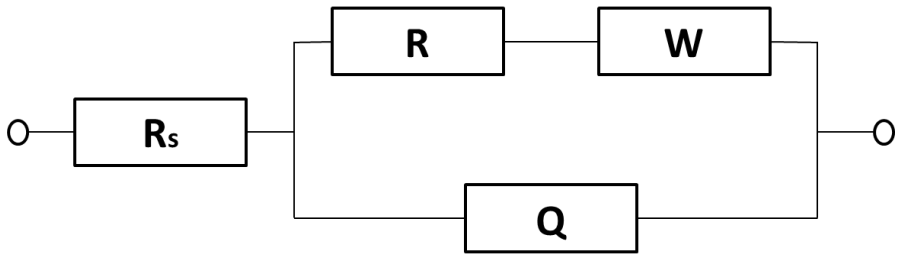

Figure 3.1 – Randles equivalent electrical circuit adapted from Barsoukov and Macdonald (2005).

Bode plots on the other hand are most commonly used for non-Faradaic impedance testing, when trying to detect an analyte. A demonstrated in Figure 3.3, a Bode plot has the log of the frequency on the X-axis and both the phase angle shift and the log of the impedance magnitude on the Y-axis (Barsoukov & Macdonald, 2005). The impedance magnitude can be calculated using Eq. (3.1):

$$|Z| = \sqrt{[R^2 + (X_L - X_C)^2]} \qquad (3.1)$$

where R is resistance in Ohms, X_C is the capacitance impedance in Ohms, and X_L is the inductive impedance in Ohms which is usually found to be negligible for biological systems. The phase angle plotted is calculated using Eq. (3.2):

$$\varphi = Tan^{-1}[\frac{X_L - X_C}{R}] \qquad (3.2)$$

since the imaginary component of impedance is dependent upon the frequency it is necessary to calculate the contribution that capacitance makes to the impedance value. This can be calculated using Eq. (3.3):

$$X_C = \frac{1}{2 * \pi * f * C} \qquad (3.3)$$

where f is the frequency in Hz and C is the value of the capacitor in F (Lum, 2014).

To gather information such as the sensitivity, limit of detection and range of detection Bode (impedance versus frequency) and Nyquist (imaginary impedance versus real impedance) plots need to be generated at increasing concentrations of bacteria to analyze the total impedance response of the biosensor. The total impedance change for all of these concentrations are then compared to the baseline (no bacteria added) over the test frequency range to select the frequency which shows the greatest impedance difference between the increasing concentration of bacteria to the baseline. The frequency that has the largest impedance difference with increasing bacteria concentration will be used for all further characterization, i.e., use to plot the calibration curve to determine the sensitivity, range, and limit of detection of the biosensor (Lum, 2014).

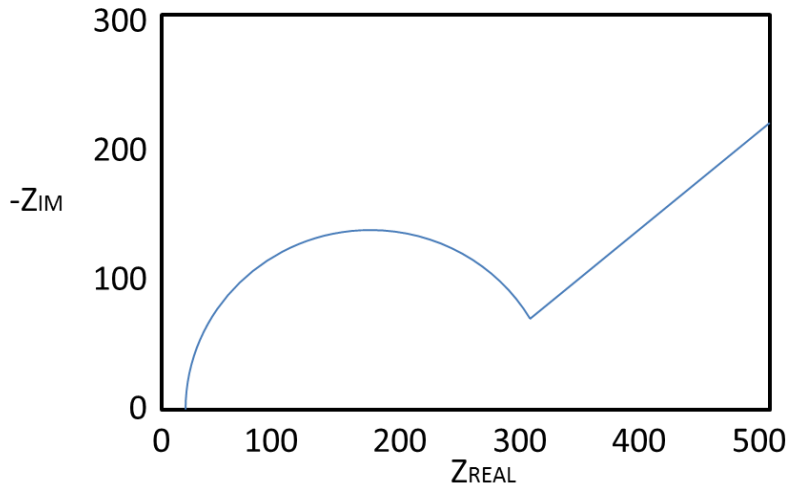

Figure 3.2 - Nyquist plot adapted from Lvovich (2012).

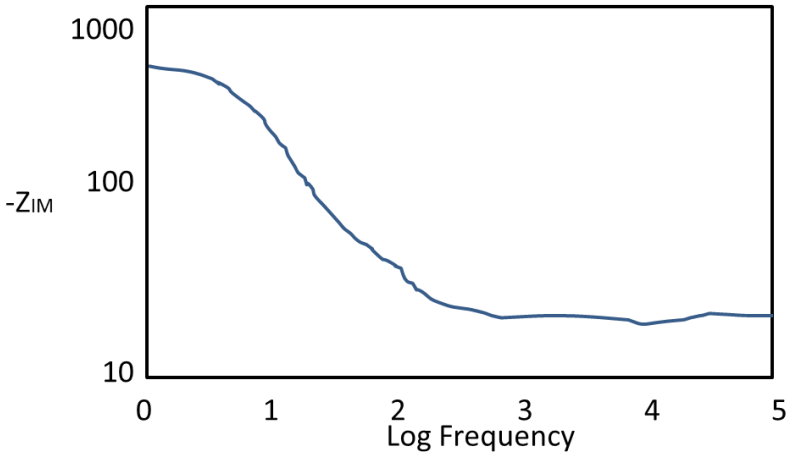

Figure 3.3 - Bode plot adapted from Lvovich (2012).

3.2. Platinum

3.2.1. Background

Platinum has been locked in the crust of the earth since before mankind walked upon it. But it wasn't until the mid-1700s that man first began to explore platinum's properties (WorldBook, 2014) and it wasn't until 1828 when William Hyde Wollaston's

process for producing a malleable form of platinum was published did commercial production take off (McDonald & Hunt, 1982). From then on the research into platinum's properties and possible applications has exploded.

3.2.2. Applications

Platinum has been used since the 1960s as an antitumor medicine, cisplatin. Cisplatin comes with some downsides though like neurotoxicity, nephrotoxicity and emetogensis, thus its dose has to be limited to deter the toxic side effects (Wong & Giandornenico, 1999). Then in the 1980s, a second generation of platinum based cancer drugs was introduced called, carboplatin, that helped to lower the side effects of the drug (Kelland, 2007). Since then the use of platinum in cancer fighting drugs has increased in recent years.

Platinum has also played an important role in the way humans get from point A to point B. Because of increasing demands for fossil fuels and energy in general it has become a priority to find new ways to improve the efficiency of our fuel sources while still maintaining low emissions. Platinum has become a vital part of this optimization because it is highly catalytic and stable for fuel cells and petroleum products (Chen & Holt-Hindle, 2010).

Lastly, platinum has been used as one of the building blocks in many biosensors because of its high electrical conductivity. The sensitivity of an electrochemical biosensor is heavily dependent upon its ability to capture electrons and convert them into a measurable signal. One of the ways that a higher sensitivity can be achieved is increasing the electroactive surface area by adding nanomaterials, like platinum

nanoparticles, that are good electron carriers into the surface of the working electrode. Platinum nanoparticles and other nanometal particles increase the electroactive surface area by increasing the conductive surface area (Claussen et al., 2010; McLamore et al., 2011; Shao et al., 2010; Vanegas et al., 2014). Wang et al. (2012) designed a biosensor that was comprised of platinum nanoclusters and multi-walled carbon nanotubes to detect glucose in samples. Their sensor showed a limit of detection of 1 μM and a linear range of 3 μM to 12.1 mM. Siriviriyanun et al. (2013) created a biosensor that was comprised of platinum nanoclusters, multi-walled carbon nanotubes, dendrimers and enzymes to detect organophosphorus pesticide. Their sensor showed marked improvement in sensitivity as the amount of platinum clusters adhered to the sensor increased. Finally, Ren et al. (2012) made a sensor to detect glucose that was comprised of platinum nanocubes, chitosan, glucose oxidase and nafion on a platinum electrode. Their sensor showed a low detection limit (0.5 μM), high sensitivity (35.92 μA mM^{-1} cm^{-2}), and a linear detection range (1×10^{-6} to 5×10^{-3} M).

3.3. Graphene

3.3.1. Origins: Graphite

Graphite is a naturally occurring carbon based mineral that consists of carbon sheets, stacked and held together by weak Van der Waals forces (Georgakilas, 2014). These carbon sheets have a structure similar to that of a 2D honey comb and when separated from each other are called graphene. Graphene has become highly prized in the nanotechnology field for its electrical and chemical properties. Researchers have found uses for it in many electronic applications such as solar panels, thin films and

sensors (Choi & Lee, 2012). However, chemically speaking, pure graphene can be considered an inert material, making it difficult to chemically bond to other materials. This, combined with the issue of obtaining pure graphene has made its counterparts graphene oxide and reduced graphene oxide a favorable alternative. Graphene oxide (GO) is similar to graphene in that it is a single layer of graphite; however, GO also has functional end groups such as carbonyl, carboxyl and hydroxyl groups from which other materials can be chemically bound to the GO (Luedtke, 2015). The downside of these functional groups become evident when evaluating the electrical properties of GO since it has been found to act as something of an electrical insulator (Karteri, Karataş, Al-Ghamdi, & Yakuphanoğlu, 2015; Liu et al., 2013). Yet, when GO is reduced the composition of the material begins to exhibit traits similar to that of pure graphene with moderate electrical conductivity, making it popular for use in a number of electronic devices (Shao et al., 2010).

3.3.2. Synthesis and Reduction of Graphene Oxide

The majority of modern methodologies for procuring GO are derived from the Hummers method. The process is executed by oxidizing graphite in a solution of potassium permanganate and sulfuric acid. The end result is a thin film that can be placed into an aqueous solution. The GO can then be reduced using chemicals such as hydrazine, $NaBH_4$ and ascorbic acid (Luedtke, 2015).

3.3.3. Applications

Graphene's electrical, mechanical and thermal properties have lent itself to many applications. Energy storage devices and polymer nanocomposites (Zeng, Cheng, Liu,

Bai, & Jiang, 2011) are two of the leading areas where graphene has been put to use in the form of batteries (Ali et al., 2015), super capacitors (Sankaranarayanan, Venkatraman, Sundar Raj, & Mohanraj, 2014), fuel cells (Zhao et al., 2015) and solar cells (Bin Mohd Yusoff, Kim, Jang, Schneider, & Da Silva, 2015; Zhi, Cui, Chen, Xie, & Huang, 2015). Graphene is particularly handy for solar cells since graphene oxide can be put into solution and used to create transparent electrodes for the solar panels(Bin Mohd Yusoff et al., 2015). One area that has also exploded with the use of graphene is chemical sensors and biosensors.

Biosensors have become very fond of using graphene and it's byproducts because of its ability to improve the electron transport of a biosensor and in turn increasing the sensitivity of the device (Luedtke, 2015). Some instances where graphene has been used in biosensors include hormones (Li et al., 2015), cancer cells (Lin et al., 2015) and glucose (Shao et al., 2010; Shi et al., 2012; Zeng et al., 2011) detection. One specific instance involves the use of ssDNA tagged with a fluorescence marker that became quenched when it was bound to functionalized graphene oxide (Lu, Yang, Zhu, Chen, & Chen, 2009). However, if the ssDNA came into contact with its complement ssDNA then it would detach from the graphene oxide and begin to glow again, indicating that the complementary ssDNA was in fact present in the sample. Another group, Vanegas et al. (2014), compared several different biosensors on platinum electrodes (Pt/Ir) all made out of various graphene, reduced graphene (rGO) and nano-platinum (nPt) coatings (Pt/Ir–GO, Pt/Ir–nPt–GO, Pt/Ir–rGO–nPt, Pt/Ir–nPt–rGO–nPt). The sensors were tested to find the sensitivity, limit of detection and response time of

hydrogen peroxide. The Pt/Ir–RGO–nPt and Pt/Ir–nPt–RGO–nPt hybrid nano-materials exhibited significantly improved electrochemical performance over all other carbon metal nanohybrids. Pt/Ir–nPt–RGO–nPt modified electrode demonstrated the highest amperometric sensitivity of all the nanomaterial platforms tested (45 ± 3.2 μA mM^{-1}), a response time of roughly 3 seconds and a limit of detection at 0.14 ± 28 μM. Lastly, Wang et al. (2014), decided to use modified graphene and gold nanoparticles as an electrode substrate with anti-*E. coli* O157:H7 antibodies attached on the surface. Their results showed that the sensor possessed impressive sensing performance, with a wide linear range (1.5 CFU mL^{-1}), a low detection limit (1.5×10^3 CFU mL^{-1}), and no significant interference from other *E. coli* strains, *Staphylococcus aureus*, or *Listeria monocytogenes* meaning a good specificity to the desired target.

3.4. Chitosan

3.4.1. Origins: Chitin

Chitin is the second most abundant polysaccharide based biopolymer in the world, beaten only by cellulose and comes from the word, Chiton, which in Greek is, a coat of nails. It was first identified by the French scientist, Henri Braconnot, in 1811 after he had managed to extract the Chitin from mushrooms (Muzzarelli et al., 2012). Twelve years later, another French scientist, Antonie Odier, confirmed Braconnot's findings but this time in insects and plants, and named the material, Chitine.

The chemical name for chitin is poly-N-acetyl-d-glucosamine and it is the main material found in the exoskeletons of invertebrates, crustaceans and insects in the Animalia kingdom, as well as the cell walls of the fungi kingdom. The chitin is used to

support and protect the organism's delicate internal parts from outside sources that could cause damage, like the organism's natural predators. Normally, the chitin found in animals is associated with other compounds essential to life, such as lipids, calcium carbonate, proteins and color pigments and the Chitin found in fungi is usually found with other polysaccharides like cellulose (Belgacem & Gandini, 2008). Because chitin can be so heavily involved with these other materials it is normally very common to include a filtration step of some kind to separate out the chitin from the rest so that it can be further processed. Even within the different producers of this biopolymer there can be a degree of difference between the final products based on the organism. Over the course of a year, some ten gigatons of chitin will be produced and hydrolyzed by these creatures which could be harvested for use in biopolymer production (Shahidi & Abuzaytoun, 2005).

3.4.2. Chemical Structure

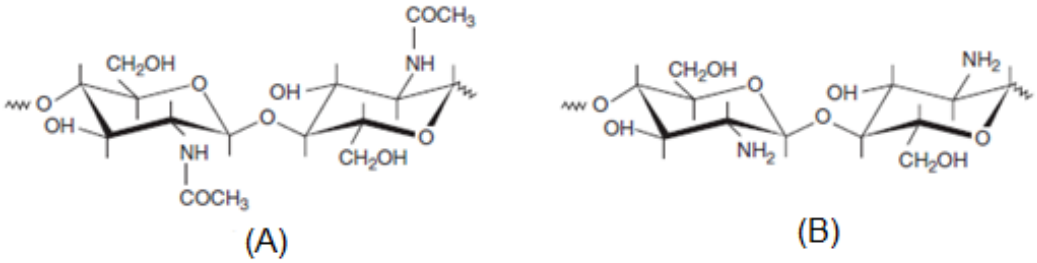

Figure 3.4 - Chemical structure of chitin (A) and chitosan (B) adapted from Belgacem and Gandini (2008).

The chemical structure of chitosan as illustrated in Figure 3.4 is very similar to that of chitin and even other polysaccharides like cellulose, with the main difference

between chitin and chitosan being the removal of the $COCH_3$ group from the structure and the addition of a hydrogen to the nitrogen group allowing for NH_2 to be formed. With the formation of this amine group, the chitosan then has greater functionality and lends itself to creating bonds with other chemicals such as glutaraldehyde and N-hydroxysuccinimide (NHS).

3.4.3. Deacetylation

Deacetylation is the process of removing acetyl groups from a material and is usually naturally occurring in very small amounts in chitin. As stated above, there can variation among the producers of this material and degree of deacetylation is by far the largest reason for this. For example, in animals the spots of deacetylation are very random and can lead to variance in the chitin's properties; whereas chitin produced by fungi has been found to have a much more predictable structure that allows for smaller changes in the materials properties (Belgacem & Gandini, 2008). When the degree of deacetylation (%DD) reaches past 50% the chitin can then be referred to as the biopolymer, chitosan (Rinaudo, 2006). After this occurrence the material also becomes soluble in acidic solutions, creating pH sensitivity. As the degree of deacetylation changes, other properties of chitosan can be subject to change such as the chain flexibility, mechanical properties, pore size, metal binding and biodegradation capabilities (Chen, Domard, Muzzarelli, Tokura, & Wang, 2011).

3.4.4. Polyelectrolyte Gels

Chitosan is a polyelectrolyte, meaning that when made into a gel it creates a charged polymer network containing fixed macro-ions in the chain of the biopolymer.

They have the special ability, like all hydrogels, to adsorb up to two thousand times their weight in water, while remaining insoluble in the water itself. Furthermore, polyelectrolyte gels can also be subjected to electrically induced contractions when placed between electrode plates. They act so peculiar when in contact with electricity, that scientists have even studied these gels as a means to bio-mimic muscles for artificial organs (Tanabe et al., 2008).

3.4.5. Molecular Weight

The molecular weight of chitosan can vary greatly with the degree of deacetylation (Tsaih & Chen, 2003). With this variation also comes change in the physical and chemical properties of the material such as its chain flexibility, zeta potential (charge distribution), pH-response, rheological and mechanical properties (Rong Huei & Hwa, 1996) and the pore sizes that can be formed when creating a hydrogel. All of these then affect the potential applications of chitosan such as its ability to hold water in use in cosmetics, anti-microbial activity in food applications and chitosan's propensity to aid in wound healing (Khoushab & Yamabhai, 2010).

3.4.6. Production of Chitosan

Since chitosan will never be found in a pure form, it is essential to purify the base material, which in most cases is shellfish, for processing. As illustrated in Figure 3.5, the process begins by first separating the shells from the main body of the crustacean. This is already a common occurrence in food production for seafood like shrimp where the shell is normally discarded as waste. From there the shells must be ground down to allow for the de-proteination and demineralization to take place (Belgacem & Gandini,

2008). De-proteination is the process of removing all of the remaining proteins in the material. This is usually done by placing the ground shells into a dilute alkali, under heat. Demineralization uses a dilute mineral acid like hydrochloric acid, to remove any unwanted organic salts or minerals from the material (Hudson & Smith, 1998). After separating and washing the material is now primarily all chitin. The chitin can be further purified for its own applications if desired. To complete the change to chitosan; however, it is necessary to further deacetylate the material using hydrolysis, which is the removal of chemical bonds via the addition of water. For the hydrolysis to take place a concentrated alkali, such as a 50% sodium hydroxide solution, and heat in the temperature range of 120^{o}C is applied to the chitin for approximately two hours under nitrogen to produce chitosan. The end step of hydrolysis can be performed several times until the desired degree of deacetylation of the material is reached. Once this is complete the chitosan can then be washed, dried and ground down to a powder for distribution.

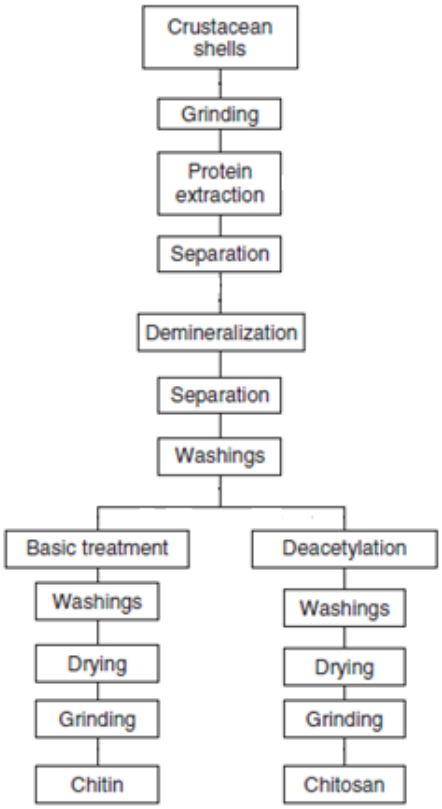

Figure 3.5 - Process of chitin to chitosan from crustaceans, adapted from Belgacem and Gandini (2008).

Once the chitosan has been ground down it can then be made into a hydrogel. Hydrogels are swollen, three-dimensional polymer networks that are hydrophilic in nature and allow for a large amount (at least 20% w/v) of water to be stored with in them (Ottenbrite, Huang, & Park, 1996; Ravi Kumar, 2000). All hydrogels have the ability to shrink and swell in volume with the addition or elimination of water to the gel. But some hydrogels have also been developed that have the ability to exhibit the same volume change when their environmental conditions are altered such as, temperature,

amount of light or pH. Chitosan is one of these environmentally sensitive materials with a capacity to shrink or swell when the pH of the system is altered (Yao, 2012).

To produce a hydrogel, the chitosan powder is normally first placed in an acetic acid solution and stirred until dissolved. The solution can then be mixed with glutaraldehyde in a homogenizer to form a stronger polymer network, before being drop coated onto another substance or placed in a dish, then dried. To safeguard that the hydrogel will remain unreactive while being stored, a solution of sodium hydroxide is applied to the gel and then washed with water to neutralize the pH (Kim, Shin, Lee, Lee, & Chung, 1997).

Chitosan can also be made into nanofiber structures that can be adhered to metallic surfaces via either electrospinning or electrodeposition. Electrospinning is a process that can procure small diameter fibers that can reach into the nanoscale; however, it is prone to having a large diameter variance. For this set up as illustrated in Figure 3.6A, a high powered voltage source is applied to a metering pump to create a large electric field between the syringe tip and the plate used to catch the spun material. As the hydrogel is extruded out of the tip, the strong charge of the polymer is attracted to the opposing charge of the plate and a stream of material begins to flow between the two. Since chitosan is a highly viscous material it can be very difficult to electro-spin by itself so in most instances the material is blended with another polymer like polyethylene oxide (PEO) or poly-vinyl alcohol (PVA) to lower the viscosity of the solution while still enabling the chitosan to make use of it pH sensitivity (Kriegel, Arrechi, Kit, McClements, & Weiss, 2008). Also shown in Figure 3.6B is a scanning electron

microscope (SEM) image of a finished Chitosan-PEO nanofiber that demonstrates the random, almost spider web like structure that results from electrospinning.

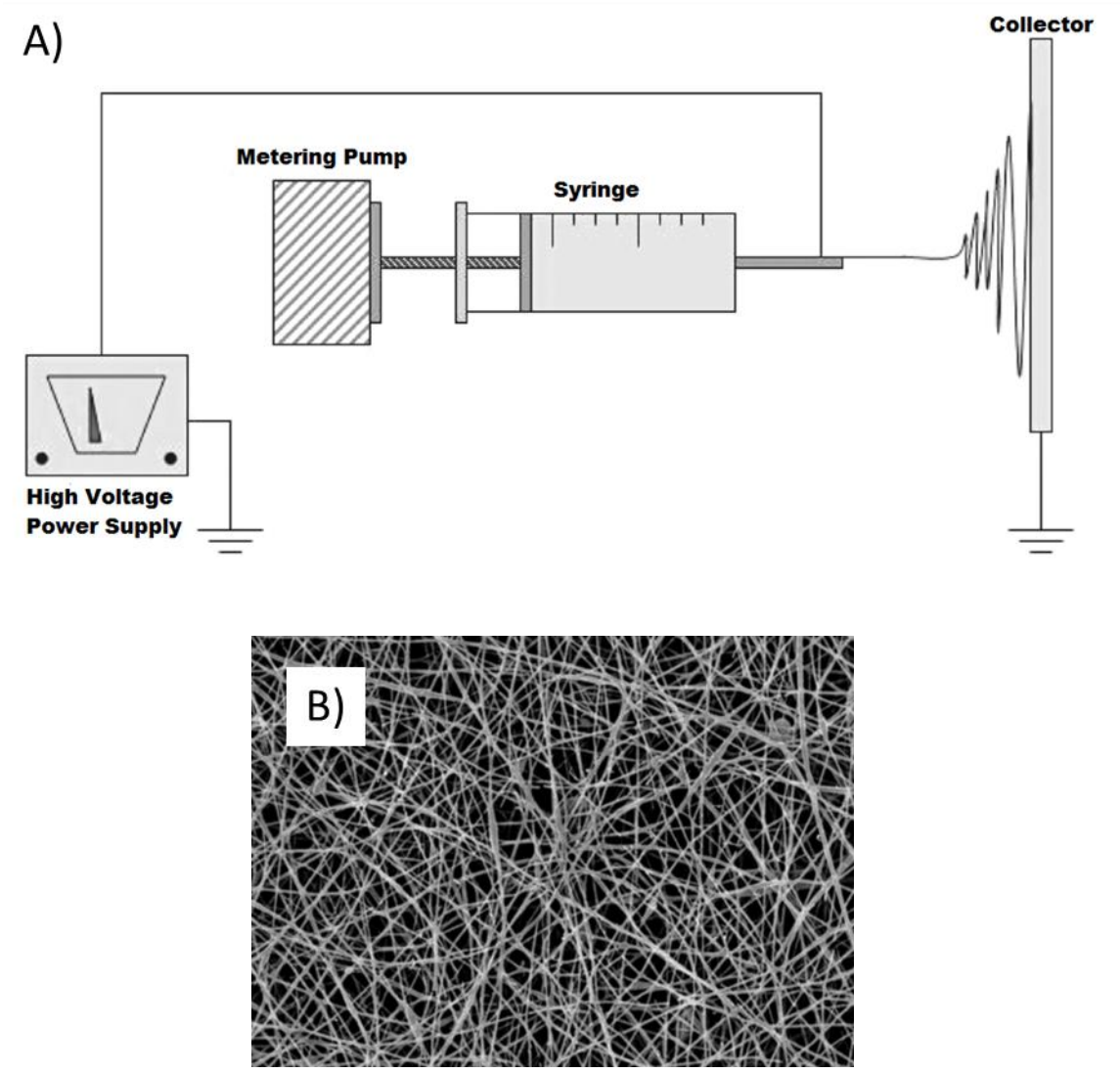

Figure 3.6 – A) Production of chitosan fibers and B) SEM image of a final chitosan-PEO composite of nanofibers at 10,000x magnification, adapted from Kriegel et al. (2008).

Polymer brushes are molecules covalently grafted into long chains on a surface (Milner, 1991). They can be formed using electrodeposition. This process uses an

electric field to move charged particles in a liquid onto an electrode that can produce a thin film that looks similar to fingers extruding out of the electrodes surface. The thickness of the thin film on the surface was highly time-dependent, so the longer you ran the electrodeposition the thicker the film ended up (Ma, Pang, & Zhitomirsky, 2011). Unlike other methods, electrodeposition requires no cross linking agents and has a relatively quick process to yield results (Wang et al., 2014).

3.4.7. Applications

Chitosan has wide ranging areas of applications as seen in Table 3.1 below, everything from health care, food safety, agriculture practices, and water treatment to biosensors. Some of these applications will be discussed in the following sections.

Table 3.1 – Types of products produced from chitin and chitosan and their potential applications, adapted from Hudson and Smith (1998).

Chitosan Form	Applications
Beads	Metal Chelation Waste Water Treatment Drug Delivery Enzyme Immobilization
Coatings	Surface Modifications Textile Finishes Seed Coatings for Improved Seed Germination Paper Sizing
Fibers	Medical Textiles Sutures
Films	Membranes Wound Care Packaging
Adsorbent Powders	Waste Water Treatment Animal Feed Additive Microcrystalline Forms Pharmaceuticals
Shaped Objects	Orthopedics Contact lenses
Solutions and Gels	Cosmetics Waste Water Treatment

Wound Healing

Chitosan has been found to in a number of studies to have the capability to enhance wound healing and repair. A case by Howling et al. (2001) discovered that chitosan can control the movement of neutrophils and macrophages such that the repair processes fibroplasia and re-epithelialization, were improved. It was also noted that the cells, dermal fibroblasts and keratinocytes, found in the outer layer of the skin were aided when chitosan was added. It did; however, appear that the effectiveness of the

dermal fibroblast proliferation was heavily dependent upon the degree of deacetylation of the chitosan, with only high %DD aiding in fibroblast growth.

One of the main reasons that chitosan is able to promote healing occurs because it is a polyelectrolyte material that can form polyelectrolyte bonds with other materials like poly-anion heparin, which can have anticoagulant properties in blood and angiogenic properties to help heart problems (Lahiji, Sohrabi, Hungerford, & Frondoza, 2000). Taking advantage of this property, the United States government has even designed and implemented bandages made with chitosan for use in their military (Becker, 2003). They found that the bandages were very effective at reducing bleeding and stopping severe hemorrhages (Wedmore, McManus, Pusateri, & Holcomb, 2006).

Health Benefits

For more than a decade chitosan has been researched and commercially sold as a dietary supplement to promote weight loss, and fight ulcers and high cholesterol in humans. Different forms have been produced such as chitosan tablets (Muzzarelli, Frega, Miliani, Muzzarelli, & Cartolari, 2000), dietary fibers (Hughes, 2002) and as a rapidly soluble chitosan supplement all to reduce body in overweight persons that also consume a high-fat diet. Of the three supplements, chitosan based dietary fibers appear to have to the best health benefits such as lowering the low-density-lipoprotein (LDL) cholesterol levels as well as creating a feeling of fullness that can prevent over eating. When chitosan is consumed it also helps slow the adsorption of sugar into the body that helps maintain blood sugar and insulin levels from having large fluctuations like ones that patients with type 2 diabetes can experience (Hughes, 2002).

As stated before, chitosan has been found to cause compelling changes to a body high in cholesterol. Much of the research has used animals such as rats to test the effect that different molecular weight chitosan can have on the hypocholesterolemic activity. It was found that the lower the molecular weight of the chitosan, the better it did to reduce cholesterol (Hirano et al., 1990; Sugano, Fujikawa, Hiratsuji, & Hasegawa, 1978; Ylitalo, Lehtinen, Wuolijoki, Ylitalo, & Lehtimäki, 2002). Chitosan can inhibit cholesterol using its amine groups as an acceptor of hydrogen to form positively charged (NH_3) amino groups, creating a salt when in the presence of hydrochloric acid. The fatty acids and other lipids present in the body then become attracted to the amino group on the chitosan (Ylitalo et al., 2002). It is thought that the binding to chitosan is what inhibits the adsorption of lipids into the body, preventing them from becoming artery blocking agents.

A study by Ito et al. (2000) also worked with chitosan to determine its health benefits, this time evaluating its effectiveness at treating stomach ulcers. Their results found that a low molecular weight chitosan when taken orally, in a low dose, proved helpful at preventing and treating gastric ulcers in rats. High molecular weight chitosan was also tested, but found to be less effective at treatment than the lower molecular weights ones.

Drug Delivery and Release

When chitosan is made into a film it tends to show very little swelling in water. To mediate this effect in drug delivery and release systems, chitosan is normally mixed with a more hydrophilic polymer such as poly(vinyl alcohol) (PVA), calcium alginate, or

gelatin to add stability to the encapsulation. Once a material has been encapsulated in the chitosan it can be held there until called upon to be released. One method for controlled release uses chitosan's pH sensitivity to swell at low pHs and shrink in a high pH system (Yao, Yin, Xu, & Wang, 1995).

Some other reported delivery applications for chitosan include, chitosan/ polyethylene glycol/ alginate miscrospheres for heparin (Chandy, Rao, Wilson, & Das, 2002) and chitosan/ xanthan microcapsules to protect drugs against stomach acids (Chellat et al., 2000) and as a possible candidate for non-viral gene delivery to the body (Lee, Kwon, Kim, Jeong, & Jo, 1998).

Prosthetic Coatings

Prosthesis is a man-made device that has been designed to replicate a part of the body that has been lost via either trauma or disease. When chitosan is applied as a film to the hydroxyapatite layers of the prosthetic, it has been shown that bone regeneration and strengthening increases with the addition of the polymer. Chitosan was also shown to increase the integrity of the implant as a whole (Avetta et al., 2014).

Food Packaging and Preservation

Chitosan has the ability to act as an antimicrobial polymer against organisms like bacteria, yeast and fungi that can find their way into food products (Devlieghere, Vermeulen, & Debevere, 2004). It is considered to be a chelating agent, meaning that it can bind with certain trace metals to stop the creation of microbial growth (Cuero, Duffus, Osuji, & Pettit, 1991). When added to a fresh food product, such as its packaging film, chitosan can use its power of chelation to prevent food spoiling and

pathogenic microorganisms from growing. Some examples of pathogens are *Staphylococcus aureus, Salmonella* Typhimurium, *Bacillus cereus, Escherichia coli* and *Proteus vulgaris* (Rodríguez-Núñez et al., 2012; Simpson, Gagne, Ashie, & Noroozi, 1997). Another effect of employing chitosan into a food's packaging has to do with chitosan's ability to control the flow of moisture and air from the product to the surrounding environment. With the flow of these essential building blocks of organism proliferation being highly regulated, it then makes more difficult for microbial activity to persist. Furthermore, there is the added benefit from this reduced moisture and air transfer between the packaging and the environment of a delaying in the ripening for fruits and vegetable, consequently reducing their respiration rate and increasing their shelf life (Binsi, Ravishankar, & Srinivasa Gopal, 2013). However, packaging alone may not be enough to stop the growth of pathogens in food so the use of food preservation additives may need to be employed.

Other studies have invested the application of chitosan as a food preservation additive directly to foods like mayo. One study by Oh et al. (2001) examined chitosan's effect in mayo on four different organisms, *Lactobacillus plantarum, Lactobacillus fructivorans, Serratia liquefaciens* and *Zygosacchaomyces bailii*. Their results showed an initial marked decrease in the microbial growth, though some of the strains were able to begin regrowth over an extended period of time. Like with packaging, chitosan additives have likewise been researched for fresh fruits in the form of edible coating to slow the rate of ripening and decay of the material (Martinon Gaspar & Moreira, 2012; Moreira, Roura, & Ponce, 2011). But one of the largest areas of research for chitosan's

application occurs in meat preservation with a number of studies examining chitosan's effectiveness to prolong the shelf life of items like fish (Abdollahi et al., 2014), snow crab (Kamil et al., 2002), bologna, ham and pastrami (Ouattara, Simard, Piette, Bégin, & Holley, 2000), and several other cooked meats (Darmadji & Izumimoto, 1994).

Agriculture

As stated earlier, chitosan has the ability to act as an anti-fungal agent. This can not only be applied to food processing and packaging, but the actual process of growing the food as well. For example, a layer of chitosan was applied to the root system of a pear tree and it was seen that the amount of fungal growth in the tree dropped off dramatically. This allowed the tree to flourish and increased crop production (Meng, Yang, Kennedy, & Tian, 2010). In addition, chitosan is a good prospect for the encapsulation of biocides that would combat diseases and organisms that may want to harm the crop, such as, viruses found in strains of potatoes, tobacco, alfalfa, peanut and cucumber plants (Chirkov, 2002; Ottenbrite et al., 1996; Pospieszny, 1997).

Water Purification

Chitosan can also be used in the practice of sand filtration of water as an additive to reduce the amount of turbidity in the system. Chitosan can do this by binding with the very small sedimentation particles that are trying to be removed from the water. Along with sediment particles, chitosan can also absorb heavy metals, phosphorus and oils that may be present in the water (Mishra, Mishra, & Tiwari, 2011).

One country that has already taken advantage of chitosan's ability to remove heavy metals would be Japan. For many years they have used the amine groups in

chitosan to bond with metal ions (Simpson, Gagne, & Simpson, 1994). Even the environmental protection agency (EPA) in the United States has allowed the application of chitosan to waste water treatment since the late 1980s, so long as the treatment concentration does not exceed 10 mg/L.

Biosensors

One of the newer fields of technology for chitosan applications is biosensors. A number of papers have incorporated chitosan into sensors that can detect glucose, hydrogen peroxide and tyrosinase (Mishra et al., 2011). By adding chitosan, the biosensor can then be controlled to hold or release the bio-recognition agent using pH variation. In addition, chitosan can act as a barrier to protect the bio-recognition agent from damage or decay, prolonging the shelf life of the biosensor.

Burrs et al. (2015) where they created a rGO/nPt base on an electrode and then attached four different hydrogels, including a chitosan hydrogel with alcohol oxidase mixed into it to detect methanol. Electrochemical tests were then run to determine the effective surface area (0.2 ± 0.06 cm^2), sensitivity to methanol (0.46 ± 0.2 μAmM^{-1}), limit of detection (100 ± 20 μM), linear range (100 to 2500 μM) and response time (4.3 ± 0.8 s). This study showed chitosan coated electrodes together with PNIPAAM (poly-N-isopropylacrylamide) had significantly better performance characteristics i.e., sensitivity, ESA, response time, shelf-life, limit of detection, compared to other hydrogels-coated electrodes (silk and nanocellulose). Shahdost-fard et al. (2013) used electrochemical testing and constructed a nanocomposite biosensor with carbon nanotubes, ionic liquid and chitosan to detect adenosine. ssDNA probes and aptamers

were adhered to the sensor. The sensor had a detection limit of 150 pM and a sensitivity of 0.67 μAnM^{-1} with a concentration range of up to 0.4 μM. Chitosan biosensors have even been used to detect bacteria. Abdelhamid and Wu (2013) created a sensor that was comprised of multifunctional graphene magnetic nanosheets coated with chitosan to detect *P. aeruginosa* and *S. aureus*. Analysis was based on Fourier transform infrared spectroscopy (FTIR) tests the limit of detection was approximately 5×10^2 CFU mL^{-1} with a range of detection from 900 to 4750 CFU mL^{-1}.

3.5. Aptamers

3.5.1. Background

Aptamers are isolated oligonucleotide sequences that can be used to detect almost any kind of molecule. The process by which aptamers are created is called systematic evolution of ligands by exponential enrichment (SELEX) (Jayasena, 1999). Random nucleic acids are first incubated with the desired target molecules (Figure 3.7). The nucleic acids that bind are then separated from the rest and the target molecules are removed. Next, the separated nucleic acids are amplified using an enriched library of nucleic acids resulting in many new aptamers. This process is then repeated until the desired amount of aptamers has been produced (Kedzierski, Khoshnejad, & Caltagirone, 2012). Aptamers have long been compared to antibodies because they exhibit similar properties when used for diagnostic purposes with the exception of a higher affinity and specificity to the molecule that is trying to be detected. There is an ever increasing need for fast and accurate diagnostic assays to detect diseases and aptamers provide the required affinity and robustness fill that void.

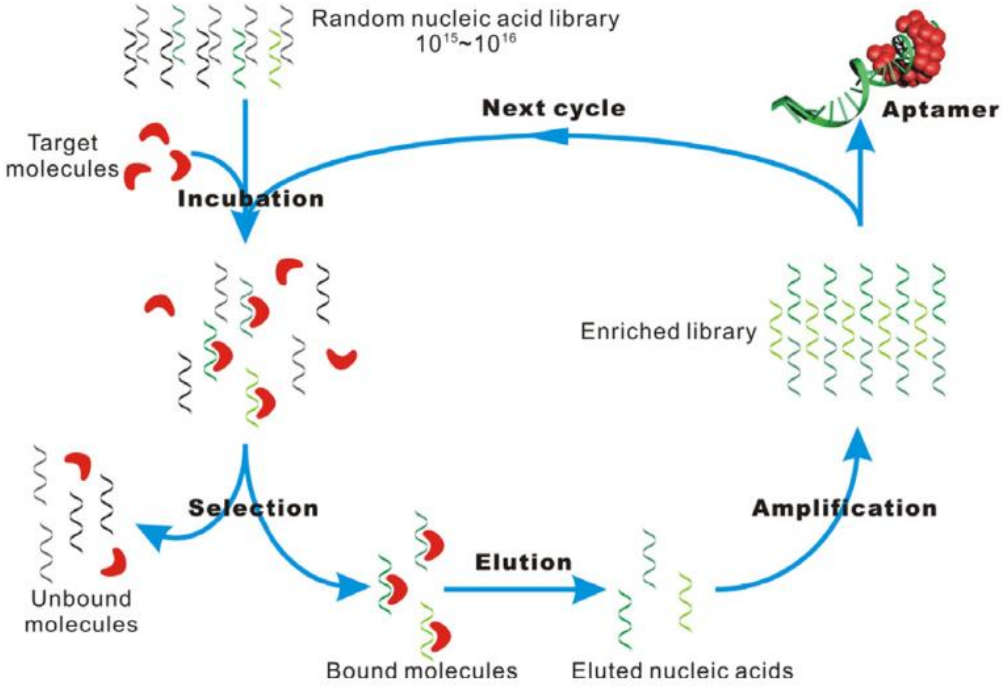

Figure 3.7 - Aptamer production cycle adapted from Song et al. (2008).

3.5.2. Antibodies versus Aptamers

Antibodies are proteins in blood plasma and other fluid located outside of cells that are created to fight off infections in the body and are part of a mammal's immune system (Lipman, Jackson, Trudel, & Weis-Garcia, 2005). Antibodies are the current standard by which molecules can be identified and are used over a wide range of applications (Jayasena, 1999). As a result, antibodies have become the basis for many disease identification tests. Aptamers, the synthetic cousin of antibodies has many of the same applications as antibodies and both have limitations and advantages. Table 3.2 gives a summary on these advantages and limitations.

Table 3.2 – Advantages and limitations of antibodies and aptamers (Jayasena, 1999; Kedzierski et al., 2012; Keefe, Pai, & Ellington, 2010; Ni et al., 2011; Pendergrast, Marsh, Grate, Healy, & Stanton, 2005; Vermeer & Norde, 2000).

	Antibodies	**Aptamers**
Advantages	-Pharmacokinetic properties of antibodies are good for the human body -Large size prevents renal filtration that can extended circulating half-lives -Not susceptible to nuclease degradation -High specificity to the target organism/molecule -The technology is readily available because no intellectual property claims are valid - Widely used as a bio-recognition agent	-Produced chemically in a readily scalable process -The chemical process involved in production is not prone to bacterial contamination -Non-immunogenic -Smaller size allows for easy entry into biological compartments -High specificity to the target organism/molecule -Can usually be reversibly denatured -Dyes or functional groups can be easily added during synthesis - Stable shelf life (> one year at room temperature)
Limitations	-Difficult to scale up without product variability because it is produced biologically -Prone to viral or bacterial contamination -Can be immunogenic -Large size limits bioavailability -Limited specific targeting of cell parts -Susceptible to irreversible denaturation; limited shelf life -Attachment of dyes or functional groups can reduce effectiveness -Can have some thermal instability	-Pharmacokinetic properties can be variable -Small size makes them susceptible to bodily filtration and a shorter half-life -Unmodified aptamers are highly susceptible to serum degradation -The technology is currently an intellectual property

Even with these limitations, aptamers have the potential to overcome these problems by, for example, adding conjugates to increase the half-life and optimizing the material that holds the aptamer to protect it from degradation (Keefe et al., 2010).

3.5.3. Applications

One of the most common applications for aptamers is its use in biosensors (Kedzierski et al., 2012). Aptamers are better than other receptors such as antibodies and enzymes for a number of reasons. First, because of their ability to be highly specific towards a range of biological materials, such as small molecules to even whole cells and second, due to the aptamers high specificity towards only one target, this also means that the biosensor is highly selective. A biosensor that is highly selective means that you can use the biosensor with a sample that has many different types of pathogens or interferents molecules in it and not have to worry about interference in your readings from the other pathogens or molecules. Lastly, aptamers can be made in a synthesized process that will be consistent and chemically stable unlike an antibody (Song et al., 2008).

There are many examples of aptamers used in biosensors to detect pathogens (Shahdost-fard et al., 2013; Singh et al., 2012; Wu et al., 2012). Many of these studies used aptamers in combination with some kind of composite to their structure to improve the sensitivity of the aptasensor by increasing the surface area of the biosensor and in turn, increasing the amount of aptamers that could be loaded onto the surface (Shahdost-fard et al., 2013; Singh et al., 2012; Wu et al., 2012). An example would be of the biosensor developed by Duan et al.(2015) that attached *Vibrio parahaemolyticus*,

and *Salmonella* Typhimurium aptamers onto quantum dots and carbon nanoparticles to simultaneously detect both pathogens using dual fluorescence resonance energy transfer (FRET). The sensor had a limit of detection at 25 CFU/mL for *V. parahaemolyticus* and 35 CFU/mL for *S.* Typhimurium with a range of detection from 50 to 10^6 CFU/mL. Another example comes from Khezrian et al. (2013) that attached human immunoglobulin E aptamers onto a multiwalled carbon nanotubes/ionic liquid/chitosan nanocomposite surface to detect the immunoglobulin using the impedance method for detection. The sensor had a limit of detection of 37 pM with a range of detection from 0.5 to 30 nM. This is just a few of many aptamer based biosensors that have been reported (Hamula et al., 2011; Torres-Chavolla & Alocilja, 2009; Velusamy et al., 2010).

3.6. *Listeria*

Listeria monocytogenes is a gram-positive psychrotroph bacteria that has caused numerous outbreaks of illness and death over the years (Farber & Peterkin, 1991). The infection usually affects those with weak immune systems such as the elderly, newborns and pregnant women. It has even been estimated that some 1600 illnesses and 260 deaths from *L. monocytogenes* occur annually in the United States alone (CDC, 2015). The infective dose of *L. monocytogenes* is undetermined likely due to variations within strains, the complexity of the food matrix that the pathogen is in and the host that has been infected. However, it has been reported in cases of raw food products that fewer than 1,000 cells may be all that is needed to cause the illness in individuals that are susceptible (USDA, 2012). The CDC (2015) reports common symptoms of a person that

has contracted listeriosis as having a fever, muscles aches, diarrhea or some other kind of gastrointestinal problems. Digestive problems caused by *L. monocytogenes* can crop up in as short as a few hours to a few days leading to hospitalization and death. However, the serious form of the infection can stay in incubation in the body for up to 3 months and cases like this have been known to cause septicemia and meningitis (USDA, 2012). Some food products that have had a *Listeria*'s outbreak include a number of cheese and dairy products, prepackaged caramel apples, cantaloupes and the most recent outbreak involving Blue Bell Creameries Ice Cream (CDC, 2015). Potential sources of contamination for *Listeria* entry into food are raw food materials, food handlers, incoming air and the food processing environment itself. The largest of these threats being after the food is processed and it comes in contact with other surfaces (USDA, 2012). Because of the severity with which the infection can take hold in a person and it's prevalence to be spread onto food products that have a short shelf life, it is important to find methods of detection that are faster than the most popular method, i.e.; culturing the bacteria from samples; so real-time PCR and biosensors have become an area of research for the detection of these bacteria (Cheng et al., 2014; Eun Jeong et al., 2014).

The government has taken steps to improve food safety such as the Food Safety and Modernization Act (FSMA), which will come into effect in 2016, which allows the FDA to ensure a higher level of public health by focusing more on preventing food pathogen outbreaks instead of just reacting to problems after they take place. The FDA is using legislative mandates to make comprehensive, science-based preventive controls compulsory for all food products. These mandates require the food industry to develop

plans to identify and monitor areas in food production that pose potential hazards (FDA, 2015). A strong government effort to pass such a law only reinforces the need for real-time pathogen detection methods that can be used as a preventive measure to catch contaminated food products before they reach the public.

The current industry recommendations from the FDA suggest testing critical food contact surfaces at least once a week and for critical non-food-contact surfaces, at least once every two weeks. As it pertains to ready-to-eat food products, which are more susceptible to contamination, the FDA recommends that if a food that supports the growth of *Listeria* contains greater than or equal to 0.04 CFU of *L. monocytogenes* per gram of food product trigger corrective actions such as detaining, recalling or even destroying potentially contaminated food. Non-*Listeria* growth supporting foods have a less stringent recommendation of 100 CFU per gram of food and similar corrective actions (FDA, 2008). The number of samples that should be tested per lot is contingent upon the level of percent positives a company wants to ensure for, an outline of the possible samples is shown below in Table 3.3 (Kornacki, 2005). However, a review by Tompkin (2002) found for most food processes that have a step to kill *Listeria*, like cooking, the chances of contamination can drop to below half a percent. This means that it would be very impractical for most companies to test enough samples so that a high confidence of detecting contaminated lots based on the low incidences of contaminants.

Table 3.3 – Relationship between incidence of microbial contamination and potential for recovery, adapted from Kornacki (2005).

Test Number Needed to Detect One or More Positives per Lot			
Percent Positives	Number of Analytical Units to Be tested (n)		
% Positive	90% Confidence	95% Confidence	99% Confidence
100	3	4	4
10	23	30	46
1	230	299	461
0.1	2303	2996	4605
0.01	23026	29963	46052

3.7. Methods of Bacteria Detection

The food industry has to maintain a high standard of safety since their products can directly affect the health and safety of its consumers. Accordingly, a number of methods have been developed over the years to test products for bacterial contamination. The traditional method for bacteria detection is the plate count technique. Where the sample is liquefied, filtered and diluted before being spread over growth medium. The medium is then left to sit for 24 to 72 hours in an incubator to allow for bacteria colonies to form. Then, the colonies are counted and any dilutions made are accounted to find the original bacteria concentration. The whole procedure can take up to a week to report final results (Bajwa, Tan, Bahreyni, & Mehta, 2013). The advantage of this technique is its simplicity and ability to distinguish viable cells. However, the disadvantages include time required to run the test, high detection limit requiring pre-enrichment steps for microorganism detection, as well as the tests specificity since regular media such as tryptic soy agar will not discriminate between different kinds of bacteria. However,

more selective agars, like Oxford Listeria agar can be used to hinder the growth of unwanted bacteria (USDA, 2012).

Newer techniques for bacteria detection in food include quantitative polymerase chain reaction (PCR) and enzyme-linked immunosorbent assay (ELISA). Quantitative PCR allows for the collection of data in real time as the test is being completed unlike the normal PCR, which would only give the amount of material collected at the end of the test. This is done by monitoring the fluorescence signal that is given off from the target nucleic acids. For the first few cycles in the process there will be little change in the fluorescence and as the target nucleic acids begin to attach the fluorescence output will increase (ThermoFisher, 2014). The ELISA procedure first starts with the coating of a capture antibody into microplate wells. The test samples are then incubated in the microplate wells to allow any antigen proteins (i.e., target analyte) to attach to the antibodies. A second antibody used for protein detection is then introduced and incubated; next a horseradish peroxidase enzyme conjugate is added to bind to the detection antibody. After a third incubation a substrate solution is used to change the enzyme into a color signal that will be directly proportional to the amount of target analytic in the test sample (ThermoFisher, 2015). Modern molecular methods like PCR and ELISA have the advantages over plate counting because they can test more than one sample at a time, are quicker to run and often allow for very specific pathogen detection. However, both techniques have some disadvantages such as the specificity can still result in detecting pathogens that are close in relation, both cannot distinguish between

living and dead pathogen cells and both techniques require a technical professional and costly reagents and equipment to run the tests (Lum, 2014).

Many food companies still use the standard plate counting technique which can lead to delayed notification about contaminated products and government agencies use PCR to confirm an outbreak using the genetic code of a microorganism; however, it cannot distinguish bacteria from live or dead. If biosensors can be designed to detect pathogens with the same specificity and reliability as plate counting, there is an opportunity to speed up the notification time about contaminated products and in turn save lives. As seen in Table 3.4, there are a number of advantages to biosensors over other methods of detection, with few downsides, so more research into this area needs to be conducted.

Table 3.4 - Advantages and disadvantages of bacteria detection methods (Abubakar et al., 2007; Bakthavathsalam, Rajendran, Saran, Chatterjee, & Jaffar Ali, 2013; Daniels & Pourmand, 2007; Kärkkäinen et al., 2011; Yoon & Kim, 2012).

Detection Method	Advantage	Disadvantage
Plate Counting	-Accurate -Inexpensive - Viable cells are counted	-Need a trained technician and specific laboratory for analysis -Time consuming (5-7 days) -Pre-enrichment step needed for detection - High detection limit
ELISA	-Short Test Time	-Low specificity compared to plate count method and PCR -Multiple reagent steps - Limited reagents shelf-life - Expensive -Need a trained technician for analysis -Cannot distinguish between live and dead cells
PCR	-More accurate than plate counting and ELISA	-Requires 10-20 hours for complete analysis -Expensive -Need a trained technician for analysis - Cannot distinguish between live and dead cells
Real-time PCR	-Faster than PCR	-Expensive -Need a trained technician for analysis - Cannot distinguish between live and dead cells
Biosensors	-Quick Test Time -Easy to miniaturize -Can have label-free operation -Low detection limit -Easy to operate and analyze	-Specificity depending upon bio-recognition agent - Reproducibility - Limited shelf-life

CHAPTER IV

MATERIALS AND METHODS

4.1. Materials

Chloroplatinic acid, 11-mercaptoundecanoic acid (11-MUA), chitosan (Medium molecular weight, 75-85% deacetylated, 200-800 cP), buffered peptone water (BPW) and lead acetate were purchased from Sigma Aldrich (St. Louis, MO). The platinum/iridium (Pt/Ir) electrodes, reference electrode (Ag/AgCl) and Pt auxiliary electrode were purchased from BASinc. (West Lafayette, IN). Glutaraldehyde, 25% (w/w) aqueous solution, and single layer graphene oxide were purchased from ACS Materials (Medford, MA). The *Listeria* aptamers that target Internalin A (47 DNA bases, $K_d = 10^3$ CFU/mL, 14811.63 g/mole) were purchased from Genelink (Hawthorne, NY). MES (2-[morpholino]ethanesulfonic acid), NHS (N-hydroxysuccinimide) and potassium nitrate were purchased from Alfa Aesar (St. Louis, MO). Sodium chloride and potassium chloride were purchased from EM Science (Darmstadt, Germany), EDC (1-ethyl-3-[3-dimethylaminopropyl]carbodiimide) were purchased from ThermoScientific (Waltham, MA) and potassium ferrocyanide were purchased from Ward's Science (Rochester, NY). Tryptose phosphate broth (TPB) were purchased from HiMedia (Mumbai, India) and the tryptic soy broth (TSB) were bought from Becton, Dickson and Company (Sparks, MD). Petrifilm-Rapid Aerobic Count Plates were purchased from 3M (St. Paul, MN). Finally, potassium phosphate monobasic was purchased from Fisher chemicals (Pittsburg, PA).

4.2. Electrode Preparation

4.2.1. Electrode Schematic

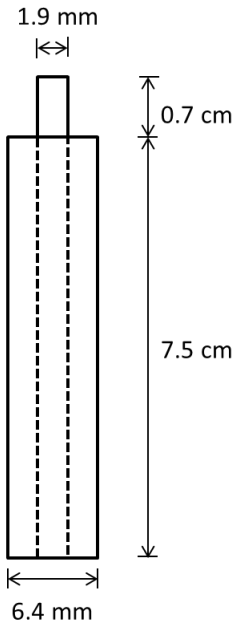

Figure 4.1 – Schematic of working (Pt/Ir) electrode.

The electrode used for all testing was purchased from BASinc. (West Lafayette, IN). The actual working surface that each biosensor platform was attached onto was on 1.9 mm in diameter platinum/iridium (Pt/Ir) (Figure 4.1).

4.2.2. Electrode Cleaning

Pt/Ir electrodes were cleaned using the methodology outlined by the electrodes' manufacturer. Briefly, electrodes were first rinsed with water and methanol to wash away any adhered material on the surface and then gently wiped dry. A white nylon disk (BASinc. West Lafayette, IN) was rinsed with distilled water and then three drops of a 1 μm diamond polish solution were placed on evenly onto the disk. The electrode was

then placed face down on the disk and moved in a figure eight pattern for 1 minute in each figure eight direction. Next, the electrode was washed with methanol to remove any remaining grit. A micro cloth disk (BASinc. West Lafayette, IN) was then wetted with distilled water and 3 drops of alumina polish were evenly added to the pad surface. The electrode was then polished again using the same figure eight pattern as before. Lastly, the electrode was rinsed with water, then methanol and gently dried.

4.3. Solutions Preparation

4.3.1. Phosphate-Buffered Saline (PBS) Solution

The PBS solution were made using 0.2 g of potassium chloride, 8 g of sodium chloride, 1.44 g of disodium phosphate and 0.24 g of monopotassium phosphate, dissolved in 1 L of distilled water and adjusted to pH 7.2 (FSIS, 2013).

4.3.2. Aptamer Storage Solution

Tris-EDTA buffer was made using a 10mM Tris and 1 mM EDTA that was adjusted to pH 7.5 using a 5 M NaOH solution (Genelink, 2004).

4.3.3. Antibody Storage Solution

Distilled water (0.5 mL) was added to the antibody vial. The vial was rotated until the lyophilized pellet was completely dissolved. Then, 0.5 mL of glycerol was added to the antibody vial and the solution was pipetted up and down several times to thoroughly mix. Prior to use, the desired concentrations were reached using PBS and was used immediately (KPL). The solution was stored at 5°C.

4.4. PGP Coating Procedure

4.4.1. First Platinum Layer Attachment

A plating solution that contained 1.44% (w/w) chloroplatinic acid and 0.002% (w/w) lead acetate in distilled water were prepared and then Pt nanoparticles were deposited on a Pt/Ir electrode using 10 V (constant potential) for 90 s (Figure 4.2) using a BK Precision single output, programmable DC power supply (Yorba Linda, CA) following the procedure previously described by (Vanegas et al., 2014).

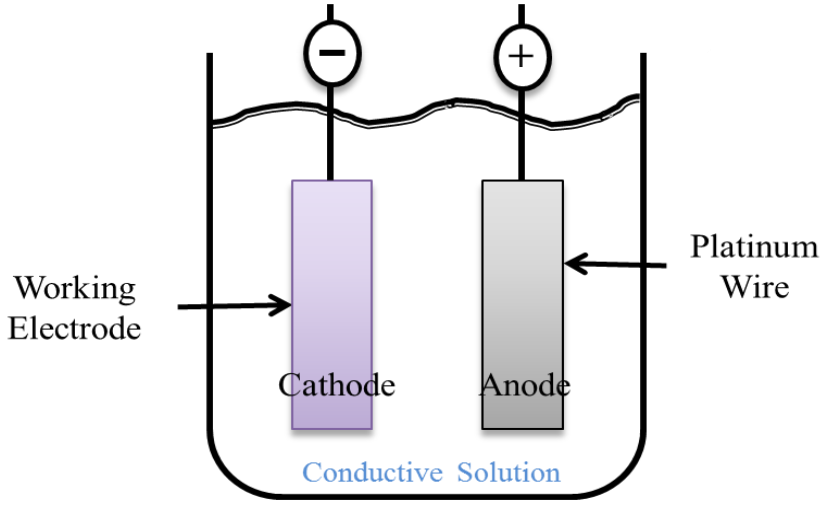

Figure 4.2 – Schematic of electrodeposition of platinum onto electrode surface.

4.4.2. Reduced Graphene Oxide Suspension Preparation and Attachment

A graphene oxide solution was prepared using graphene oxide in distilled water at a 2 mg/ml concentration and then ultra-sonicated for 30 minutes at 40% power (40 Watts) and 90% pulsing time, with a titanium micro tip and a UP400S Ultrasonic Processor (400 Watts, 24 kHz) (Hielscher, Inc., Ringwood, NJ). Then, 500 µL of the graphene oxide solution were agitated for 5 minutes with 2 mg of ascorbic acid to

produce reduced graphene (GOx). Next, 2 μL of this solution were drop coated on to the electrode surface. Electrodes will then be dried for 1 min at room temperature and 30 s under hot air using a blow dryer (Style by Revlon 1875 Watt dryer, New York, NY) before being spin coated for 30 s at 1700 rpm and 1 min at 3500 rpm (Burrs et al., 2015). The spin coater was built using a Benchtop Router Table with 1-3/4 HP Router and a Router Speed Control Dial from Harbor Freight (Calabasas, CA).

4.4.3. Second Platinum Layer Attachment

The second layer of Pt was adhered onto the Pt-GOx composite electrode using the same plating solution (Figure 4.2) as procedure 4.4.1 at 10 V for 30 s (Vanegas et al., 2014). This PGP coating was the platform for all of the biosensors tested in this study.

4.5. Chitosan Nanobrushes Coating Procedure

First, one gram of chitosan was mixed in 100 mL of distilled water. The solution's pH was then lowered to below 5 using a 2.5 M HCl solution and mixed further. Next, the chitosan was adhered to the PGP surface via electrodeposition. The PGP coated electrode was placed in 10 mL of the chitosan solution where electrodeposition at 3V for 5 minutes using a BK Precision single output, programmable DC power supply (Yorba Linda, CA) was applied producing chitosan (CHT) nanobrushes (Luo, Xu, Du, & Chen, 2004). The electrodeposition set-up was the same as seen in Figure 4.2, with the exception that the chitosan solution was used instead of the conductive solution used in 4.4.1.

4.6. Aptamer Biosensor

4.6.1. Aptamer Design

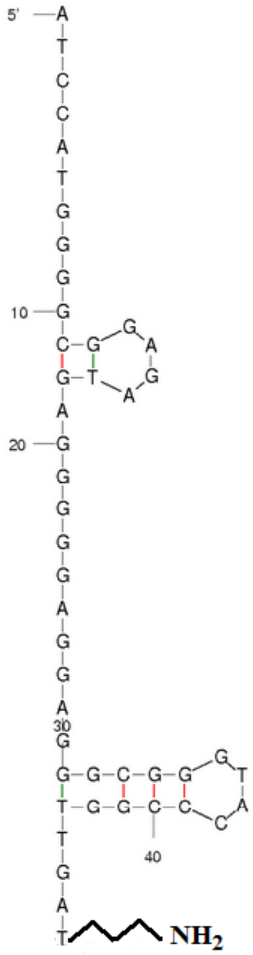

Figure 4.3 - Structure of the *Listeria monocytogenes* aptamers with amine ending modified from Aptagen (2015).

Synthesized aptamers, seen in Figure 4.3, were purchased from Gene Link Inc. (Hawthorne, NY) that is inherent to the strain of *Listeria* serotype *monocytogenes*. The aptamers have also shown a proclivity for attachment to the strain *Listeria innocua* in preliminary testing. This is likely because the aptamers are specially designed to detect

protein internalin A, which can be found in both strains (Ohk, Koo, Sen, Yamamoto, & Bhunia, 2010). The aptamers were specially designed with an amine functional group, as seen in Figure 4.3, at the termination site of the aptamer to allow for covalent bonding with the carboxyl functional group on the linking compound (i.e., chitosan or 11-MUA). The same aptamers with a thiol functional end group were also used for testing on the PGP coating.

4.6.2. Aptamer Attachment onto a PGP Surface

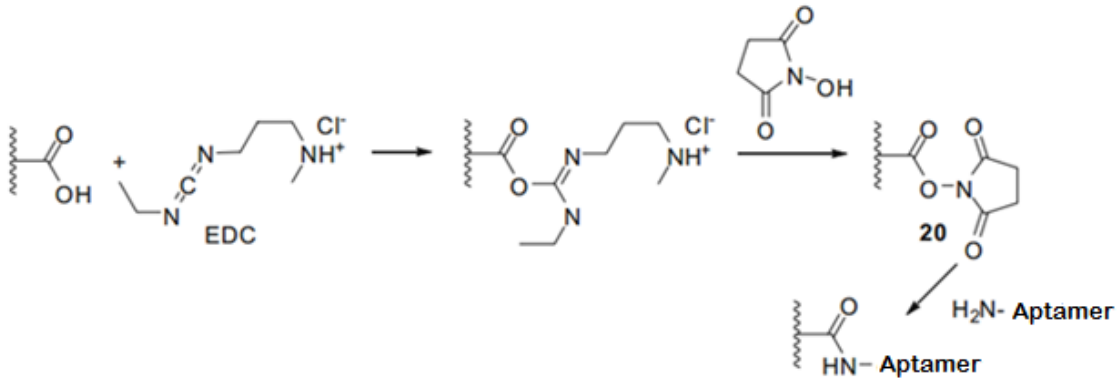

Figure 4.4 - Chemical process for attachment of amine ended aptamers onto PGP electrode via the chemical linkers, EDC and NHS modified from Balamurugan et al. (2008).

To attach the aptamer to the PGP coated sensor, the electrode surface must first be prepared with a SAM composed of 11-MUA. First, a solution of 131 mg of 11-MUA in 4 mL of ethanol were prepared. The PGP-coated electrode were placed in 500 µL of this solution and reacted for 30 minutes at room temperature. Next, 1.6 mg of EDC were added directly to 4 mL of a 10 mM phosphate buffer solution (PBS, pH 7.2). Then, 2.4 mg of NHS were added to the solution and mixed. The complete EDC/NHS reaction

can be seen in Fig. 4.4. The electrode was then placed in 500 μL of the EDC/NHS solution for 2 hours at room temperature under agitation (Jantra et al., 2011). Amine terminated aptamers were rehydrated using aptamer storage solution based on the nmols of aptamers to a concentration of 10 μM. Aptamers were further diluted in aptamer storage solution to the desired testing concentrations 100, 200 and 400 nM (Park, Baig, Lee, Moon, & Yoon, 2014; Taghdisi et al., 2015). Unused aptamers in solution were stored at -80^{o}C. Finally, the functionalized electrode was placed into the solution containing the hydrated aptamers and allowed to react for 2 h at room temperature under agitation. Finished electrodes were stored in the aptamer solution at 5^{o}C until further use.

Thiol terminated aptamers were rehydrated using aptamer storage solution based on the nmols of aptamers to a concentration of 10 μM. Aptamers were further diluted in aptamer storage solution to the desired testing concentrations 100, 200 and 400 nM (Park et al., 2014; Taghdisi et al., 2015). Thiol terminated aptamers solution (2 μL) were then drop coated onto the PGP surface and allowed to dry at room temperature for 30 minutes (Vanegas et al., 2014). Finished electrodes were stored in the aptamer solution at 5^{o}C until further use.

4.6.3. Aptamer Attachment onto a PGP-Chitosan Nanobrush Surface

Immobilization of the aptamers took place on the chitosan nanobrushes using the chemical linker glutaraldehyde. Glutaraldehyde contains aldehyde functional groups which can form bonds with materials that have amino functional groups as seen in Figure 4.5 (Balamurugan et al., 2008). Both the chitosan hydrogel and the aptamers are

composed of amino-terminated groups, making the choice to use glutaraldehyde a simple one.

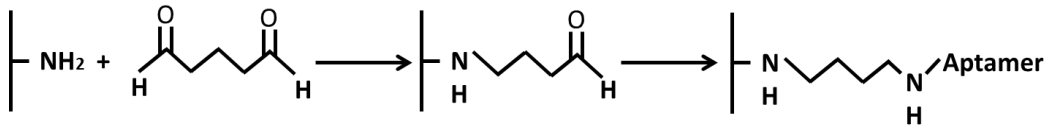

Figure 4.5 - Chemical process for attachment of aptamer onto chitosan hydrogel via the chemical linker, glutaraldehyde modified from Balamurugan et al. (2008).

A 10% w/v solution of glutaraldehyde was prepared and 500 μL of the solution was used for each chitosan coated electrode. The electrode sat in the solution for 2 hours at room temperature before the electrode was transferred to the aptamer solution for 2 hours. The aptamer concentrations were the same as the PGP + amine aptamers in section 4.6.2. The electrodes were stored in the aptamer solution at 5^{o}C.

4.7. Antibody Biosensors

PGP-antibody and PGP-CHT-antibody electrodes were prepared and tested for limit of detection, range and sensitivity using the exact same methodology and as the PGP + amine aptamer and PGP + CHT + aptamer electrodes as mentioned above (Section 4.6.2 and 4.6.3). The polyclonal goat based anti-*Listeria* antibodies used were purchased from KPL, Inc. (Gaithersburg, MA) and the concentrations tested were 50, 100 to 200 nM based on the literature (Cummins et al., 2014).

4.8. Experimental Design

4.8.1. Experimental Set-up

All electroactive surface area (ESA) and electrochemical impedance spectroscopy (EIS) tests were performed with a 3 electrode cell set up with a platinum working electrode, Ag/AgCl reference electrode and a platinum auxiliary electrode (Figure 4.6), using a potentiostat (CHI6044E) and software version 12.04 from CH Instruments (Austin, TX). The tests were all done in 20 mL of testing solution. Testing solutions varied depending upon the test being performed.

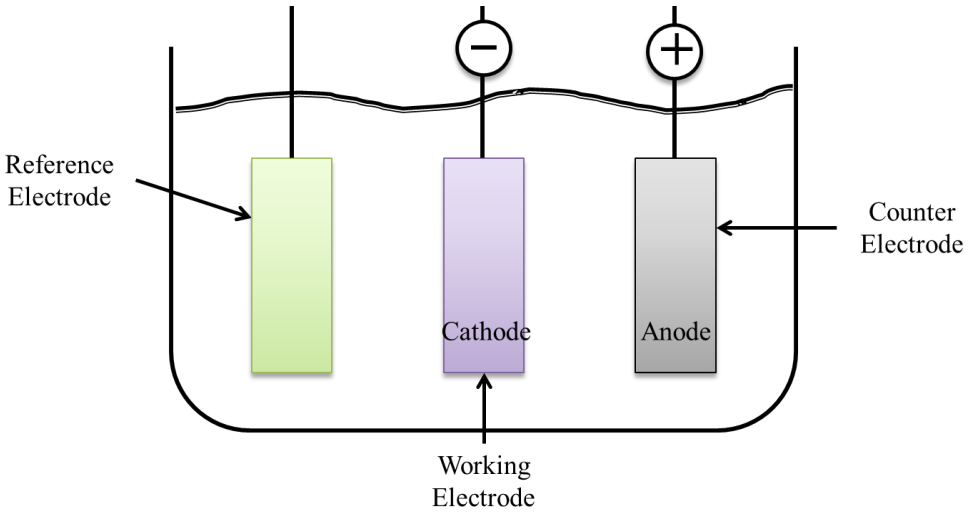

Figure 4.6 – Electrochemical set-up for all cyclic voltammetry (CV) and electrochemical impedance spectroscopy (EIS) testing in 20 mL of testing solution.

4.8.2. Capture Probe Loading

The tests were done in a 20 mL solution of 4 mM potassium ferricyanide trihydrate and 1 M potassium nitrate in distilled water. Cyclic voltammetry (CV) was performed using a sweep range of 650 mV with switching potential were used with a 30

second quite time. For effective surface area tests a range of scan rates from 50, 100, 150 to 200 mV/s were used.

Electrochemical impedance spectroscopy (EIS) was performed with the same 3 electrode cell set up as the CV testing. The tests were done in a 20 mL solution of 4 mM potassium ferricyanide trihydrate and 1 M potassium chloride in distilled water. An initial DC voltage of 0.25 V was applied to a frequency range of 1 Hz to 100 kHz with 100 mV AC amplitude.

4.8.3. Electroactive Surface Area (ESA) Analysis

The electroactive surface area was determined using the reduction current (i_p) peaks (Hamann, Hamnett, & Vielstich, 2007; Shi et al., 2012) from each scan rate and the Randles-Sevcik equation (4.1):

$$i_p = (2.69 \times 10^5) n^{3/2} D^{1/2} C A v^{1/2} \quad (4.1)$$

where n is the number of transferred electrons for the redox reaction, D is the diffusion coefficient (6.70×10^{-6} $cm^2 s^{-1}$), C is the molar concentration of ferricyanide trihydrate (4 mM), A is the effective surface area (cm^2), and v is the scan rate (Vs^{-1}). For cyclic voltammetry using $Fe(CN)_3^{-6}$, the value of n is equal to one, due to the following half reaction taking place at the electrode:

$$Fe(CN)_3^{-6} + e^- \rightarrow Fe(CN)_4^{-6} \quad (4.2)$$

By using equation (4.1), a well-established linear relationship is shown to exist between i_p and $v^{1/2}$. A linear regression for i_p versus $v^{1/2}$ was created and a slope k was obtained then, after manipulation of equation (4.1), A can be represented in equation (4.3) as:

$$A = k/((2.69 \times 10^5)n^{3/2}D^{1/2}C) \quad (4.3)$$

4.8.4. PGP + CHT+ 100 nM Aptamer Actuation Test

The PGP + CHT + 100 nM aptamer sensor was tested in two different pH testing solutions to determine which pH produced the highest ESA and also to examine if changing the pH multiple times affected the sensors ability to produce the same ESA at each pH. Two ESA testing solutions were prepared using the same CV testing solution ($Fe(CN)_3^{-6}/NO_3^-$) as in procedure 4.8.2, one at pH 5 and one at pH 7 using a 2.5 M HCl solution to lower the pH . The biosensor was placed in the pH 5 solution and tested using the normal CV testing procedure. After testing was finished the sensor was placed in the pH 7 testing solution and CV testing was completed. This process was then repeated and all the data collected for analysis.

4.8.5. Bacteria Cultures

L. innocua (ATCC 33090) and *L. monocytogenes* (ATCC 15313) were resuscitated in TPB, by two identical consecutive transfers and incubating for 24 hours aerobically at 35°C. Both *Listeria* strains were used to see if a general *Listeria* biosensor could be developed. *Staphylococcus aureus* (ATCC 25923) was resuscitated in TSB, by two identical consecutive transfers and incubating for 24 hours aerobically at 35°C. Cultures were maintained on tryptic soy agar (TSA) slants stored at 4°C for no more than 3 months. Transfers from slants were made similarly to the resuscitation method to prepare microorganisms for testing with the biosensor. The total aerobic plate counts were measured in triplicate. Samples of the bacteria were serially diluted in BPW and enumerated on petrifilms (3M aerobic plate count, St. Paul, MN). Petrifilms were

incubated for 48 hours at 35°C before counting the colony growth and the results were reported as CFU/mL of bacteria solution (AOAC, 1990b).

4.8.6. PGP + CHT + 100 nM aptamer Capture Efficiency Test

To determine the ideal testing conditions based on chitosan nanobrushes actuation, cyclic voltammetry (CV) was run on the biosensors under a number of conditions, as seen in Table 4.1, to determine the highest peak current (i_p) possible. The testing condition with the highest peak current meant that it had the highest electron transport and would therefore give the best sensitivity, selectivity, linear range, and detection limit. For each testing condition, 2 containers with 20 mL of PBS at pH 7 were prepared. If the testing condition required, the pH of the PBS was lowered to 5 using a 2.5 M HCl solution. Then, an aliquot of *Listeria innocua* was added until the concentration of *L. innocua* in the container equal 10^3 CFU/mL. The biosensor was first placed into one solution and left for 20 minutes before being transferred to the other solution container for CV testing.

Table 4.1 – Outline of pH testing conditions tested on PGP + CHT + 100 nM aptamer electrodes.

Testing Condition	**pH biosensor sits in**	**pH biosensor is tested in**
1	5	5
2	5	7
3	7	7
4	7	5

4.8.7. Biosensor Bacteria Loading Test

This test was conducted to observe the change in the voltage output of the biosensors, i.e., current peak and voltammagram's shape, as bacteria was attaching itself to the surface of the sensor. The aptamer and antibody attached biosensors (PGP+50 nM antibodies, PGP + 100 nM amine aptamers, PGP + 400 nM thiol aptamers and PGP + CHT + 100 nM aptamers) were immersed in a PBS solution with pH based on the results from section 3.8.6 with increasing concentrations, (from 10 to 10^7 CFU/mL) of the *Listeria innocua* suspension (*Listeria monocytogenes* was used for PGP + 400 nM thiol aptamers) for approximately 15 min, and then tested using cyclic voltammetry (CV) at a 100 mV/s scan rate. CV was performed using a sweep range of 650 mV with switching potential were used with a 30 second quite time.

4.8.8. Biosensor Testing

To determine the limit of detection, range and sensitivity of different biosensor platforms electrochemical impedance spectroscopy (EIS) analysis was employed with the same testing settings as for the capture probe loading in section 4.8.1 and 4.8.2. *L. innocua* and the electrodes were prepared the same as for CV testing using PBS at pH 7 as the testing solution for the PGP only electrodes. The PGP+CHT electrodes were tested on pH solutions based on the results from section 4.8.6.

Selectivity of the biosensor involved the use of the same previously used *L. innocua* strain, as well as *Staphylococcus aureus* (ATCC 25923). *S. aureus* was chosen because it was a Gram-positive bacteria readily available in the laboratory and comparable to *Listeria* which is also Gram-positive. The use of bacteria from the same Gram-staining provided a

comparable challenge to the biosensor in terms of selectivity. The procedure followed the same one used to find the sensitivity of the electrode as the set up described in the paragraph above, with the exception that *S. aureus* and *L. innocua* were both added at room temperature to the PBS at the same increasing concentrations from 10 to 10^7 CFU/mL. Similarly, pH values were adjusted based on the results from section 4.8.6.

4.8.9. Biosensor Testing in Vegetable Broth

Biosensors (PGP+CHT+100 nM amine terminated aptamers and PGP+CHT+200 nM antibodies) were tested in sterilized vegetable broth to determine the sensitivity, limit of detection and linear range of detection. The procedure followed the methodology outlined in section 4.8.8 with the exception that *L. monocytogenes* was used instead of *L. innocua*.

4.8.10. Sensitivity and Selectivity Analysis

Sensitivity and selectivity were found using EIS data. The imaginary impedance values were gathered at each bacteria concentration and a change in normalized impedance was found, as seen in Equation (4.4):

$$\Delta Z_N^{''} = \frac{Z_C^{''} - Z_0^{''}}{Z_0^{''}} \qquad (4.4)$$

where $\Delta Z_N^{''}$ (Ohms) is the change in normalized imaginary impedance, $Z_C^{''}$ (Ohms) is the imaginary impedance at the concentration being tested and $Z_0^{''}$ (Ohms) is the measured imaginary impedance when no bacteria is present in the testing solution. The impedance values were plotted taken over a range of frequencies at increasing bacteria concentrations, Bode (impedance versus frequency) and Nyquist (imaginary impedance

versus real impedance) plots, to analyze the total impedance response of the biosensor. The normalized impedance change for all of these concentrations were then compared to the baseline (no bacteria added) over the test frequency range to select the frequency which showed the greatest impedance difference between the increasing concentration of bacteria to the baseline. The frequency that had the greatest normalized changes in imaginary impedance with increasing bacteria concentration was then used for graphing the calibration curve (log imaginary impedance change versus log bacteria concentration). The logarithmic concentration (CFU/mL) of the bacteria was plotted against the corresponding logarithmic change in normalized imaginary impedance (Ohms) for the selected frequency. The sensitivity (dimensionless, log Ohms/log CFU/mL) of the biosensor was then determined based on the slope of the line from the plotted data (Varshney & Li, 2007). Selectivity was found in the same manner as the sensitivity under the presence of interferents, i.e., *Staphylococcus aureus* and vegetable broth.

4.8.11. Range of Detection Analysis

The range of detection was determined by plotting the logarithmic bacteria concentration versus the logarithmic normalized change in impedance. The range was determined to be the linear region of the plot (Cunningham, 1998).

4.8.12. Limit of Detection Analysis

The limit of detection (LOD) for each biosensor was estimated from equation (4.5):

$$LOD = \frac{3\sigma}{s} \qquad (4.5)$$

where the standard deviation (σ) is determined from repeated measurements of the normalized change in imaginary impedance in cell-free electrolytes (baseline), and the sensitivity (*s*) is determined in the same fashion as section, 4.8.10 (Radhakrishnan, Jahne, Rogers, & Suni, 2013).

4.9. Microscopic Analysis

Imaging of the surface of the PGP and PGP + Chitosan biosensors were done using a Quanta 600 FEG scanning electron microscope (SEM) from FEI (Hillsboro, Oregon) at the Texas A&M University Microscopy Imaging Center (College Station, TX). The SEM tests were performed at 25 V and 5000x and 10000x magnifications. The electrodes were first coated with a 10 nm layer of platinum using a Cressington sputter coater 208 HR (Watford, United Kingdom) before being examined to improve the conductivity of the electrodes surface. To get the coating on the electrode, the top plate of the sputter chamber was lifted off and the samples were placed on the base plate. The top plate was closed and the coater was turned on and switched to the thickness controller. The argon gas supply was opened and thickness monitor was zeroed. The thickness set point was established (10 nm). Once the pump indicated that it was ready then the "Cycle/stop" button was pressed to begin the coating process. After the desired height was reached, the coating stopped automatically. Electrodes were retrieved after the machine was switched off and allowed to ventilate (Cressingtion, 2015) prior to SEM imaging.

4.10. Statistical Analysis

A completely randomized design with equal replications was used in this study. All experiments were performed in triplicate as independent experiments and results were expressed as mean ± standard deviation. Data analysis was performed using SPSS software (version 21.0 for Windows). Differences between variables were tested for significance by one-way analysis of variance (ANOVA) and significantly different means ($p < 0.05$) were separated by the Tukey test.

CHAPTER V

RESULTS AND DISCUSSION

5.1. Actuation Test

The actuation test was performed to determine the electroactive surface areas (ESAs) at each pH 5 and 7 for future testing as well as to determine if the chitosan would degrade when the pH was changed multiple times. Representative CV curves at each pH change are shown in Figure 5.1. The ESA value for pH 5 was 0.0359 ± 0.0001 cm^2 and the value for pH 7 was 0.0478 ± 0.0169 cm^2, for each cycle respectively. The repetitions of the pH change showed no degradation of the nanobrushes as seen in Figure 5.2. This implies that the chitosan brushes have a reversible behavior and that they would have more than single use capabilities. The pH sensitivity of chitosan is derived from the presence of amino groups in the chitosan. When the chitosan is placed into an acidic solution the free hydrogens attach to the amino acids resulting in an osmotic swelling force. If the chitosan is then placed into a basic solution the cationic amino acids revert back to their regular form as the extra hydrogen atom is drawn towards the negatively charged OH groups present in the base solution, as this occurs, the chitosan collapses (Yao, 2012). This reversibility has also been noted in literature previously, for instance in the review by Yi et al. (2005). In their review they discuss how these different pH changes allow for different chemistries to be used to functionalize chitosan in different ways that can improve the materials components, like elasticity.

Figure 5.2 shows this concept from an electrical stand point. When the pH is 5, the material became swollen, increasing resistance to electrical flow in the system.

Conversely, when the pH was increased to 7 the chitosan shrank which allowed for easier flow. This means that pH 7 is the best pH to do all future electrochemical testing. The study by Burrs et al. (2015) came to a similar conclusion and only used chitosan at pH 7.1 for further testing. It could be hypothesized that this would also be the best condition for bacteria detection at pH 7 based on the nanobrushes response. Therefore, a further test was conducted to confirm that pH 7 was the best pH to do electrochemical detection involving bacteria.

Instances of chitosan shrinking and swelling have been noticed in other studies. Cui et al. (2014) for example, noted in their testing of chitosan/gelatin hydrogels that at both pH 1.2 and 7.4 the hydrogel swelled. When the hydrogel was submerged in pH 1.2, the swelling ratio was much larger when at pH 7.4 and as the chitosan content increased so did the swelling ratio. However, when the pH was at 7.4, the swelling ratio was much smaller and as the percent of chitosan increased, the swelling ratio decreased. Knowing this, it can be hypothesized that this swelling behavior will be good for capturing bacteria and a further test will be done to determine which pH will be best to let the bacteria attach to the surface and which pH will be best to do electrochemical tests.

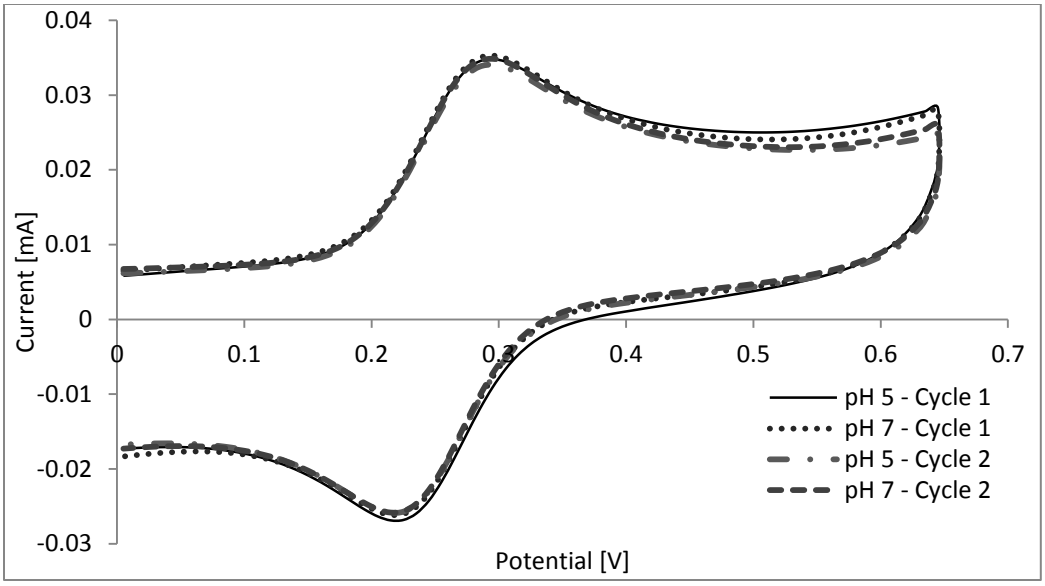

Figure 5.1 – CV curves of PGP + CHT coated electrodes in varying pHs, each test was repeated three times.

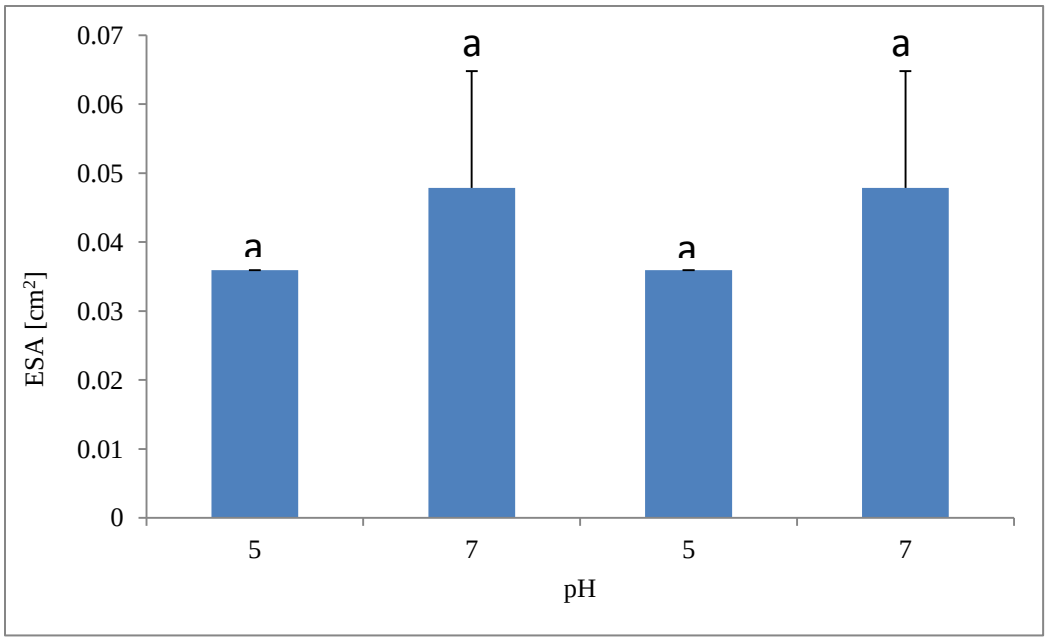

Figure 5.2 – ESA values of PGP + CHT coated electrodes in varying pHs over two cycles, each test was repeated three times. Error bars represent standard deviation for each test condition. [a,b]Means which are not followed by a common superscript letter are significantly different ($P < 0.05$).

5.2. Electroactive Surface Area (ESA)

Cyclic Voltammograms (CV) curves and Cottrell plots for all electrode treatments tested can be seen in the appendix (Figures A.1 thru A.36) with the full range of scan rates (50, 100, 150, 200 mV/s) tested for each coating and bio-recognition agent concentration. Each CV curve exhibited a response similar to a reversible couple with redox peaks and the PGP electrodes seen above, signifying that a diffusion controlled reaction as seen in Equation 5.3A, occurred at the electrode-solution interface where the diffusion layer was smaller than the surface area of the electrode (Hamann et al., 2007).

$$Fe(CN)_3^{-6} + e- \rightarrow Fe(CN)_4^{-6} \qquad (5.1)$$

A correlation coefficient (R^2) of 0.99 or higher was found for each linear regression of all the electrode treatments from the Cottrell plots, which was later used for electroactive surface area (ESA) calculations using the Randles-Sevick equation (Eq. 4.1). ESA values for all sensing platforms can be observed in Tables 5.1 and 5.2. A high ESA value implies good electron transfer on the surface of the sensor (Shao et al., 2010). The following sub-sections will compare all of the electrodes treatments to each other and to the literature.

5.2.1. Bare, PGP and PGP + Chitosan Coating Comparison

Figure 5.3A shows CV of bare, PGP, and PGP + Chitosan as representative cyclic voltammograms at a 100 mV/s scan rate. Each CV curve exhibited a response similar to a reversible couple with redox peaks, signifying that a diffusion controlled reaction was taking place at the interface of the electrode-solution (Burrs et al., 2015). Cottrell plots shown in Figure 5.3B were created to calculate the electroactive surface

area (ESA) of each modified electrode using the Randles-Sevick equation (Eq. 4.1). The surface area for bare electrode was found to be 0.0179 ± 0.0001 cm^2, when the PGP coating was applied to the electrode the surface area increased to 0.0236 ± 0.0039 cm^2. Compared to the basic PGP coating there is a significant increase in the surface area of the electrode when the chitosan was added, from 0.0236 ± 0.0039 cm^2 to 0.0305 ± 0.0017 cm^2.

When comparing ESA for all the PGP coating procedures with the literature, Shi et al. (2012) reported a smaller ESA value (6.0 ± 0.56 $x10^{-3}$ cm^2) than found in this research (0.0236 ± 0.0045 cm^2), whereas Vanegas et al. (2014) reported a higher ESA value (0.148 ± 0.064 cm^2). This is likely due to differences in PGP coating procedures. Shi et al. (2012) and Vanegas et al. (2014) both use the same electrodeposition procedure as this research, the main difference lies in the graphene addition. Shi et al. (2012) and Vanegas et al. (2014) both use a similar drop coating procedure; however, Shi et al. (2012) only allowed their electrodes to dry for 30 minutes and Vanegas et al. (2014) allowed their electrodes to be dried overnight before the final platinum coating was deposited, which could have influenced the amount of reduced graphene deposition. This research used a drop coating followed by a spin coating methodology that appears to have produced middle range reduced graphene deposition and consequently middle range ESA values.

When comparing ESA values for PGP + Chitosan coating procedures with the literature, Burrs et al. (2015) reported a higher ESA value (0.2 ± 0.06 cm^2) than in this study (0.0305 ± 0.0025 cm^2). This is likely due to differences in PGP and chitosan

coating synthesis procedures. In their study, the PGP coating was created by using sonoelectrodeposition to adhere nano-platinum on to the surface. Then a suspension of graphene oxide was reduced with ascorbic acid and ultrasonicated and 2 μL of the solution was spin coated for two cycles at 2621 rpm for 30 seconds, followed by 5738 rpm for 60 seconds. After spin coating, a second layer of nano-platinum was then applied using the same procedure as the first nano-platinum coating. This research used a drop coating and spin coating methodology for PGP coating. For the chitosan coating, Burrs et al. (2015) chose to make chitosan hydrogels and entrap the enzyme that they tested with into the hydrogel before spin coating over the PGP surface, while this research chose to use electrodeposition to attach chitosan to the PGP surface and used covalent binding in the form of EDC/NHS chemical reactions to attach the aptamers or antibodies.

When comparing these two methods of bio-recognition attachment it becomes apparent that the covalent binding technique used in this research has several advantages over the entrapment method. For instance, compared to entrapment techniques, covalent binding often produces a higher quality surface structure that increases the amount of bio-recognition agent that can attach to the surface of the electrode. Secondly, the bio-recognition agent is not embedded inside a hydrogel with less access to the target agent as with the entrapment method. Thirdly, covalently attached components tend to be more durable than entrapped components because they leach less from the reaction layer and overall tend to show more stability in the long term when tested under tough conditions such as stirring or washing (Cunningham, 1998). However, covalent binding has to be

controlled to avoid excessive or unwanted crosslinking, which could block or inactivate bio-recognition agents' active sites for target recognition. Excessive crosslinking could further causes polymers to over-crosslink hindering their desirable properties; i.e., electron conductivity, hydrophilicity, porosity, stimuli responsiveness (Sapsford et al., 2013). Ultimately, the differences in synthesis methods for these two studies reflected on the surface conductivity and consequently the ESA values observed. From the observed results, the PGP and PGP + Chitosan coatings were used to determine the best loading of bio-recognition agents and for future biosensor tests.

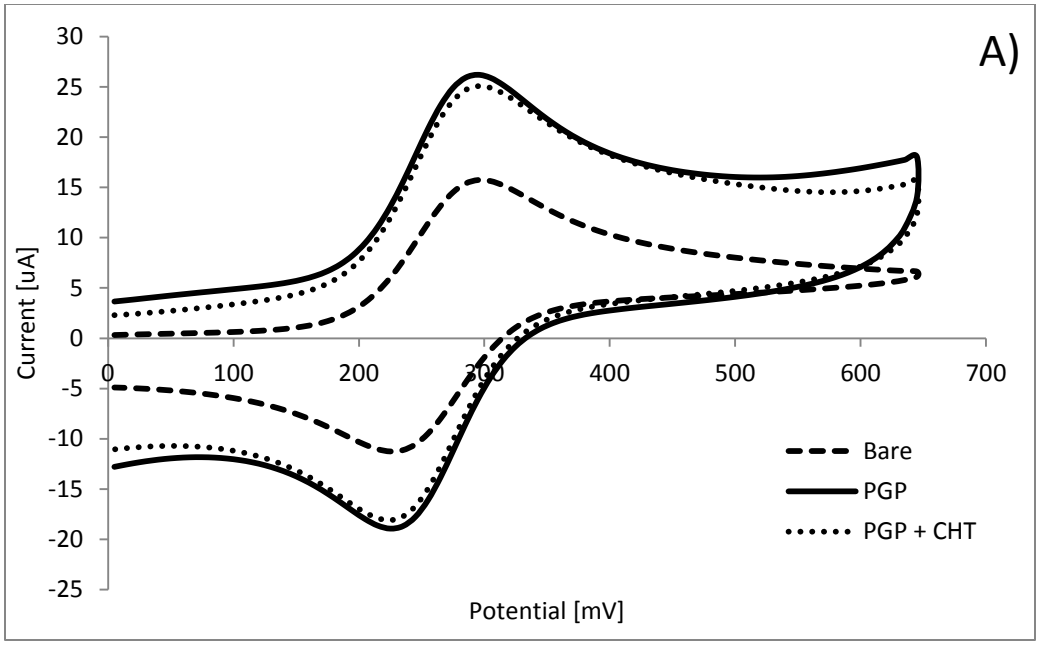

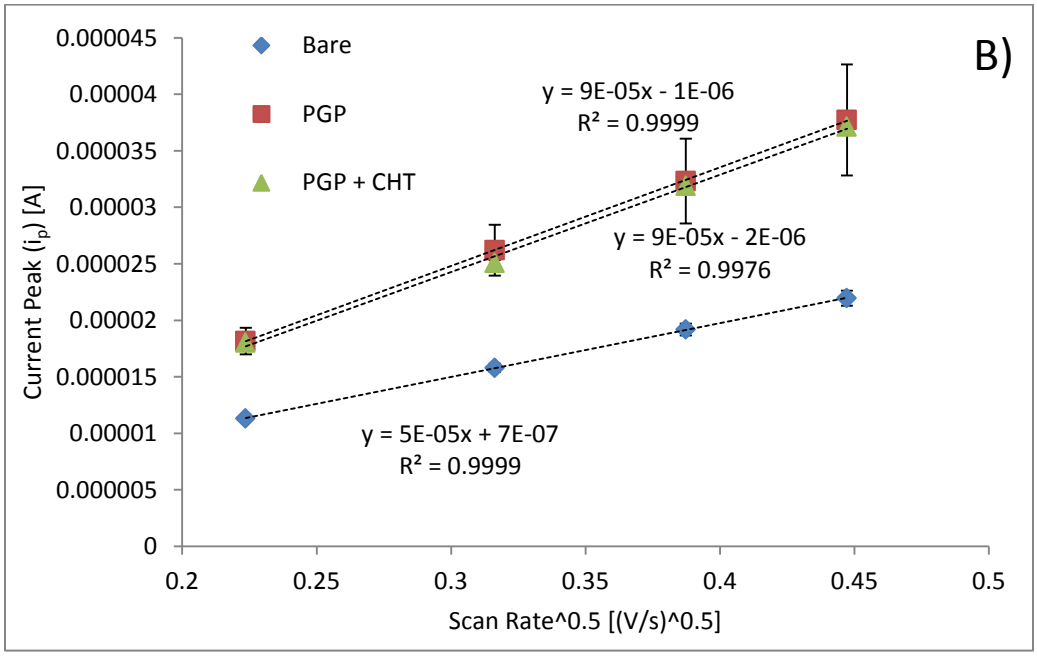

Figure 5.3 – A) Representative cyclic voltammograms of Bare, PGP and PGP + CHT electrodes in 4 mM $Fe(CN)_6$/1 M KNO_3 solution at 100 mV/s scan rates, each test was repeated three times. B) Characteristic Cottrell plot of Bare, PGP and PGP + CHT electrodes, each test was repeated three times. Error bars represent standard deviation for each test condition.

5.2.2. PGP with Different Aptamer Loading and Group Termination

Two PGP + aptamer sensors were created, each with a different group termination (thiol and amine) and different aptamer concentrations were tested to determine the best loading for each PGP + aptamer sensor. The highest electroactive surface area for the PGP + thiol aptamers was 0.0718 ± 0.029 cm^2 and occurred at the 400 nM aptamer concentration, which was about 4 times higher than the bare Pt/Ir electrode. The PGP + thiol aptamer electrodes also showed an incremental ESA increase as the aptamer concentration increased. As seen in Figure 5.2, the ESA values for the electrodes never decreased as the thiol aptamer concentrations increased indicating that the concentrations tested may not have been large enough to reach a saturation point for the aptamers on the electrodes surface. The highest electroactive surface area for the PGP + amine aptamers at 0.0478 ± 0.047 cm^2 and occurred at the 100 nM aptamer concentration, which was about 2.5 times higher than the bare Pt/Ir electrode. Electrode loading saturation may have occurred at the 400 nM concentration for the PGP + amine aptamer concentration as seen by the drop in ESA values (Figure 5.4).

Statistical analysis revealed that only the PGP + 400 nM thiol aptamer was statistically significant from the bare electrode and all other PGP + bio-recognition agent concentrations were not statistically different. Since there was no statistical significance between any PGP + aptamer based sensors, the sensor with the largest ESA value for each aptamer conjugation was chosen to use for future biosensor testing. The PGP + 400 nM thiol aptamer had the highest ESA so it could be hypothesized that the thiol

aptamers contributed more to the electrical conductivity of the electrode than when the PGP + amine aptamers were attached to the surface. A study by Fink and Schonenberger (1999) were the first to show that DNA strands had good electron conductive properties. They found that the resistivity values were comparable to those of conducting polymers, and indicate that DNA transports electrical current as efficiently as a good semiconductor. They also found that molecules attached to the DNA by a covalent bond such as with the PGP + amine aptamer could affect the electronic structure of the DNA and in turn, affect the conductivity of the DNA itself (Fink & Schonenberger, 1999). One reason for the higher ESA could be the way that the aptamers were attached to the biosensors surface. The amine aptamers were attached to the PGP coated sensor after the surface was prepared with a self-assembled monolayer (SAM) composed of 11-MUA, followed by EDC and NHS crosslinking reaction. A SAM had to be created to allow the amine terminated aptamers to attach to the PGP surface since an amine ended would not attach to the surface on its own like the thiol aptamers would. It has been shown in the literature that SAMs can affect the ESA value of electrode surfaces. Claussen, Wickner, Fisher, and Porterfield (2011) conducted a study using alkane-thiol self-assembled monolayers with glucose sensing enzymes which concluded that increasing the length of the SAM can decrease ESA values, the sensitivity of the device, as well as alter the limit of detection and shift the linear region of detection up to higher concentrations.

For the amine terminated aptamers loading multiple solution transfers were required for functionalization including 11-MUA deposition, EDC/NHS activation

(Jantra et al., 2011), and aptamer attachment and each step was a 2 h process. While for the thiol terminated aptamers, a solution of aptamer was drop coated onto the PGP surface and allowed to dry at room temperature for 30 minutes (Vanegas et al., 2014). Since the PGP electrodes had to be placed in different solutions to attach the amine aptamers, some of the graphene on the electrode, which is water soluble, could have fallen off while sitting in the solution. This would have reduced the conductivity on the surface of the electrode and in turn, lower the resulting ESA values for the PGP + amine aptamer electrodes. The study by Taghdisi et al. (2015) used a series of increasing concentrations of aptamer (0, 10, 25, 50, 100, 200, 500, and 1500nM) to detect insulin. Their results showed that the best concentration of insulin binding aptamers for the rest of their tests was 200 nM. Their aptamer loading results were then taken into consideration for this study's aptamer loading tests. Ohk et al. (2010) created the aptamers used in this study. In their work, they made an antibody/aptamer biosensor that used a 337.5 nM concentration of aptamers for their testing.

5.2.3. PGP with Antibody Loading

A PGP + antibody sensor was created with polyclonal goat based anti-*Listeria* antibodies and different antibody concentrations were tested to determine the best loading. The highest electroactive surface area for the PGP + antibodies was 0.0359 ± 0.0001 cm^2 and occurred at the 50 nM antibody concentration, which was about 2 times higher than the bare Pt/Ir electrode. Statistical analysis revealed that no PGP + antibody concentrations were statistically significant from one another so the largest ESA value was chosen to use for future biosensor testing. The PGP + antibody sensors were

created using the exact same methodology as the PGP + amine aptamer electrodes (Section 4.6.2) and the concentrations tested were 50, 100 to 200 nM based on the literature (Cummins et al., 2014). Cummins et al. (2014) used a 100 nM concentration of monoclonal antibodies to detect Ricin using surface plasmon resonance (SPR) measurements. Electrode loading saturation may have occurred at the 100 nM and 200 nM concentrations (Figure 5.4) for the PGP + antibody as seen by the drop in ESA values. Since the PGP + antibody and PGP + amine aptamer electrodes used the same attachment technique a close comparison between the two should be made. Statistical analysis revealed that there was no significant difference between the two bio-recognition agents on ESA values. However, it should be noted that the aptamer sensors had larger ESA values over all its concentrations, than the highest antibody concentrations (100 nM and 200 nM) for the antibody sensors, only the 50 nM antibody had an ESA value in the range of the aptamer sensors. The antibodies also have a larger molecular weight of 160,000 g/mole (KPL) than the aptamers which have a molecular weight of 14,811.63 g/mole (Aptagen). Implying that more of the aptamers were able to load onto the surface of the electrode because of their small size and in turn have higher ESA values than the antibody electrodes and potentially higher sensor sensitivity.

Table 5.1 - Average electroactive surface areas of electrodes with PGP coatings loaded at different concentrations of bio-recognition agents.

Electrode	ESA [cm^2]
Bare	0.0179 ± 0.0001^{a}
PGP	$0.0236 \pm 0.0045^{a,b}$
PGP+100 nM amine Aptamers	$0.0478 \pm 0.0207^{a,b}$
PGP+200 nM amine Aptamers	$0.0478 \pm 0.0207^{a,b}$
PGP+400 nM amine Aptamers	$0.0335 \pm 0.002^{a,b}$
PGP + 100 nM thiol Aptamers	$0.0478 \pm 0.0207^{a,b}$
PGP + 200 nM thiol Aptamers	$0.0478 \pm 0.0207^{a,b}$
PGP + 400 nM thiol Aptamers	0.0718 ± 0.0359^{b}
PGP+50 nM Antibodies	$0.0359 \pm 0.0001^{a,b}$
PGP+100 nM Antibodies	$0.0311 \pm 0.0021^{a,b}$
PGP+200 nM Antibodies	$0.0323 \pm 0.0036^{a,b}$

^{a,b}Means within a column which are not followed by a common superscript letter are significantly different ($P < 0.05$). Each test was repeated three times.

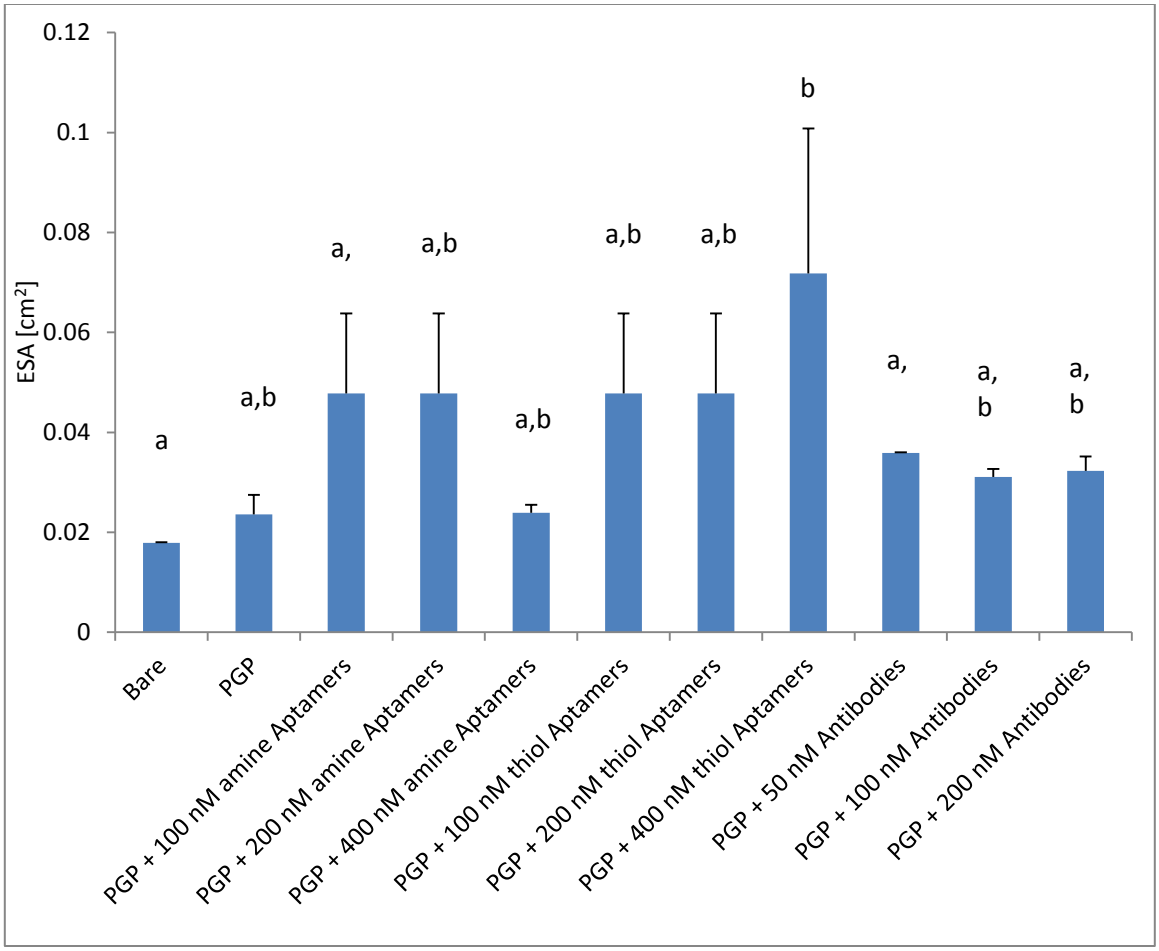

Figure 5.4 – Comparison between PGP electroactive surface areas at various bio-recognition agent concentrations, each test was repeated three times. Error bars represent standard deviation for each test condition. [a,b]Means which are not followed by a common superscript letter are significantly different ($P < 0.05$).

5.2.4. PGP + Chitosan Aptamer Loading

A PGP + CHT + aptamer sensor was created using the amine terminated aptamers and different aptamer concentrations were tested to determine the best loading. Amine aptamers were chosen for further testing with the PGP + CHT electrodes because of its ability to readily bind to the chitosan via glutaraldehyde crosslinking reaction (amine-amine binding) (Balamurugan et al., 2008), unlike the thiol ended aptamers. The

three concentrations tested were the same as for the PGP + aptamer loading tests to determine if a notable increase would take place in aptamer attachment in comparison to the PGP + aptamer electrode.

The addition of 100 nM concentration amine ended aptamer bio-recognition agents further increased the ESA to 0.0335 ± 0.0033 cm^2 (Figure 5.3). This was also found to be the highest ESA for the PGP+CHT coatings tested. Statistical analysis revealed that no PGP + CHT + aptamer concentrations were statistically significant from one another so the largest ESA value was chosen to use for sensitivity testing. Further statistical analysis also showed that the PGP + CHT + aptamer electrodes did not have significantly different ESA values to the PGP + amine aptamer counter parts. However, it should be noted that the PGP + aptamer sensors had larger ESA values for the 100 nM and 200 nM concentrations, than the highest ESA value for the PGP + CHT + aptamer sensors, though not statistically significant. One possible reason that the PGP + CHT + aptamer sensors had lower ESA values could have to do with the chemistry used to attach the aptamers to each platform. As discussed above, the PGP + amine aptamers used the SAM method of attachment with EDC/NHS crosslinking chemistry (carbonyl-amine binding); the PGP + CHT + aptamer electrodes used a 10% w/v solution of glutaraldehyde for attachment (amine-amine binding). The PGP + amine aptamer electrode was crosslinked using the heterobifunctional crosslinker (EDC/NHS) group and there is only one site on 11-MUA that can be used for attachment (carbonyl end group); whereas the PGP + CHT + aptamer electrode used the homobifunctional crosslinker (glutaraldehyde), which allowed for random crosslinking between chitosan

chains and aptamer/antibody NH_2 groups. Homobifunctional crosslinkers cannot provide the same degree of precision as the heterobifunctional crosslinkers (Sapsford et al., 2013). Therefore, it is possible that the glutaraldehyde was less effective at attaching the aptamers to the chitosan brushes than EDC/NHS to the SAM on the PGP surface.

5.2.5. PGP + Chitosan Antibody Loading

A PGP + CHT + antibody sensor was created using the same antibodies from the previous section (5.2.3) at different concentrations to determine the best loading. The three concentrations tested (50 nM, 100 nM and 200 nM) were the same as for the PGP + antibody loading tests to determine if a notable increase would take place in antibody attachment in comparison to the PGP + antibody electrode. PGP + CHT + antibody bio recognition agents were tested and it was observed that at their highest ESA value (0.0305 ± 0.0035 cm^2), the antibodies were only equal to that of the PGP+CHT electroactive surface area. Since the PGP + CHT + antibody and PGP + CHT + aptamer electrodes used the same attachment technique a close comparison between the two should be made. Statistical analysis revealed that there was no significant difference between the two bio-recognition agents.

This could have occurred for a number of reasons, first, because the antibodies which have a molecular weight of 160,000 g/mole (KPL) are larger in size than the aptamers which have a molecular weight of 14,811.63 g/mole (Aptagen), thus limiting the antibodies ability to successfully attach to the sensors surface. Secondly, as seen in Figure 5.5, the ESA values for the electrodes never decreased as the antibody concentrations increased indicating that the concentrations tested may not have been

large enough to find a saturation point for the antibodies on the electrodes surface. Statistical analysis revealed that for all PGP + CHT + antibody concentrations tested, there were no statistically significant differences from one another so the largest ESA value was chosen to use for future biosensor testing. Another possible reason that the PGP + CHT + antibody sensors had lower ESA values could have to do with the chemistry used to attach the antibody to each platform. As discussed above, the PGP + antibody used the SAM method of attachment with EDC/NHS crosslinker; the PGP + CHT + antibody electrodes used glutaraldehyde crosslinker. So it is possible that the glutaraldehyde was less effective at attaching the antibody to the chitosan brushes than the EDC/NHS to the SAM on PGP surface.

L. monocytogenes is a bacterium with the potential to cause death in high-risk populations. Therefore, sensors that show the ability to detect *L. monocytogenes* with high sensitivity and a low limit of detection are highly desirable. The composite nanomaterials used in this project could provide a platform for biosensors when combined with bio-recognition agents like aptamers.

Table 5.2 - Average electroactive surface area of electrodes with PGP + CHT coatings loaded at different concentrations of bio-recognition agents.

Electrode	ESA [cm^2]
Bare	0.0179 ± 0.0001^{a}
PGP	$0.0236 \pm 0.0045^{a,b}$
PGP+Chitosan	$0.0305 \pm 0.0025^{a,b}$
PGP+CHT+100 nM amine Aptamers	$0.0335 \pm 0.0041^{a,b}$
PGP+CHT+200 nM amine Aptamers	0.0251 ± 0.0001^{a}
PGP+CHT+400 nM amine Aptamers	0.0239 ± 0.0041^{a}
PGP+CHT+50 nM Antibodies	0.0197 ± 0.0076^{a}
PGP+CHT+100 nM Antibodies	$0.0287 \pm 0.0001^{a,b}$
PGP+CHT+200 nM Antibodies	$0.0305 \pm 0.0076^{a,b}$

[a,b]Means within a column which are not followed by a common superscript letter are significantly different ($P < 0.05$). Each test was repeated three times.

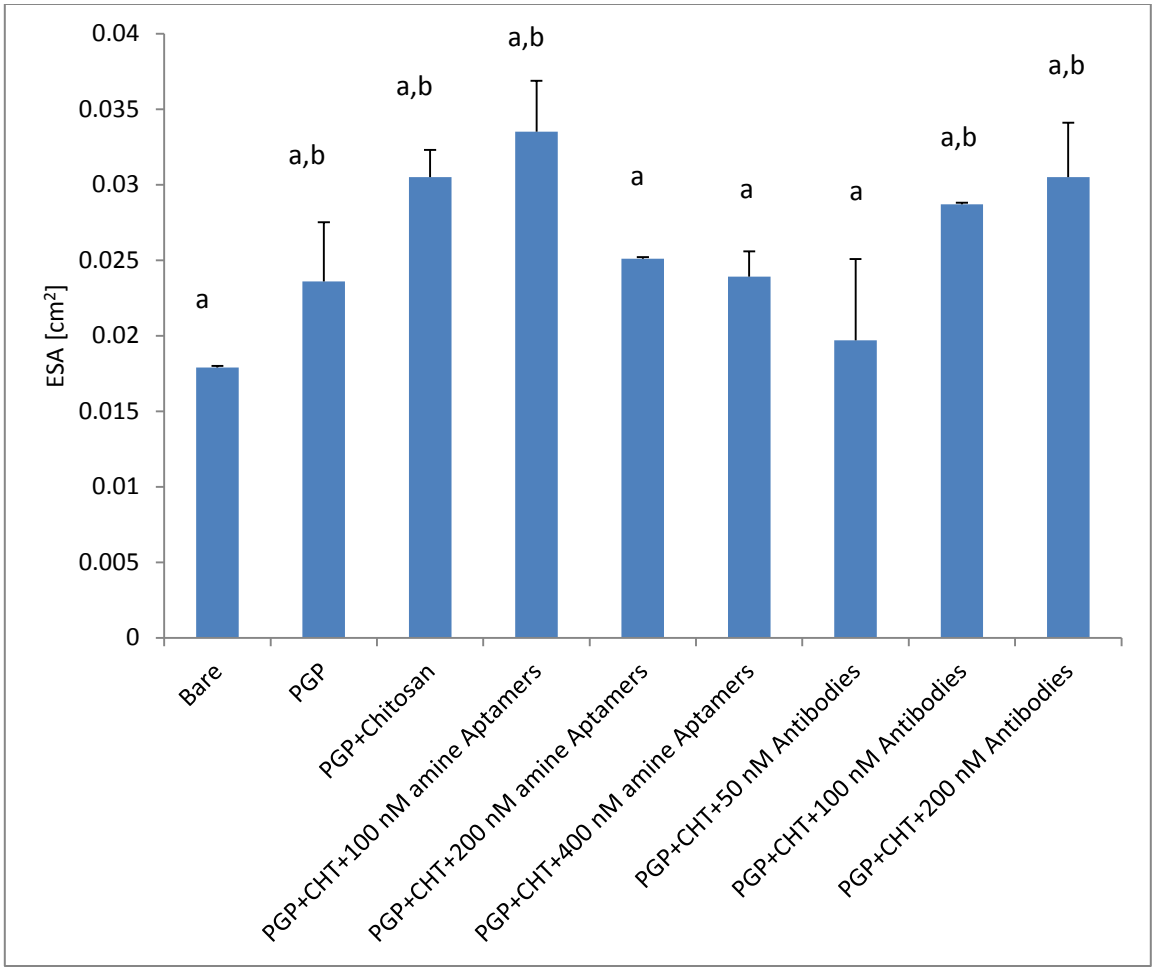

Figure 5.5 - Comparison between PGP+ CHT electroactive surface areas at various bio-recognition agent concentrations, each test was repeated three times. Error bars represent standard deviation for each test condition. [a,b]Means which are not followed by a common superscript letter are significantly different ($P < 0.05$).

5.3. Circuit Fitting Analysis of Electrodes

Figures 5.7A and 5.8 show representative Nyquist and Bode plots for bare, PGP with 100 nM aptamer, and PGP-CHT with 100 nM aptamer electrodes in PBS at a potential of 100 mV (AC), 0.25 mV (DC) and frequency range of 1 Hz–100 kHz. Figure 5.7B is a zoomed in graph of the Nyquist plot with a frequency range of 3414 Hz to 100 kHz from Fig. 5.7A and shows the lack of semicircular region that is typically seen in a

Nyquist plot at higher frequencies. CHi software was used to estimate the charge transfer resistance (R) and other circuit components (solution resistance (R_s), Warburg impedance (W), and double-layer capacitance (Q)) based on the Randles equivalent circuit model (Fig. 3.1) and shown below (Fig. 5.6), the values for all of the components can be seen in Table 5.3.

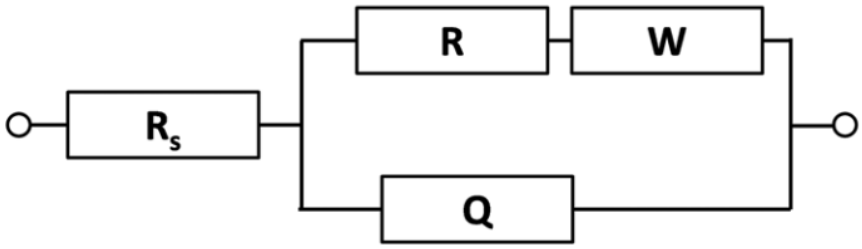

Figure 5.6 – Randles equivalent electrical circuit adapted from (Barsoukov & Macdonald, 2005).

The charge transfer resistance for the bare electrode ($8.9 \times 10^{11} \pm 9.51 \times 10^{10}\ \Omega$) is much higher than the modified electrodes. No semicircular region was measureable for PGP + 100 nM amine aptamer and PGP + CHT + 100 nM aptamer electrodes as seen in Fig. 5.7A and 5.7B, this indicates a fast electron transfer with a small charge transfer resistance (Burrs et al., 2015). The PGP + 100 nM amine aptamer sensor had the lowest charge transfer resistance of $735.6 \pm 71.038\ \Omega$. A smaller resistance means that the sensor should have a higher ESA value and this proved to be true. PGP + 100 nM amine aptamers has the highest ESA value ($0.0478 \pm 0.0207\ cm^2$) of the three electrodes, followed by the PGP + CHT + 100 nM amine aptamer ($0.0335 \pm 0.0041\ cm^2$) and lastly the bare electrode ($0.0179 \pm 0.0001\ cm^2$). A similar trend was also observed for the

Warburg impedance values, which relates the impedance at the diffusion layer and it is indicated by the 45^{o} lines in the Nyquist plot (MacDonald & Andreas, 2014). Similarly, the other two components of the circuitry, i.e., solution resistance and double layer capacitance; the bare electrode showed the highest values compared to the other electrode coatings. All of the charge transfer resistance values showed a wide standard deviation for every electrode coating, this may indicate that the fitting model used by CHi software varies a lot among treatment replicates. However, the error values for all electrodes (0.0186 ± 0.00057 to 0.0327 ± 0.0002) were all very small for each replication, indicating a good fit to the equivalent circuitry.

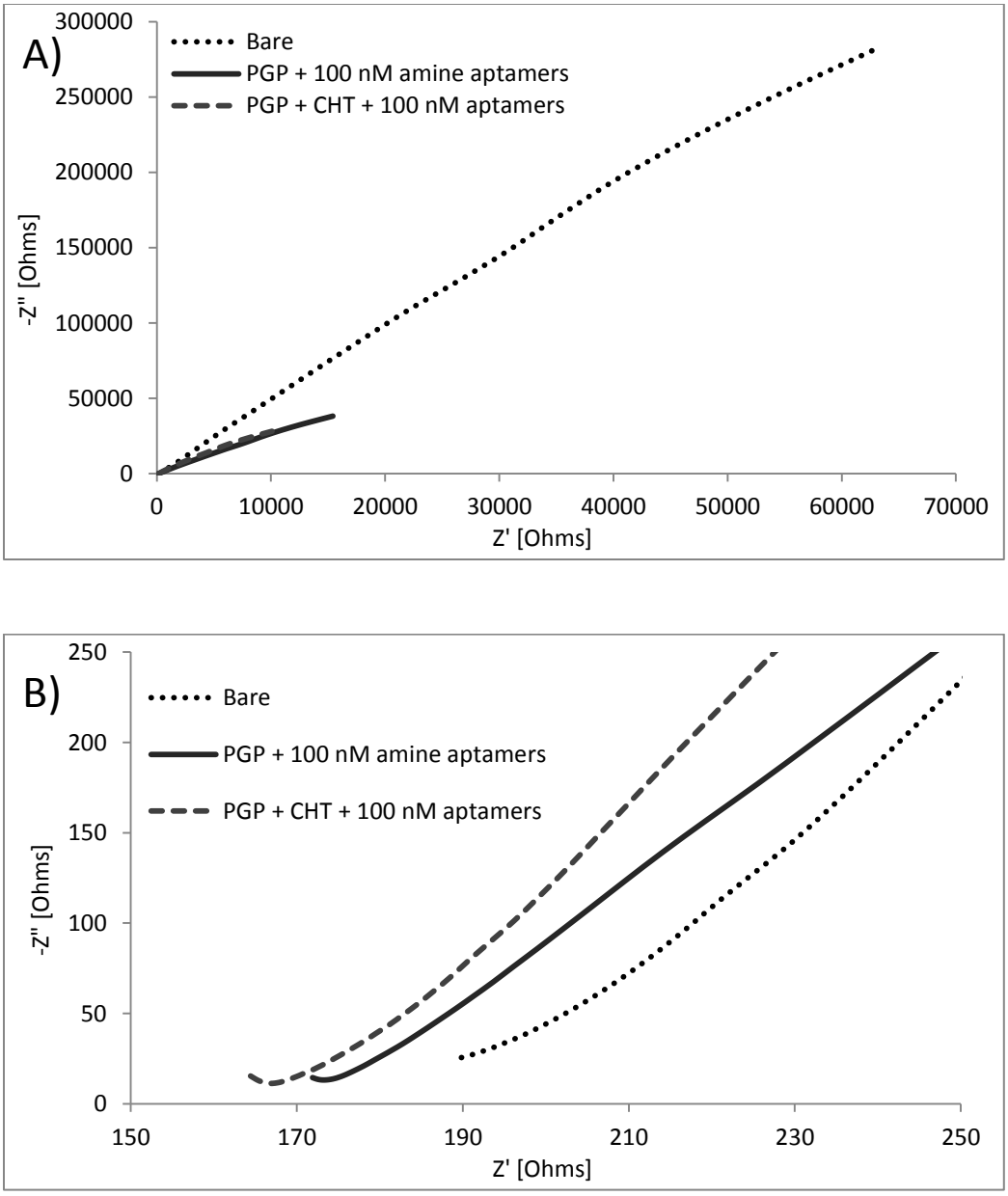

Figure 5.7 – A) Nyquist plots for for Bare, PGP + 100 nM amine aptamers, PGP + CHT + 100 nM aptamers at a potential of 100 mV (AC), 0.25 mV (DC) and frequency range of 1 Hz–100 kHz. B) Zoomed over a frequency range of 3413 Hz–85790Hz, each test was repeated three times.

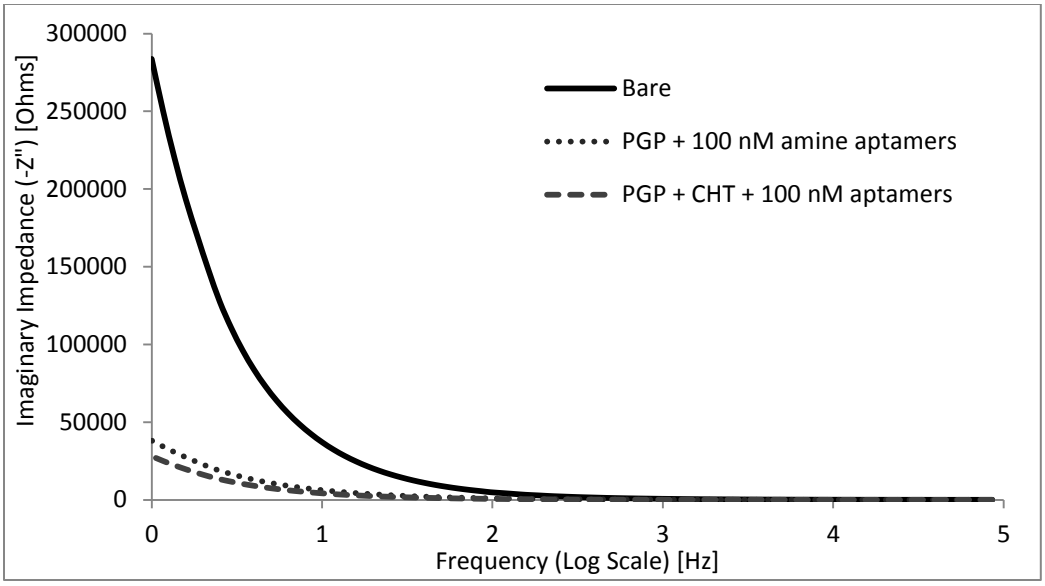

Figure 5.8 - Bode plots (imaginary impedance vs. frequency) for Bare, PGP + 100 nM amine aptamers, PGP + CHT + 100 nM aptamers treated electrodes at a potential of 100 mV (AC), 0.25 mV (DC) and frequency range of 1 Hz–100 kHz.

Table 5.3 - Circuit components for bare, PGP + 100 nM amine aptamers and PGP + CHT + 100 nM aptamers coatings.

Electrode Coating	R_s [Ohms]	W [Ohms.$s^{-0.5}$]	Q [F]	R [Ohms]	Error
Bare	195.03 ± 0.1527	$2.104x10^{11} \pm 3.53x10^{11}$	$7.21x10^{-7} \pm 4.54x10^{-9}$	$8.9x10^{11} \pm 9.51x10^{10}$	0.0327 ± 0.0002
PGP-100 nM amine aptamers	172.2 ± 1.039	$1.304x10^{-6} \pm 5.82x10^{-8}$	$4.82x10^{-6} \pm 1.52x10^{-7}$	735.6 ± 71.038	0.0186 ± 0.0006
PGP-CHT-100 nM aptamers	167.8 ± 0.7937	$3.01x10^{10} \pm 5.21x10^{10}$	$6.51x10^{-6} \pm 3.8x10^{-7}$	$3.62x10^{5} \pm 3.14x10^{5}$	0.0273 ± 0.0009

5.4. Capture Efficiency

The capture efficiency tests were performed based on pH responsiveness of chitosan to determine the optimum testing conditions for further biosensor tests. The capture efficiency test was defined based on the CV curves from the testing conditions outlined in the methodology (Section 4.8.6); these curves can be seen in Figure 5.9 for scan rate of 100 mV/s and *L. innocua* concentration of 10^3 CFU/mL. The testing condition with the highest positive curve peak on the CV curves determined the condition for which the electrode would have the highest electrochemical conductance and would in turn give the best results in further testing. Because of the lack of defined CV peaks, ESA value calculations using the Randles-Sevick equation (Eq. 4.1) could not be completed, since it requires the peak current values from the CV curves. Therefore, inferences were made solely based on the CV curves themselves.

Chitosan actuation, i.e., swelling and shrinking, is dictated by the pH of the solution. When more acid is added the pH decreases, chitosan nanobrushes become positively charged and a larger volume, i.e., swelling, can be observed because of intramolecular electrostatic repulsions. Chitosan has a pK_a value that can vary between pH 6 and 7 depending upon the deacetylation degree of the chitosan so if the solution becomes more basic then the chitosan becomes uncharged and shrinks. (López-León et al., 2005). As shown in Figure 5.9, the best testing condition was observed when the electrode was first placed in a pH 5 testing solution with bacteria and then tested in a pH 7 solution showing the highest positive CV curve, i.e., redox reaction section, when compared to the other testing conditions. A similar trend was also observed for the

oxidation reaction section of the CV curve, the same testing conditions also showed the most negative valleys. Since the chitosan is swollen at pH 5, this allowed for the aptamers to be fully exposed to the bacteria in the solution and enhanced the bacteria's attachment to the sensor. Then, when the pH was changed to 7 the chitosan shrank and allowed for an extra layer of protection for the bacteria that has been captured. Moreover, when the chitosan is collapsed and tested in pH 7 it also lowers the amount of electrical transfer charge resistance in comparison to when the chitosan is in a pH 5 solution. By exploring chitosan's pH change in this way we could define the optimum conditions by which to perform further EIS testing, which for this instance is sitting the sensor in pH 5 with the bacteria before testing in pH 7. The results found in this section were consistent with the previous section (5.1) which demonstrated ESA values being higher when electrodes were tested at pH 7 than at pH 5.

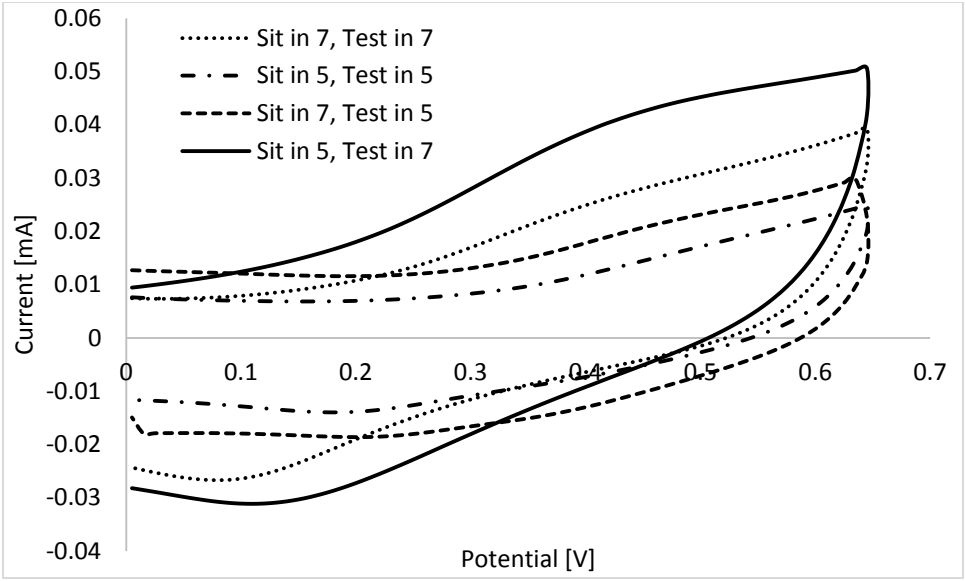

Figure 5.9 – CV curves at 100 mV/s scan rate of various testing condition under different pHs for PGP + CHT + 100 nM aptamers in a 10^3 CFU/mL concentration of *L. innocua* in PBS, each test was repeated three times.

5.5. Detection of *Listeria monocytogenes* and *Listeria innocua* in PBS using Different Biosensor Platforms

Bode and Nyquist plots with increasing concentrations of *Listeria monocytogenes* and *Listeria innocua* in PBS were created using the optimized conditions for each electrode coating: PGP + 50 nM antibody, PGP + 100 nM amine aptamer, PGP + 400 nM thiol aptamer, and PGP + CHT + 100 nM aptamer. The Nyquist and Bode plots of the PGP + 50 nM antibody can be seen below in figures 5.11A and 5.12A, respectively; and close-up Nyquist and Bode plots in 5.11B and 5.12B show incremental changes in impedance values over bacteria concentration. As seen in Fig. 5.12B, the largest difference in impedance values compared to the zero bacteria concentration (baseline) impedance values was found at 1 Hz, so all the points used in the calibration

curve for *Listeria innocua* detection (Figure 5.15) came from the impedance values found at 1 Hz. Frequency selection for plotting calibration curves for each biosensor platform followed the same approach aforementioned. Similar Bode plots were obtained and shown on figures 5.13A, 5.14A for PGP + 100 nM amine aptamer and PGP + 400 nM thiol aptamer electrode coatings, respectively. Figures 5.13B and 5.14B are close-ups showing the range of frequencies which show incremental changes in impedance values over bacteria concentration.

Each sensor tested had a detection time of approximately 17 minutes. This time was determined based on the amount of time that the sensors were allowed to sit in the bacteria suspension (15 minutes) and how long it took to run an EIS test (approximately 2 minutes). With an increase in bacteria concentration, at certain frequency ranges that varied upon the sensor platform being tested, the imaginary impedance ($-Z''$) value gradually increased, implying that more negative charge accumulated on the electrode surface (Burrs et al., 2015). These frequency ranges were selected for each sensor platform to determine sensor performance parameters, i.e., sensitivity, limit of detection, and linear range of detection. The normalized change in impedance numbers were calculated using the explanation in section 4.8.10 and equation (4.4). Since all of the sensors did not work on the same frequency and had different impedance response range, the data needed to be normalized so the biosensors could be compared to each other.

5.5.1. Detection of *Listeria monocytogenes* and *Listeria innocua* in PBS for PGP Biosensor Platforms

The mean sensitivity values towards *Listeria monocytogenes* for the PGP + 400 nM thiol aptamer and *Listeria innocua* for the PGP + 50 nM antibody and PGP + 100 nM amine aptamer respectively; are shown in Table 5.4. Of the PGP variations, the highest sensitivity was measured for the PGP + 400 nM thiol aptamers (9.81 ± 2.0 1/log(CFU/mL)) platform. This sensitivity value was approximately 4 to 8 times higher than the other two PGP electrodes, i.e., PGP + 50 nm antibody and PGP + 100 nM amine aptamer (see, Figure 5.15, 5.16 and Figure 5.17 for calibration curves of the PGP-based platforms). This large change in sensitivity could be because the PGP + 400 nM thiol aptamer biosensors were tested with *L. monocytogenes* and the other two PGP sensors were tested with *L. innocua.* Since these aptamers were designed with *L. monocytogenes* in mind it is likely that they would bind better with this specific bacteria strain instead of *L. innocua*. The aptamers affinity constant is reported to be 10^3 CFU/mL (Aptagen, 2015) and Ohk et al. (2010) who created the aptamers used in this research found that *L. innocua* had the second highest affinity, next to *L. monocytogenes*; however, this affinity was found to be non-significant in comparison to the *L. monocytogenes* affinity on their study. The antibodies used for the PGP + 50 nM antibody sensor, polyclonal goat based anti-*Listeria* antibody, on the other hand are specific to many strains of *Listeria* spp. as seen in Figure 5.10. Thus, the antibody sensor tests using *L. innocua* should give a good estimate of the sensors sensitivity and LOD for *L. monocytogenes*.

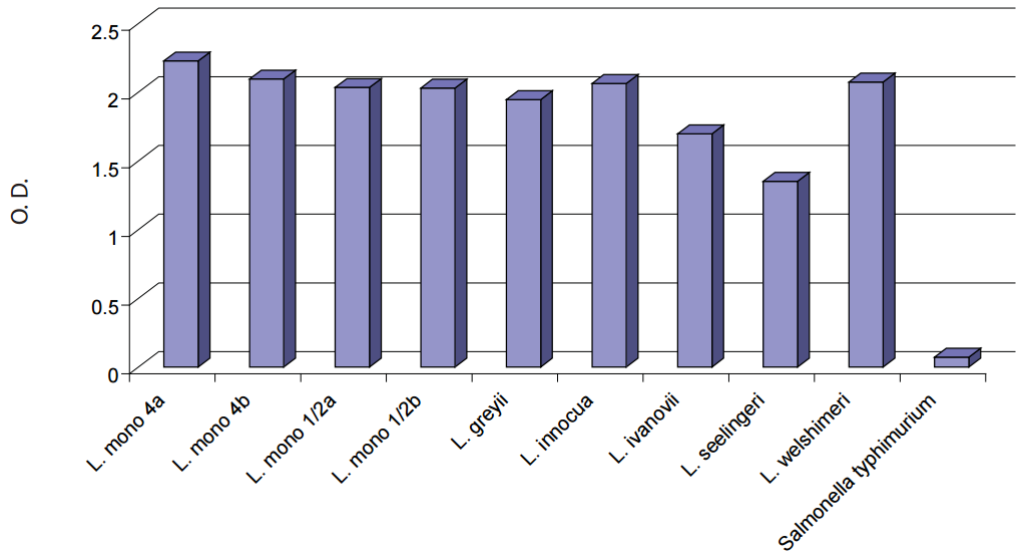

Figure 5.10 - Colorimetric assay demonstrating the specificity of the polyclonal goat based anti-*Listeria* antibody for six species of *Listeria*, including multiple strains of *L. monocytogenes* adapted from KPL (2015).

Along with sensitivity, the sensors were also tested for limit of detection and range of bacteria detection as seen in Table 5-4. The range of detection showed very little change in ranges among the electrode coatings. All of the PGP electrodes had a higher starting range value of 10^2 CFU/mL. Of the two different kinds of aptamers tested (thiol and amine) it is difficult to tell which one was the best at detecting *Listeria* since the two sensors each detected a different *Listeria* strain. Based on ESA values it could be hypothesized that the PGP + 400 nM thiol aptamers are attached in a superior manner and while the sensitivity and LOD values are better than the PGP + 100 nM amine aptamer sensor, it is impossible to know for certain which one was best without testing both sensors using the same *Listeria* strain. However, a comparison can be made based on the method of attachment. The PGP + amine aptamer sensors had a much longer

series of steps, involving the preparation of a SAM followed by covalent crosslinking of aptamers with EDC/NHS chemistry for two hours in order to attach them to the electrode's surface before testing. The PGP + thiol aptamer sensor on the other hand only required the aptamers to be drop coated onto the electrode and allowed to air dry for 30 minutes before testing. The one-step attachment process would further support the use of PGP + thiol aptamer sensors over PGP + amine aptamer sensors.

The antibody and amine aptamer electrodes for the PGP platform used the same method of attachment through SAM formation and EDC/NHS crosslinking with the bio-recognition agent and when statistical analysis of the sensitivities was conducted it was determined that the PGP + 100 nM amine aptamer and PGP + 50 nM antibody were not statistically significant. This means that both treatments would have the same performance in PBS. However, in the long term, aptamers would be a better bio-recognition agent than antibodies because of their smaller size which increases bioavailability, shelf life stability and the ease with which functional groups can be added to the aptamers (Jayasena, 1999; Keefe et al., 2010).

In a recent study, Wang, Ruan, Li, Kanayeva, and Lassiter (2008) used monoclonal antibodies immobilized on TiO_2 nanowire bundle to detect *L. monocytogenes* in PBS. They found a LOD of 10^2 CFU/mL, which is higher than the LOD found in this research. They also determined a range of detection of 10^2 to 10^7 CFU/mL which is similar to the range of detection found for the PGP + 50 nM antibody sensor in this research (10^2 to 10^7 CFU/mL). It should also be noted that Wang et al. (2008)'s testing procedure takes approximately one hour so it also has a longer response

time than this research. Overall, the PGP + 50 nM antibody sensor developed showed superior performance metrics.

Based on the sensitivity results observed between aptamer and antibody for the PGP electrode coating, which showed to not be significantly different for the same type of attachment method, it was decided to only test the PGP + CHT + aptamer coating in PBS and for future real-life challenge tests, in vegetable broth and *L. monocytogenes* it would be tested both antibody and aptamers.

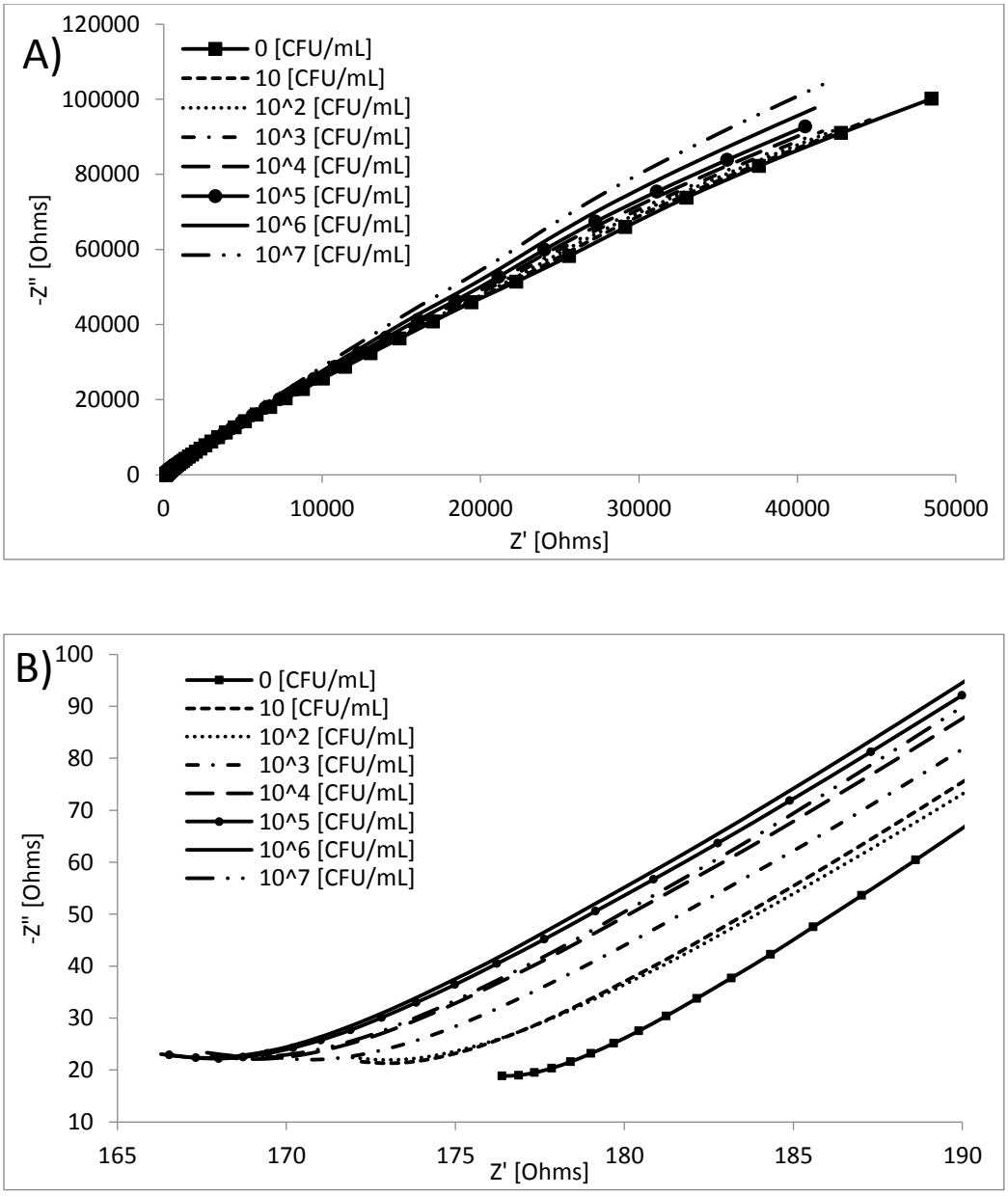

Figure 5.11 – A) Nyquist plots for PGP + 50 nM polyclonal goat based anti-*Listeria* antibodies treated electrodes at increasing *L. innocua* concentrations, at a potential of 100 mV (AC), 0.25 mV (DC) and frequency range of 1 Hz–100 kHz. B) Zoomed over a frequency range of 8579 Hz–85790Hz, each test was repeated three times. The 0 CFU/mL concentration stands for the baseline (non-inoculated PBS).

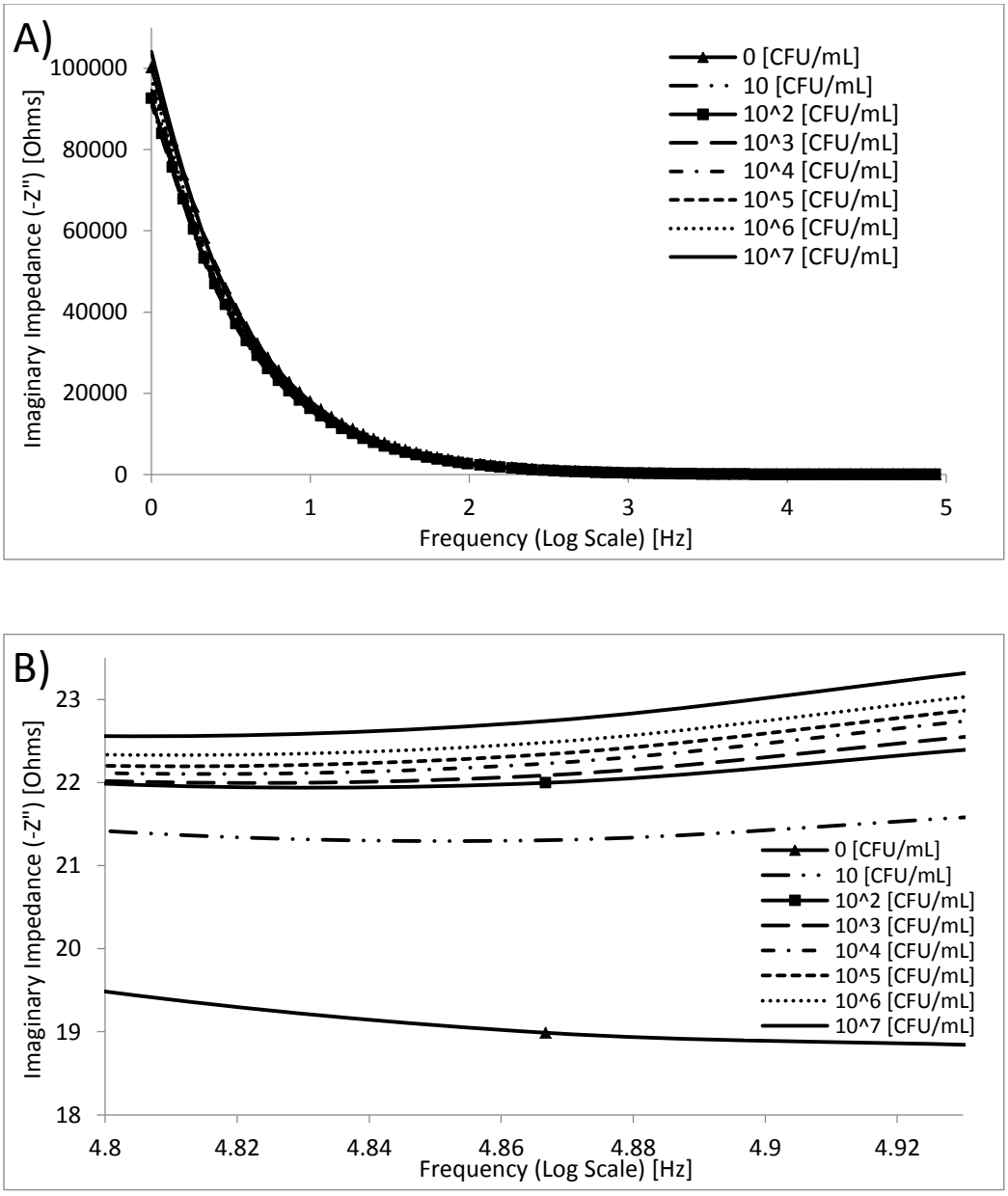

Figure 5.12 – A) Impedance spectra (Bode plot) of PGP + 50 nM polyclonal goat based anti-*Listeria* antibody electrodes incubated with different concentrations of *L. innocua* in PBS over a range of frequencies (1 Hz to 100 kHz). B) Zoomed in view over a range of frequencies (63090 Hz to 85790 Hz), each test was repeated three times. The 0 CFU/mL concentration stands for the baseline (non-inoculated PBS)

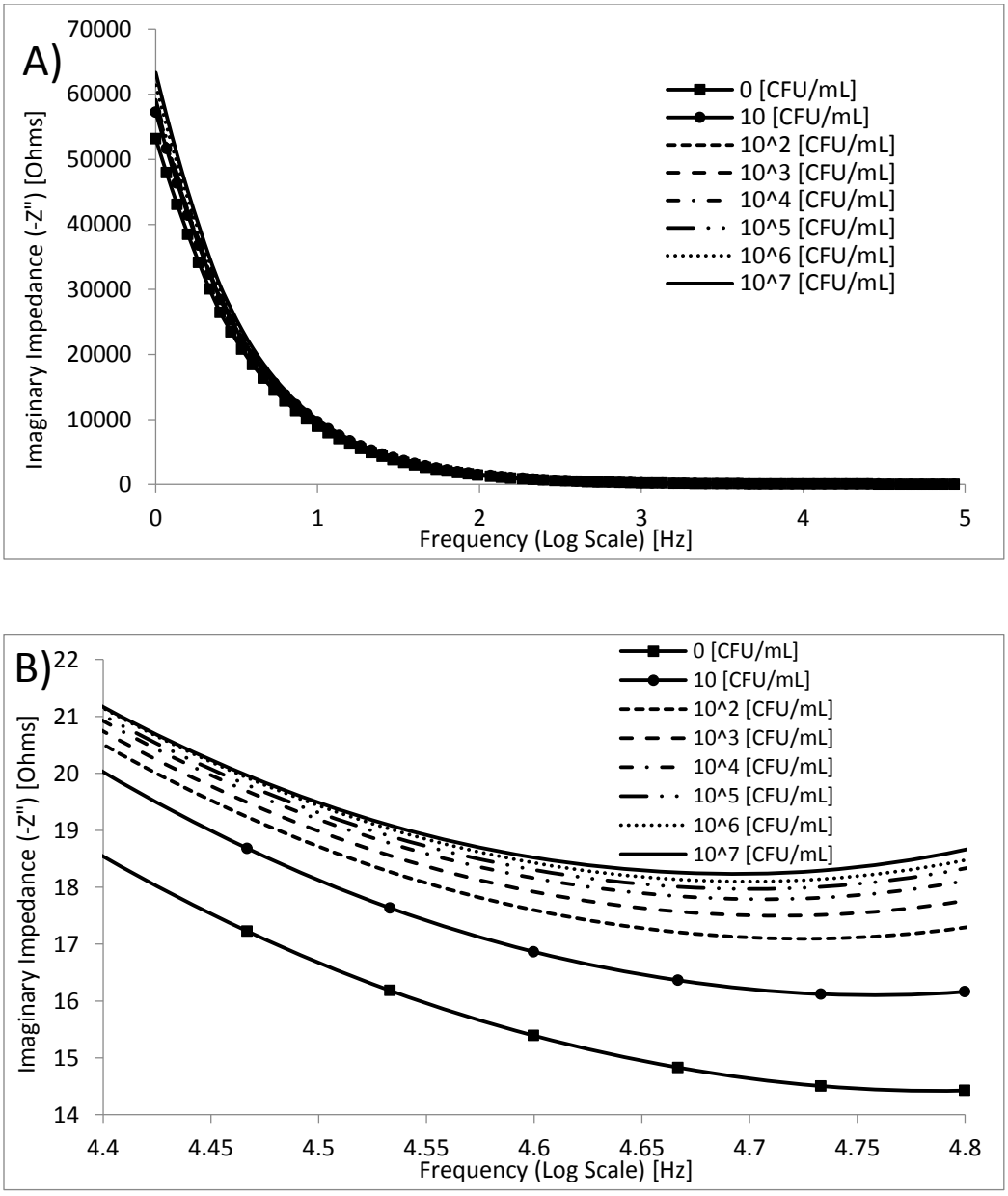

Figure 5.13 – A) Impedance spectra (Bode plot) of PGP + 100 nM amine aptamer electrodes incubated with different concentrations of *L. innocua* in PBS over a range of frequencies (1 Hz to 100 kHz). B) Zoomed in view over a range of frequencies (63090 Hz to 85790 Hz), each test was repeated three times. The 0 CFU/mL concentration stands for the baseline (non-inoculated PBS).

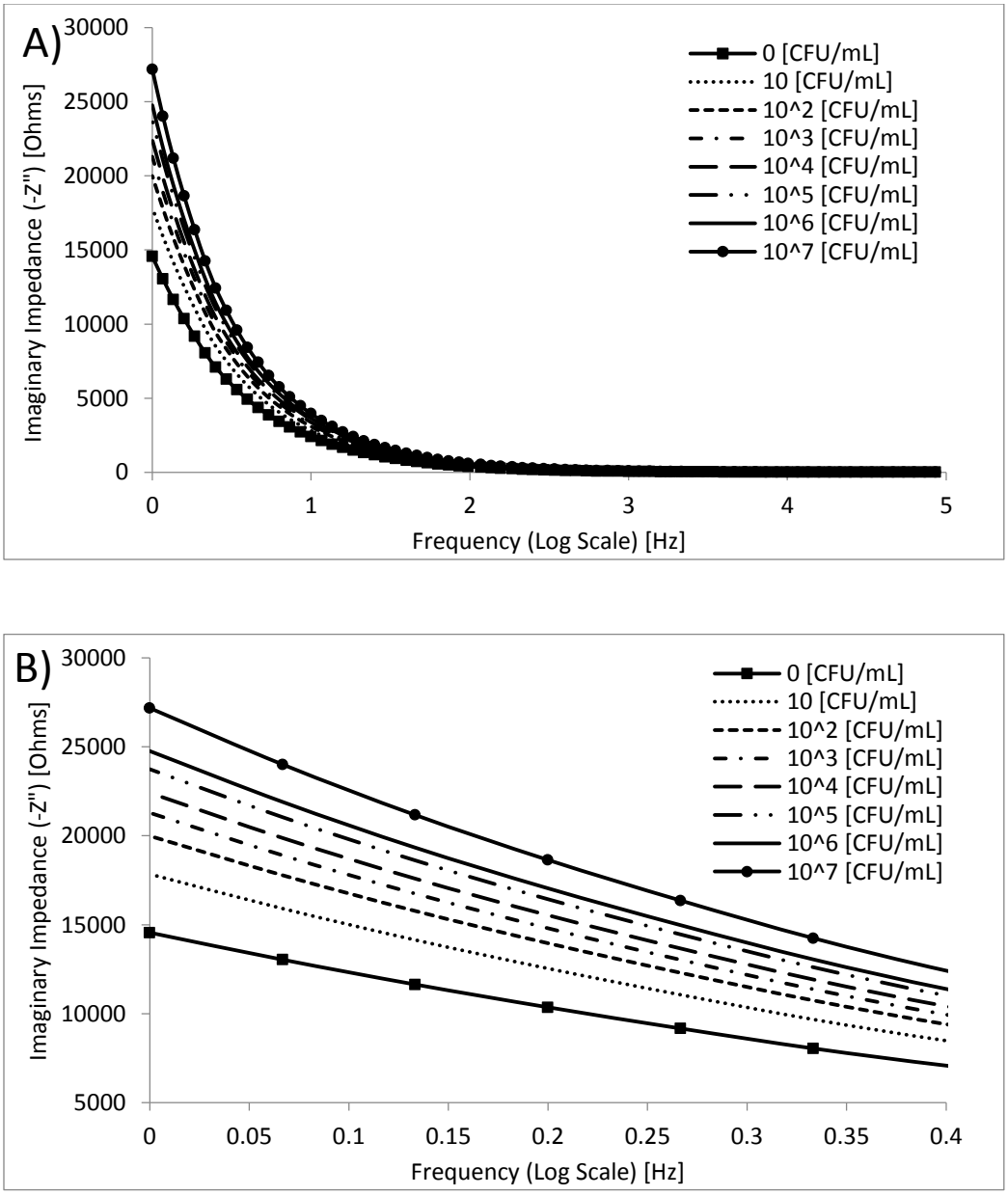

Figure 5.14 – A) Impedance spectra (Bode plot) of PGP + 400 nM thiol aptamer electrodes incubated with different concentrations of *L. innocua* in PBS over a range of frequencies (1 Hz to 100 kHz). B) Zoomed in view over a range of frequencies (1 Hz to 2.5 Hz), each test was repeated three times. The 0 CFU/mL concentration stands for the baseline (non-inoculated PBS).

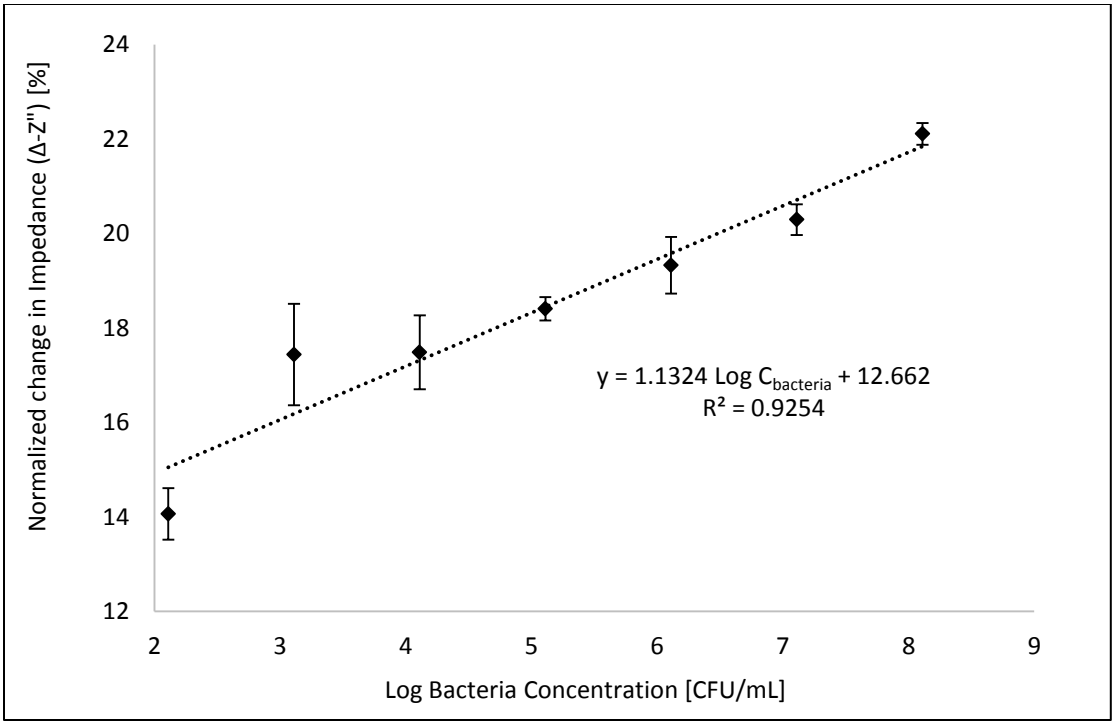

Figure 5.15 – Calibration curve for the detection of *L. innocua* in PBS at 85790 Hz using normalized impedance change versus logarithm of bacteria concentration for PGP + 50 nM polyclonal goat based anti-*Listeria* antibody biosensor. Each test was repeated three times. Error bars represent standard deviation for each test condition.

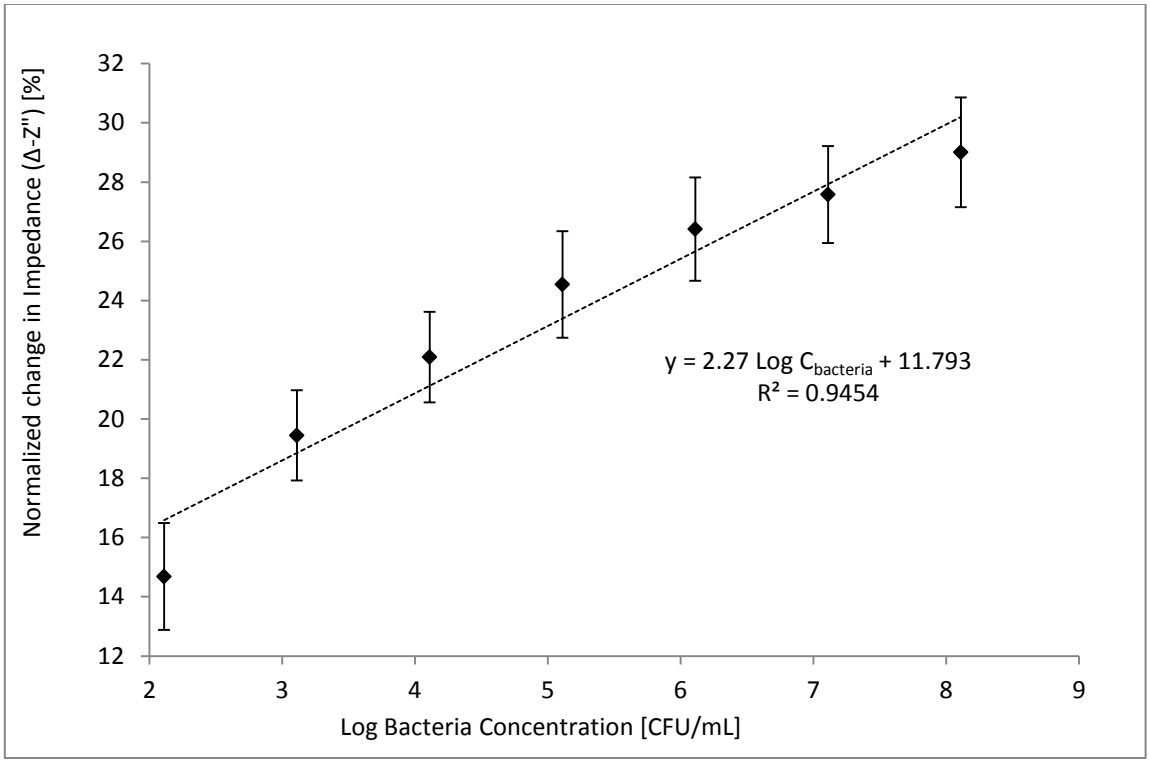

Figure 5.16 - Calibration curve for the detection of *L. innocua* in PBS at 46439 Hz using normalized impedance change versus logarithm of *L. innocua* concentration for the PGP + 100 nM amine aptamer, each test was repeated three times. Error bars represent standard deviation for each test condition.

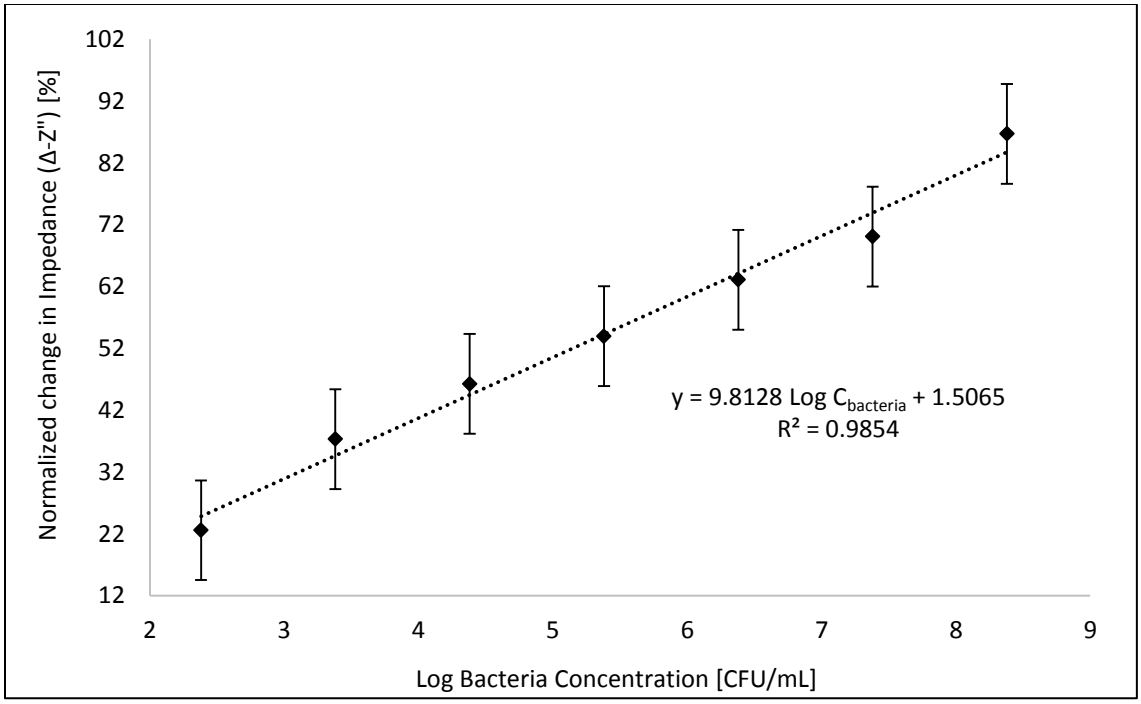

Figure 5.17 - Calibration curve for the detection of f *L. monocytogenes* in PBS at 1 Hz using normalized impedance change versus logarithm of *L. monocytogenes* concentration for the PGP + 400 nM thiol aptamer biosensor, each test was repeated three times. Error bars represent standard deviation for each test condition.

Table 5.4 - Biosensors performance results for *Listeria* spp. detection in PBS.

Biosensor platform: Electrode Coating	Frequency Selected [Hz]	Sensitivity [1/log(CFU/mL)]	Limit of Detection [CFU/mL]	Detection Range [CFU/mL]	R^2
PGP + 100 nM amine Aptamers	46439	2.27 ± 0.28^{ab}	$47.4.4 \pm 3.36^{d}$	$10^2 – 10^8$	0.9454
PGP + 400 nM thiol Aptamers	1	9.81 ± 2.0^{c}	11.2 ± 0.79^{a}	$10^2 – 10^8$	0.9854
PGP + 50 nM Antibodies	85790	1.13 ± 0.175^{a}	85.9 ± 3.73^{e}	$10^2 – 10^8$	0.9254

[a,b,c,d,e]Means within a column which are not followed by a common superscript letter are significantly different ($P < 0.05$).

5.5.2. Detection of *Listeria innocua* in PBS for PGP + CHT Biosensor Platforms and Selectivity Measurement using *Listeria innocua* and *Staphylococcus aureus*

The sensitivity values of the PGP + CHT + 100 nM aptamer sensor were measured in the presence of *Listeria innocua* only and also in the presence of two different bacteria suspensions and can be seen in Table 5.5. The Bode plots for suspension can also be seen in Figure 5.18A and 5.19A and closer in 5.18B and 5.19B to show incremental changes in impedance values over bacteria concentration. As seen in Fig. 5.18B, the largest difference in impedance values with increasing bacteria concentration was found at 1 Hz, so all the points used in Figure 5.20 (calibration curve) came from the impedance values found at 1 Hz. The second suspension contained equally increasing concentrations of *L. innocua* and *S. aureus* and had a sensitivity value of 14.25 ± 1.69 1/(CFU/mL) derived from the slope in Figure 5.21. *S. aureus* was

chosen as the interfering bacteria because similar to *Listeria* spp., *S. aureus* is also a Gram-positive bacterium and would be more likely to give a false positive reading than a Gram-negative bacterium. Furthermore, *S. aureus* is also an important foodborne pathogen (Doyle & Buchanan, 2013).

When statistical analysis of the sensitivity values was conducted, the test showed no statistical significance between the two sensitivities. This means that this sensor will be very selective towards *Listeria spp.* and should only detect this bacteria when in a medium that contains other pathogens and bacteria. Ohk et al. (2010) found a similar selectivity when they used the same aptamers as this study and some anti-listeria antibodies to compare their sensors selectivity towards *Listeria monocytogenes*. Their results showed a significant difference between testing their sensor in *L. monocytogenes* and *S. aureus*. The study by Radhakrishnan et al. (2013) also gave another instance of *Listeria* selectivity, they applied increasing concentrations of *Salmonella enterica* to their anti-listeria antibody biosensor and found no change in EIS tests as the concentration increased. It can also be noted that they found a small detection limit (4 CFU/mL) similar to this research (9.1 ± 1.1 CFU/mL). Based on this study, it is possible to make an argument that the PGP + CHT + 100 nM aptamer in this research is comparable in selectivity and limit of detection to the sensor created by Radhakrishnan et al Radhakrishnan et al. (2013) that used antibodies. In the long term, aptamers would be a better bio-recognition agent than antibodies because of their smaller size which increases bioavailability, shelf life stability and the ease with which functional groups can be added to the aptamers (Jayasena, 1999; Keefe et al., 2010).

When comparing all the electrode platforms together (Table 5.4 and 5.5) the PGP + CHT + 100 nM aptamer and PGP + 400 nM thiol aptamer sensors showed the best results when sensitivity, range and LOD were tested. Despite of the trends from the electroactive surface area data, the PGP+CHT+100 nM aptamers showed the highest sensitivity in PBS (Figure 5.20) among all the electrodes tested (12.14 ± 1.79 1/log(CFU/mL)). Analysis of variance (ANOVA) was performed to determine whether or not any effects on the response variable (impedimetric sensitivity) arising from the electrode platforms were statistically significant. Using a Levene's test of equality of error variances a p-value smaller than the critical value ($p < 0.05$) was obtained indicating that there was a significant difference in impedimetric sensitivity among some of the treatments. A Tukey test was then performed to compare the mean impedimetric sensitivity of every concentration to the set of all pairwise comparisons. The four electrode platforms were statistically different, and the sensitivity obtained from the PGP + CHT + 100 nM aptamers and the PGP + 400 nM thiol aptamers platforms were significantly greater than the other two PGP platforms tested. The PGP+CHT+100 nM aptamers also had the lowest LOD (9.1 ± 1.1 CFU/mL) and had the lowest starting range value of 10.

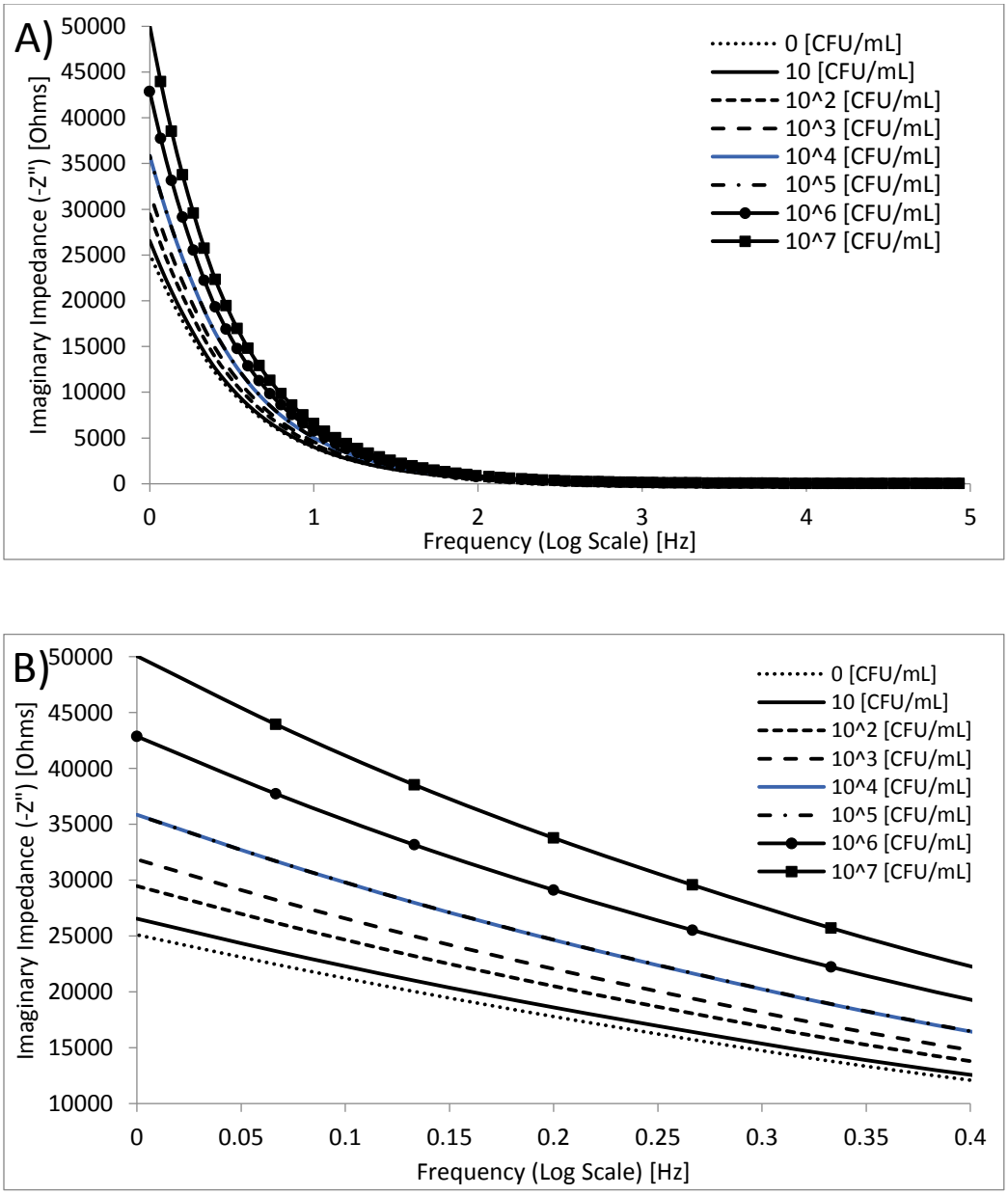

Figure 5.18 – A) Impedance spectra (Bode plot) of PGP + CHT + 100 nM aptamer electrodes incubated with different concentrations of *L. innocua* in PBS over a range of frequencies (1 Hz to 100 kHz). B) Zoomed in view over a range of frequencies (1 Hz to 2.5 Hz), each test was repeated three times. The 0 CFU/mL concentration stands for the baseline (non-inoculated PBS).

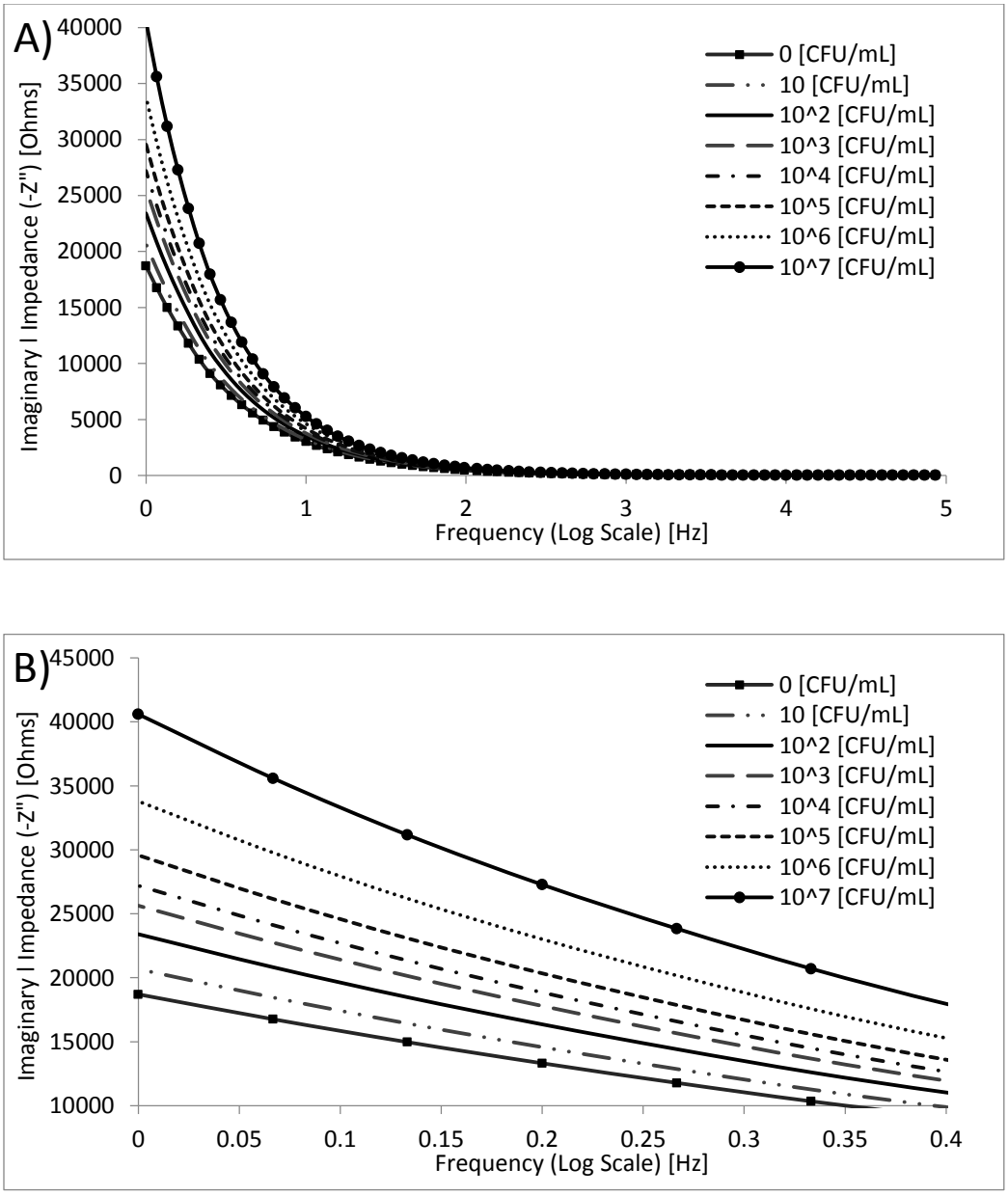

Figure 5.19 – A) Impedance spectra (Bode plot) of PGP + CHT + 100 nM aptamer electrodes incubated with different concentrations of *L. innocua* and *S. aureus* in PBS over a range of frequencies (1 Hz to 100 kHz), each test was repeated three times. B) Zoomed in view over a range of frequencies (1 Hz to 2.5 Hz), each test was repeated three times. The 0 CFU/mL concentration stands for the baseline (non-inoculated PBS).

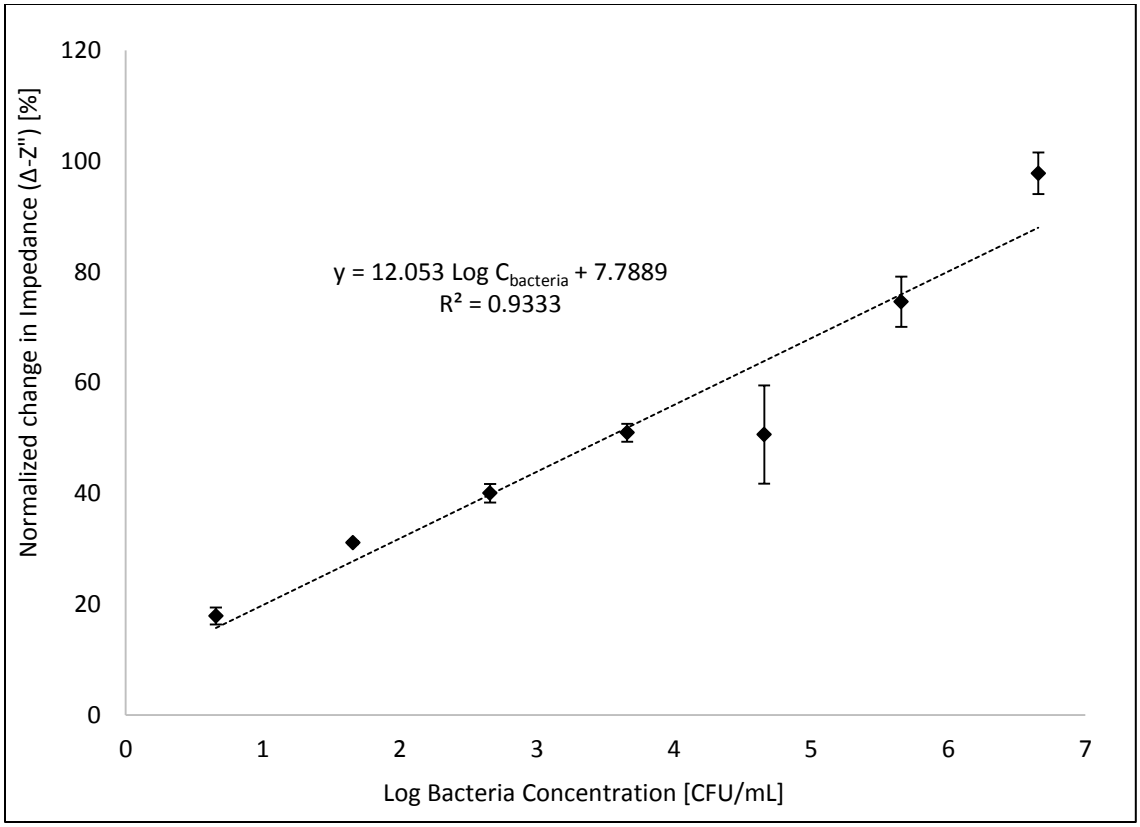

Figure 5.20 - The linear relationship between change in normalized impedance and logarithm of *L. innocua* concentration for the PGP + CHT + 100 nM aptamer in PBS at 1 Hz, each test was repeated three times. Error bars represent standard deviation for each test condition.

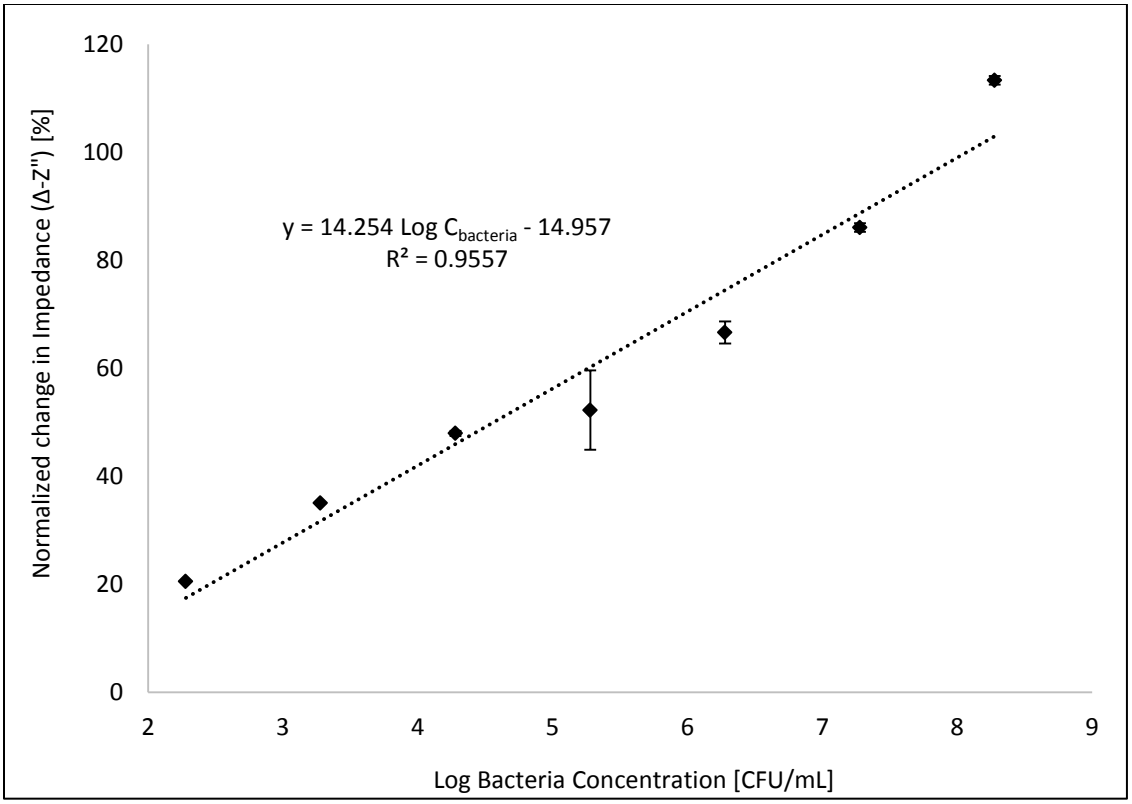

Figure 5.21 - The linear relationship between change in normalized impedance and logarithm of *L. innocua* and *S. aureus* concentration for the PGP + CHT + 100 nM aptamer in PBS, each test was repeated three times. Error bars represent standard deviation for each test condition.

Table 5.5 - PGP + CHT + 100 nM aptamer biosensors sensitivity versus selectivity comparison.

Biosensor platform: Electrode Coating	Frequency [Hz]	Sensitivity [1/log(CFU/mL)]	Limit of Detection [CFU/mL]	Detection Range [CFU/mL]	R^2
Sensitivity PGP + CHT + 100 nM Aptamers	46439	12.14 ± 1.79^{c}	9.1 ± 1.1^{a}	$10 - 10^{7}$	0.9333
Selectivity PGP + CHT + 100 nM Aptamers	1	14.25 ± 1.69^{c}	9.4 ± 0.11^{a}	$10^{2} - 10^{8}$	0.9557

[a,b,c]Means within a column which are not followed by a common superscript letter are significantly different ($P < 0.05$).

5.6. Detection of *Listeria monocytogenes* in Vegetable Broth

The PGP + CHT biosensors were also tested in a real food sample, vegetable broth. The vegetable broth is composed of water, vegetable juice concentrate, cooked vegetables (carrot, onion, celery), tomato paste, yeast extract, molasses, onion powder, potato flour, natural flavor, canola oil, cane sugar and sea salt (HEB, 2015). There have been two reported outbreaks of *L. monocytogenes* in fresh produce, one in 2011 involving cantaloupe and in 2014 involving sprouts, demonstrating the importance of testing fresh produce for *Listeria* contamination. A fresh produce sample would normally be suspended/diluted in water and homogenized prior to testing for bacteria contamination, therefore, we used vegetable broth as not only as a real-food sample with all its complexity but also as good representation of fresh produce sample suspensions.

The pH of the vegetable broth was altered to reflect the prior sections testing conditions sit the sensor first in pH 5 and then do EIS testing in pH 7. These sensors were chosen for further testing because the PGP + CHT + 100 nM aptamer showed the highest sensitivity and lowest LOD values in the previous section (5.5). PGP + CHT + 200 nM antibody sensors were tested to compare if aptamers would be more effective with the PGP + CHT coating with antibodies. Bode plots can be seen in Figures 5.22A and 5.23A and exploded Bode plots with narrow frequency ranges in Figures 5.22B and 5.23B. The calibration curves for detection of *Listeria* monocytogenes in vegetable broth for both sensors can be seen in Figures 5.24 and 5.25, which consisted of the normalized change in impedance plotted against the log of bacteria concentration. The normalized change in impedance numbers were calculated using the explanation in

section 4.8.10 and equation (4.4). As seen in Fig. 5.22B and 5.23B, the largest difference in impedance values was found at 1 Hz, so all the points used in Figure 5.24 and 5.25 came from the impedance values found at 1 Hz. The mean sensitivity and LOD values towards *Listeria monocytogenes* for the PGP + CHT + 100 nM aptamer and PGP + CHT + 200 nM antibody respectively; are shown in Table 5.6. Each sensor tested had a detection time of approximately 17 minutes. This time was determined based on the amount of time that the sensors were allowed to sit in the food sample containing bacteria (approximately 15 minutes) and how long it took to run an EIS test (approximately 2 minutes).

The EIS testing for both sensors showed similar sensitivity values, the aptamers had a sensitivity of 3.76 ± 0.34 1/log(CFU/mL) and the antibodies had a value of 4.9 ± 0.4 1/log(CFU/mL) (Figures 5.24 and 5.25). When statistical analysis of the sensitivities was conducted it was determined that the two different treatments were not statistically significant. This means that both treatments will work the same in this type of sample; implying that other bio-recognition agents or even immunosensing agents could be attached to the PGP + CHT platform and have similar detection capabilities. However, if the sample were to change to something else like yogurt for example, these numbers would likely vary. The antibodies showed a slightly lower limit of detection (23.9 ± 0.96 CFU/mL) but also a smaller range of detection $10^2 – 10^7$ CFU/mL. In the long term, aptamers would be a better bio-recognition agent than antibodies because of their smaller size which increases bioavailability, shelf life stability and durability (Jayasena, 1999; Keefe et al., 2010).

Table 5.7 summarizes the performance characteristics of the PGP and PGP + CHT nanocomposites from this study and similar sensors used for the detection of *Listeria* spp. in food products in the literature. As shown in this table, the performance characteristics such as response time, detection range and limit of detection towards *Listeria* by the PGP and PGP + CHT nanocomposites are within the range found in the literature. Ohk et al. (2010) designed an aptamer/antibody sensor that was able to detect *L. monocytogenes* in sliced ready to-eat lunch meat samples (beef, chicken and turkey) that had been inoculated with *Listeria monocytogenes* (4 CFU/sample g), their process required an 18 hour enrichment step in selective enrichment broth prior to actual testing, making the response time much longer than this research which has a response time of approximately 17 minutes. Cheng et al. (2014) also created an electrochemical sensor using self-assembled monolayers (SAM) on modified gold (Au) electrodes for the detection *L. monocytogenes* in milk. Unlike Ohk et al., Cheng et al. (2014) required no pretreatment of the sample before testing, they also found a similar linear range of detection ($10^2 – 10^6$ CFU/mL) to this research; however, they do not list a LOD. Eun Jeong et al. (2014) used Real-Time PCR to detect *L. monocytogenes* in inoculated ham, sausage, ground meat, processed milk, cheese, and infant formula. They found detection limits of 10^0 to 10^2 CFU/g or mL, depending on the food sample being tested which is lower than the LOD found in this research for some instances. However, Eun Jeong et al. (2014)'s testing procedure requires a 4 hour incubation time before testing so it does have a longer response time than this research. Furthermore, the sensors in this research, in comparison to plate counting have several advantages because plate counting is time

consuming (5-7 days) and it requires a pre-enrichment step to reach similar detection limits and personnel trained in microbiology, unlike this research.

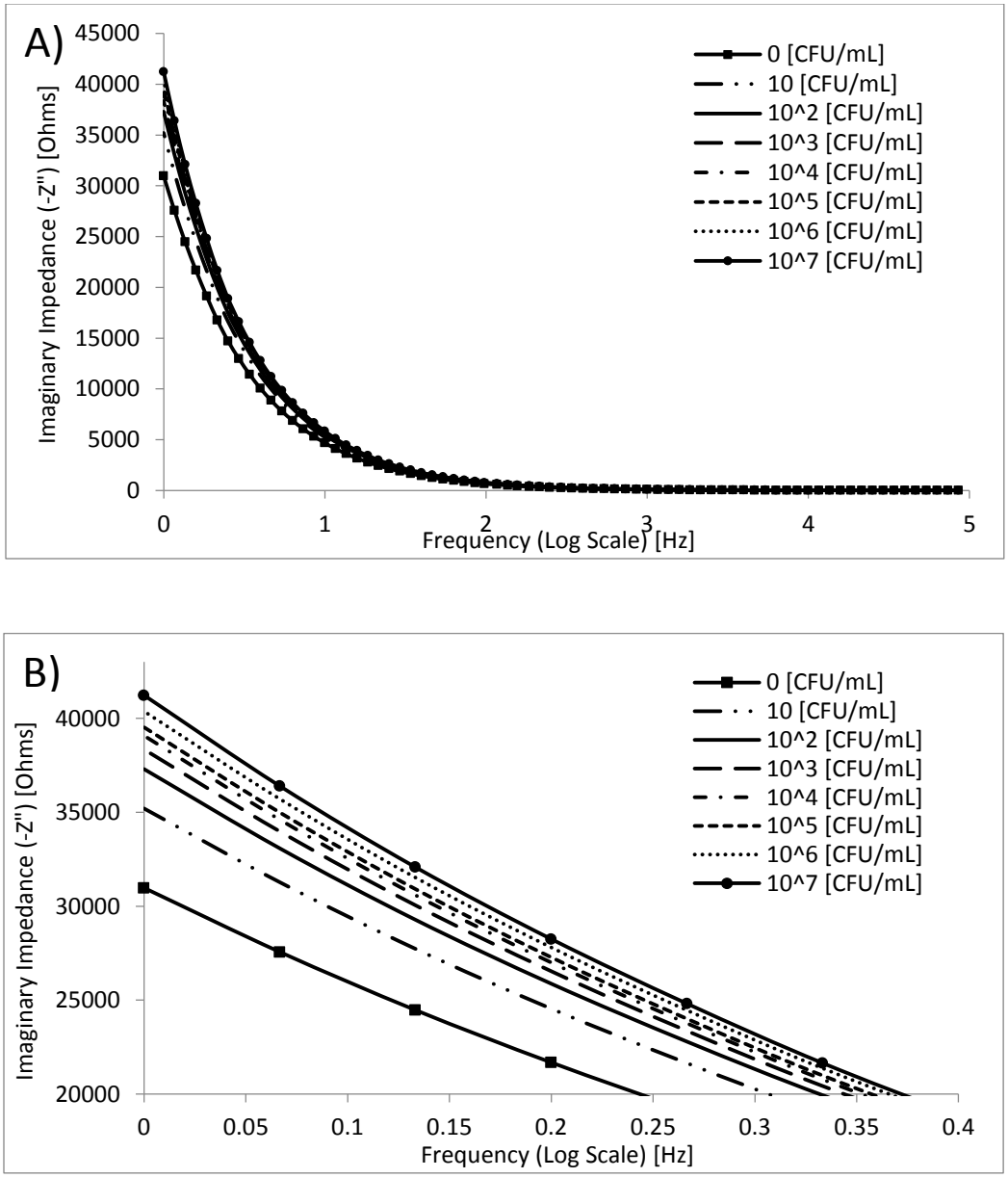

Figure 5.22 – A) Impedance spectra (Bode plot) of PGP + CHT + 100 nM aptamer electrodes incubated with different concentrations of *L. monocytogenes* in vegetable broth over a range of frequencies (1 Hz to 100 kHz). B) Zoomed in view over a range of frequencies (1 Hz to 2.5 Hz), each test was repeated three times. The 0 CFU/mL concentration stands for the baseline (non-inoculated PBS).

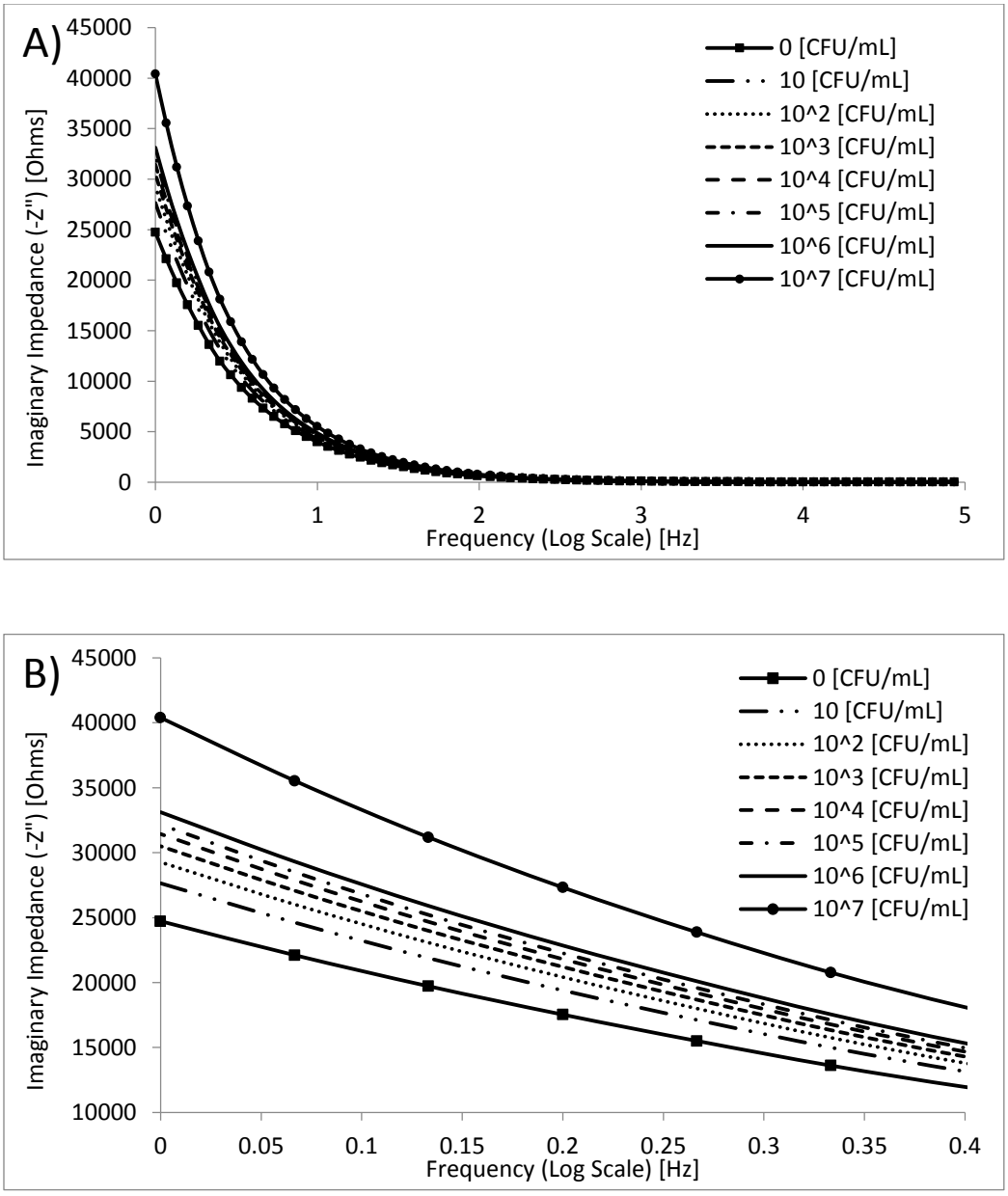

Figure 5.23 – A) Impedance spectra (Bode plot) of PGP + CHT + 100 nM aptamer electrodes incubated with different concentrations of *L. monocytogenes* in vegetable broth over a range of frequencies (1 Hz to 100 kHz). B) Zoomed in view over a range of frequencies (1 Hz to 2.5 Hz), each test was repeated three times. The 0 CFU/mL concentration stands for the baseline (non-inoculated PBS).

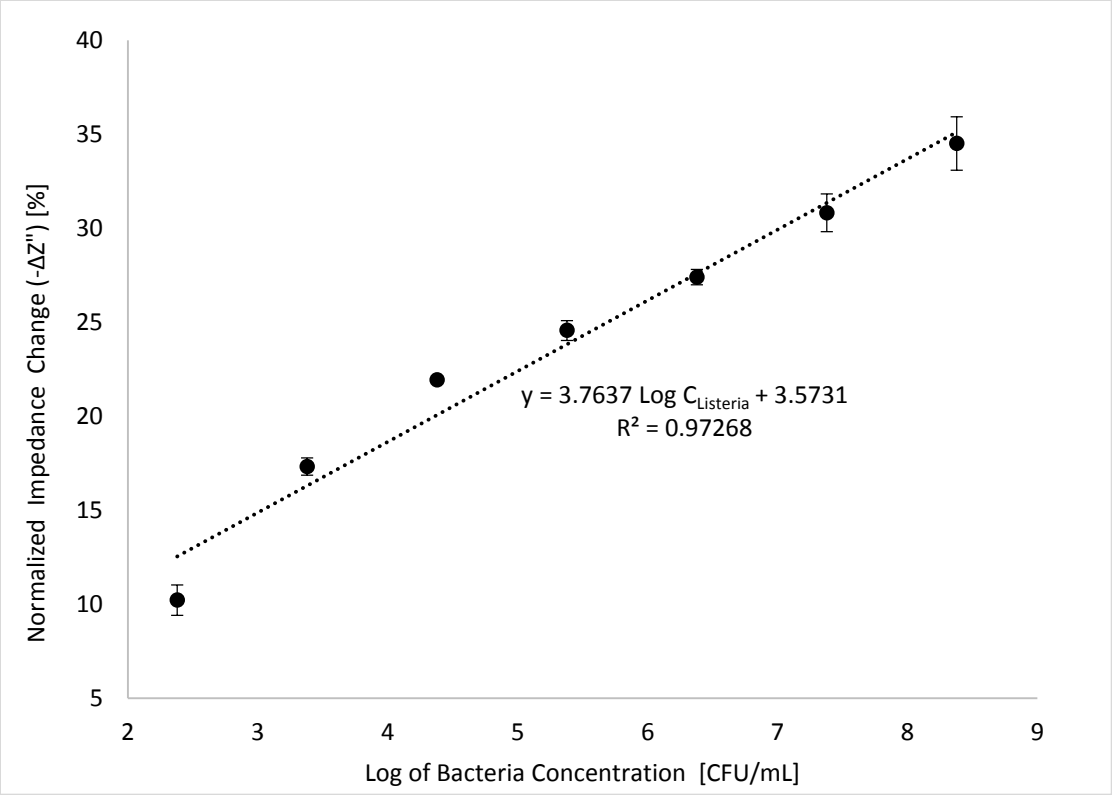

Figure 5.24 – Calibration curve for the detection of *L. monocytogenes* in vegetable broth using normalized impedance versus bacteria concentration for the PGP + CHT + 100 nM aptamer at 1 Hz, each test was repeated three times. Error bars represent standard deviation for each test condition.

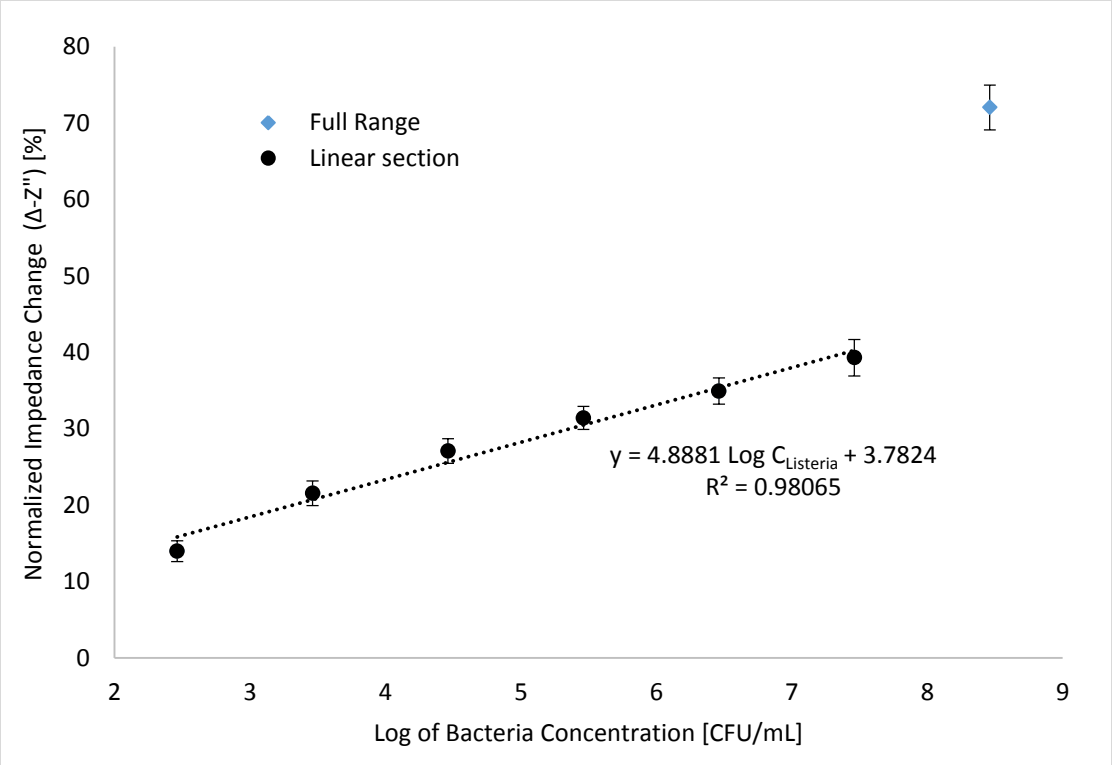

Figure 5.25 – Calibration curve for the detection of *L. monocytogenes* in vegetable broth using normalized impedance versus logarithm of bacteria concentration for the PGP + CHT + 200 nM polyclonal goat based anti-*Listeria* antibody at 1 Hz, each test was repeated three times. Error bars represent standard deviation for each test condition.

Table 5.6 - PGP + CHT electrode data for *Listeria monocytogenes* detection in vegetable broth.

Biosensor platform: Electrode Coating	Frequency [Hz]	Sensitivity [1/log(CFU/mL)]	Limit of Detection [CFU/mL]	Detection Range [CFU/mL]	R^2
PGP + CHT + 100 nM Aptamers	1	$3.76 \pm 0.34^{a,b}$	31.12 ± 0.64^{c}	$10^2 - 10^8$	0.9727
PGP + CHT + 200 nM Antibodies	1	4.9 ± 0.4^{b}	23.9 ± 0.96^{b}	$10^2 - 10^7$	0.9806

[a,b,c]Means within a column which are not followed by a common superscript letter are significantly different ($P < 0.05$).

Table 5.7 - Comparison of biosensors performance parameters for *Listeria* spp. detection.

Nanomaterial and bio-recognition agent	Mode of Detection	Microorganism Detected	Test Medium	Sensitivity	Limit of Detection	Detection Range	Response Time	Reference
PGP + 100 nM amine aptamers	Impedimetric	*L. innocua*	PBS	2.27 ± 0.28^{ab} 1/log(CFU/mL)	$47.4.4 \pm 3.36^{d}$ CFU/mL	$10^2 – 10^8$ CFU/mL	17 min	This Study
PGP + 400 nM thiols aptamers	Impedimetric	*L. monocytogenes*	PBS	9.81 ± 2.0^{c} 1/log(CFU/mL)	11.2 ± 0.79^{a} CFU/mL	$10^2 – 10^8$ CFU/mL	17 min	This Study
PGP + 50 nM antibodies	Impedimetric	*L. innocua*	PBS	1.13 ± 0.175^{a} 1/log(CFU/mL)	85.9 ± 3.73^{e} CFU/mL	$10^2 – 10^8$ CFU/mL	17 min	This Study
PGP + CHT + 100 nM aptamers	Impedimetric	*L. innocua*	PBS	12.14 ± 1.79^{c} 1/log(CFU/mL)	9.1 ± 1.1^{a} CFU/mL	$10 – 10^7$ CFU/mL	17 min	This Study
PGP + CHT + 100 nM aptamers	Impedimetric	*L. monocytogenes*	Vegetable Broth	$3.76 \pm 0.34^{a,b}$ 1/log(CFU/mL)	31.12 ± 0.64^{c} CFU/mL	$10^2 – 10^8$ CFU/mL	17 min	This Study
PGP + CHT + 200 nM antibodies	Impedimetric	*L. monocytogenes*	Vegetable Broth	4.9 ± 0.4^{b} 1/log(CFU/mL)	23.9 ± 0.96^{b} CFU/mL	$10^2 – 10^7$ CFU/mL	17 min	This Study

Table 5.7 - Continued

Nanomaterial and bio-recognition agent	Mode of Detection	Microorganism Detected	Test Medium	Sensitivity	Limit of Detection	Detection Range	Response Time	Reference
Mouse monoclonal antibody immobilized on self-assembled monolayers	Impedimetric	*L. monocytogenes*	Milk	n.r.	n.r	10^2 - 10^6 CFU/mL	n.r.	(Cheng et al., 2014)
Antibody immobilized on highly-dispersed carbon particles	Amperometric	*L. monocytogenes*	Milk and chicken extract	n.r.	10 CFU/mL	n.r.	30 min	(Chemburu, Wilkins, & Abdel-Hamid, 2005)
None	Real-Time PCR	*L. monocytogenes*	Ham and sausage homogenized in Fraser broth	n.r.	1 – 10^2 CFU/mL depending upon the sample	n.r.	9 - 10 h	(Eun Jeong et al., 2014)
Monoclonal antibodies immobilized on TiO_2 nanowire bundle	Impedimetric	*L. monocytogenes*	PBS	n.r.	10^2 CFU/mL	10^2 - 10^7 CFU/mL	1 h	(Wang et al., 2008)

Table 5.7 - Continued

Nanomaterial and bio-recognition agent	Mode of Detection	Microorganism Detected	Test Medium	Sensitivity	Limit of Detection	Detection Range	Response Time	Reference
Polyclonal antibodies and aptamers immobilized on streptavidin-coated optical waveguide	Fluorescence Intensity	*L. monocytogenes*	Sliced lunch meat of beef, chicken and turkey homogenized in Fraser broth	n.r.	10^3 CFU/mL	n.r.	>18 h	(Ohk et al., 2010)
Antibody immobilized on a polypyrrole polymer-modified electrode	Amperometric	*L. monocytogenes*	0.15 M $NaNO_3$	n.r.	10^5 Cells/mL	n.r.	30 min	(Minett, Barisci, & Wallace, 2003)

n.r.: not reported.

[a,b,c,d,e] Means within a column which are not followed by a common superscript letter are significantly different ($P < 0.05$).

5.7. Microscopic Analysis

The PGP and PGP + CHT coatings were subjected to SEM imaging and Fig. 5.26 and 5.27 show the surface characteristics of the PGP "sandwich" design. The morphology of the PGP structures observed in this study seem different to those reported by Shi et al. (2012) and Vanegas et al. (2014) who also used PGP coating methodologies for their biosensor testing. The SEM images show homogenous deposits of platinum-black and reduced graphene on the surface of the electrode, the particles sizes appear to be between 0.25 to 0.5 μm. Compared to the other two studies this research showed a much different PGP surface. SEM imaging for both studies had much more uniformly distributed particles and defined particle ridges and valleys in the surface of their sensors than the PGP sensors created in this research. When comparing SEM imaging for all the PGP coating procedures, Shi et al. (2012) had particles roughly 0.1 μm to 0.25 μm, this research had particles between 0.25 to 0.5 μm and Vanegas et al. (2014) had particles smaller than 100 nm. This is likely due to differences in PGP coating procedures. Shi et al. (2012) and Vanegas et al. (2014) both use the same electrodeposition procedure as this research, the main difference lies in the graphene addition. Shi et al. (2012) and Vanegas et al. (2014) both use a similar drop coating procedure; however, Shi et al. (2012) only allowed their electrodes to dry for 30 minutes and Vanegas et al. (2014) allowed their electrodes to be dried overnight before the final platinum coating was deposited, which could have influenced the amount of reduced graphene deposition. This research used a drop coating and spin coating methodology that appears to have produced larger, more dispersed PGP particles than the other two

studies, though not necessarily an inferior ESA value. Shi et al. (2012) reported a smaller ESA value ($6.0 \pm 0.56 \times 10^{-3}$ cm^2) than found in this research (0.0236 ± 0.0045 cm^2), whereas Vanegas et al. (2014) reported a higher ESA value (0.148 ± 0.064 cm^2). As the images show, the deposition of platinum nanoparticles and reduced graphene appears to increase surface area of the electrode. Furthermore, both materials are highly conductive, graphene oxide is approximately 10^5 S/m (Gao, Chen, Liu, Miao, & Wang, 2015) and platinum's is 9.4×10^6 S/m (De Vittorio, Martiradonna, & Assad, 2014), consequently not only the surface area was increased but also the electrodes' ESA values increased when ESA values measured electrochemically were compared. The PGP ESA values were larger ($P < 0.05$) than the bare electrode values meaning that the depositions observed must have added in the increased ESA values due to both material electrical conductivity.

Figures 5.28 and 5.29 show the PGP + CHT coating on the electrode surface when subjected to SEM. The figures show an almost hilly, forest like structure from a distance with peaks of chitosan attachment and valleys of no apparent coating. As the magnification increases it becomes apparent that in the chitosan sections the electrodeposition was successful in creating finger like structures of chitosan. Each finger looks to have a diameter of roughly 250 to 500 nm. When looking at the SEM imaging the PGP + CHT sensor appear to have a larger surface area because of the chitosan fingers, in comparison to the PGP sensors, which seems to have a lighter coating of conductive material and in turn a smaller surface area. This is further justified when surveying the ESA data, the PGP + CHT sensors showed a higher ESA value than

that of the PGP partially due to the increase in electrode surface area and the electrochemical properties of chitosan. Based on the sensitivity and limit of detection analysis it would appear as though the PGP + CHT coating was more successful than its PGP coating counterpart when amine aptamers were applied to their surfaces and tested in regular PBS solution. This was likely due to the chitosan "fingers" increasing the surface area from which the aptamers could attach. A study by Du et al. (2007) used a variable potential electrodeposition technique to create 50 nm diameter chitosan nanoparticles on a gold substrate. The research in this thesis used a single, larger (3 V), voltage potential to adhere the chitosan which maybe the cause of the particle size discrepancy. The chitosan used in this research also differs slightly (75-85% deacetylation) from the compared study who used only 85% deacetylated chitosan for their testing. Using a different degree of deacetylation can affect the length of the polymer chain, which can in turn affect the nanobrush size that is created.

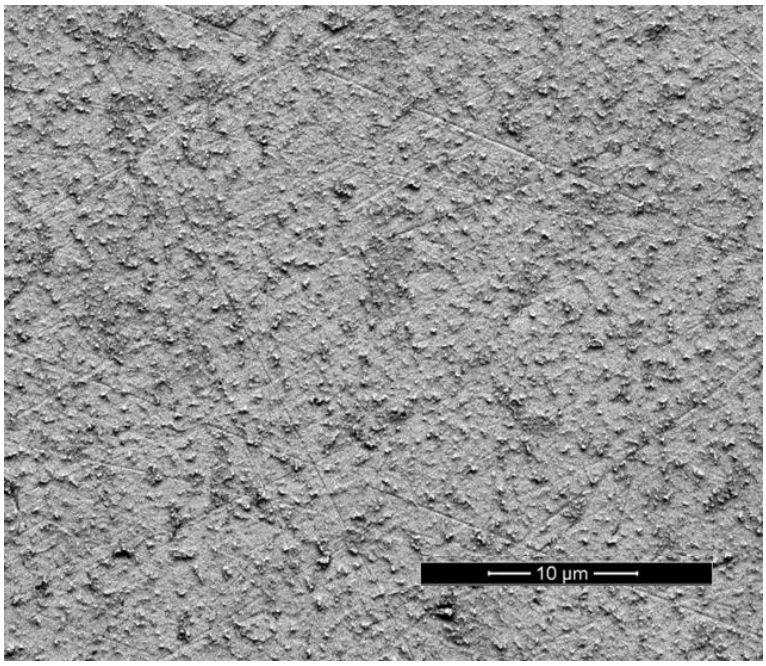

Figure 5.26 - SEM image of PGP coating at 5,000x magnification.

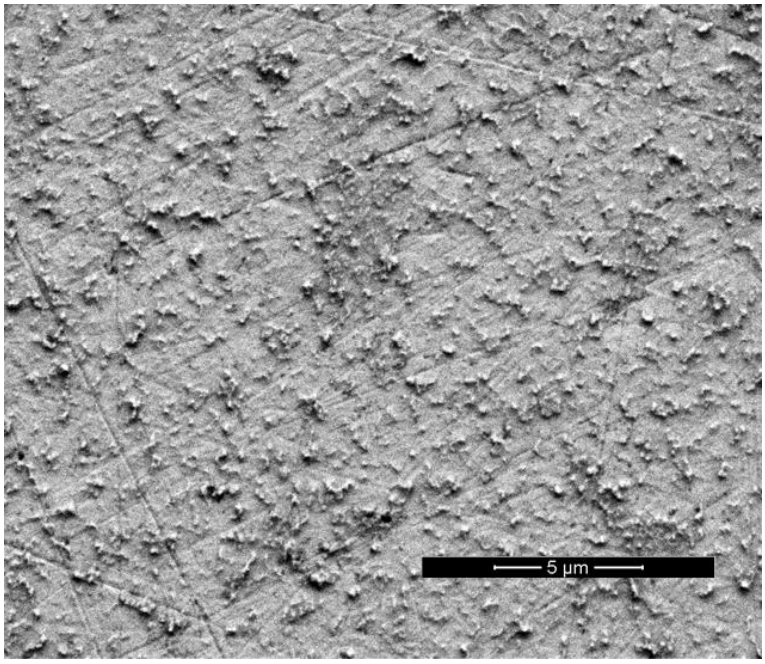

Figure 5.27 - SEM image of PGP coating at 10,000x magnification.

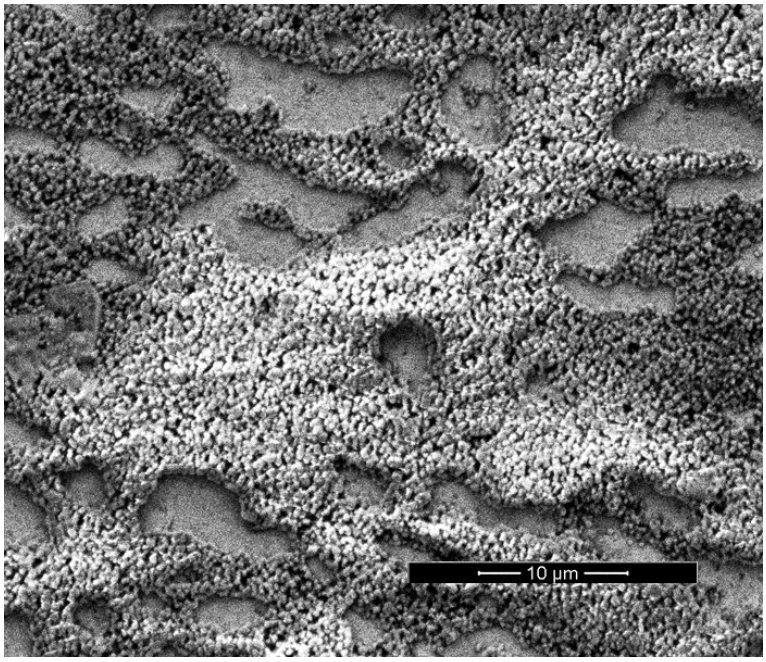

Figure 5.28 - SEM images of PGP + CHT coating at 5,000x magnification.

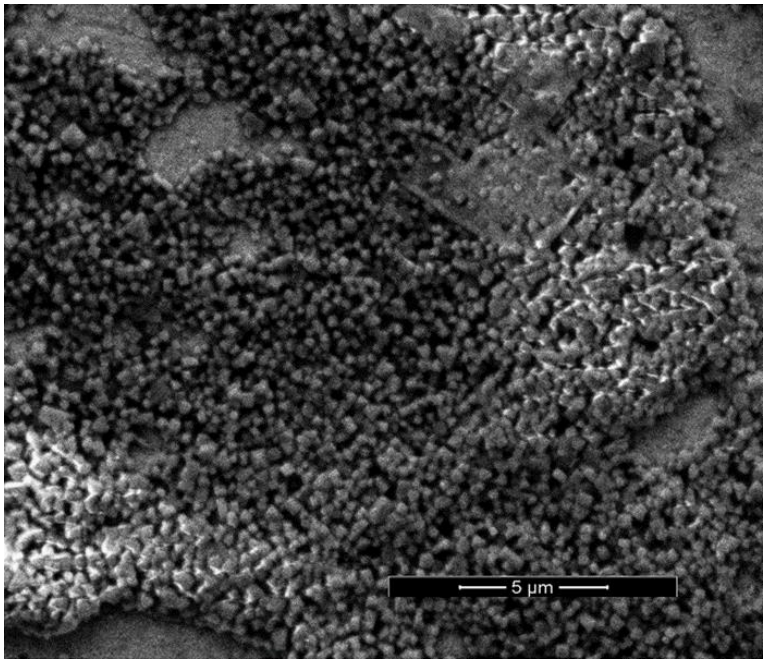

Figure 5.29 - SEM images of PGP + CHT coating at 10,000x magnification.

5.8. Real Life Application

While these sensors do have many competitive traits with other methods of detection for pathogens in ideal conditions, such as limit of detection, linear range of detection, and time of detection. There are a few considerations that need to be taken into account before it can be translated into real-life applications, for instance in production lines in the food industry. One of the most important factors would be food product being tested. For instance, in this research the food sample used was vegetable broth, while it is complex with many different chemical compounds in its make-up, it is in liquid form. For other samples such as deli meats which are solid, an extra step to liquefy the sample would need to be taken. Another factor to take into consideration is sample acidity, if a sample is more acidic, it would affect the chitosan configuration (i.e., swollen state), and potentially making the sensor less sensitive. To correct this, samples may need to have their pHs adjusted to the optimum conditions for bacteria detection.

Another factor to take into account is the sample size used for analysis. Likely, any product/processing batch that will be tested is larger in size than the 20 mL used in this study and it is also very likely that there will a low concentration of bacteria in the product/processing batch (i.e., one or two cells of bacteria in the product). It is very likely that a product/processing batch would have to be divided into multiple samples to properly detect bacteria presence and avoid false negatives which would add on to the detection time.

CHAPTER VI

RECOMMENDATIONS FOR FUTURE RESEARCH

There are still many areas of biosensors left to be explored and even within this research there are more opportunities for advancement. To start with, a shelf life study needs to be conducted to see how long the biosensor could sit before becoming compromised and to see if it would be possible to miniaturize the whole system. The durability of the system would also be important to understand to see if the biosensor could be reused. Due to the current software of the testing apparatus it would be help to create a program that does all of the analysis and gives easy to understand results.

Other options would be to apply different types of capture probes such as rRNA, DNA, lectins or enzymes to see if one is more effective in capturing bacteria as well as using other aptamers that are designed to detect other organisms such as *Escherichia coli, Staphylococcus aureus*, or other non-food pathogens. It would also be helpful to apply different hydrogels such as Poly(N-isopropylacrylamide) (PNIPAAM), silk fibroin or cellulose nanocrystals (CNC) with aptamers to see if the sensitivity and/or selectivity will show any marked differences. Since hydrogels with other types of stimuli-responsive behavior might improve capture of bacteria and sensitivity of the biosensor.

As far as the procedure used in this research it might prove helpful to explore different options. One of those options would be mixing the aptamers into the chitosan and then doing electrodeposition to see if there is a difference in biosensor performance. Also, developing a better spin coater to improve the consistency of the PGP coating since it seemed to be a source of inconsistency. Lastly, it would be helpful to determine

the thickness of the PGP and PGP + CHT coatings and fully characterize its material properties.

Finally, as far as testing is concerned it would be good to try some additional tests for further validation of the biosensor. For example, the biosensor should also be validated against false positive and false negative readings and more types of food samples to see if the sensor would still work in more complex media. Furthermore, a test should be conducted to see the selectivity with *L. innocua* and *L. monocytogenes* to determine how much the biosensor is affected if both are present in a sample. It would also be helpful to test the biosensor to see if more *Listeria* strains are able to be detected to design a broad general *Listeria spp*. sensor. Finally, tests should to run with samples that have been stored in refrigeration conditions since *Listeria* is psychrophilic and can grow under refrigeration temperatures (4-10^{o}C).

CHAPTER VII

CONCLUSIONS

In this thesis, several types of studies were conducted to develop impedance biosensors for detection of bacterial targets. *Listeria innocua* and *Listeria monocytogenes* were chosen as the target bacteria due to their importance in food safety. This study demonstrated an approach for the fabrication of hybrid composites based on chitosan, graphene oxide, and platinum. The effect of bio-recognition agents type and concentration on electrochemical performance was studied in detail and optimized for biosensor applications.

Each sensor tested had a detection time of approximately 17 minutes. This time was determined based on the amount of time that the sensors were allowed to sit in the bacteria suspension (15 minutes) and how long it took to run an EIS test (approximately 2 minutes). The PGP biosensors were tested to determine ESA with three different bio-recognition agents (amine terminated aptamers, thiol terminated aptamers and antibodies) attached to the surface and each agent was tested at three different concentrations to determine an optimum concentration for EIS testing. The optimum concentration for PGP + thiol aptamer sensors was 400 nM and the corresponding ESA value for it was 0.0718 ± 0.029 cm^2. The best concentration for PGP + amine aptamer sensors was 100 nM and the corresponding ESA value for it was 0.0478 ± 0.047 cm^2. The optimum concentration for PGP + antibody sensors was 50 nM and the corresponding ESA value for it was 0.0359 ± 0.0001 cm^2.

Further EIS testing was performed to determine each sensors properties. The mean sensitivity towards *Listeria monocytogenes* for the PGP + 400 nM thiol aptamer was 9.81 ± 2.0 1/log(CFU/mL) and towards *Listeria innocua* for the PGP + 50 nM antibody was 1.13 ± 0.175 1/log(CFU/mL) which was lower than for PGP + 100 nM amine aptamer at 2.27 ± 0.28 1/log(CFU/mL). The LOD for the PGP + 400 nM thiol aptamer was 11.2 ± 0.79 CFU/mL, for PGP + 50 nM antibody was 85.9 ± 3.73 CFU/mL, which was higher than for PGP + 100 nM amine aptamer at 47.4 ± 3.36 CFU/mL. In addition to detecting a small number of cells all the sensors were able to detect bacteria over a wide range of concentrations from $10^2 – 10^8$ CFU/mL in PBS. The PGP + 400 nM thiol aptamer had the highest ESA, sensitivity and the lowest limit of detection for the PGP platform, so it could be hypothesized that the thiol aptamers attached to the PGP surface was better than the amine aptamers.

The PGP + CHT biosensors were tested to determine ESA with two different bio-recognition agents (aptamers and antibodies) attached to the surface and each agent was tested at three different concentrations to determine an optimum concentration for EIS testing. The best concentration for PGP + CHT + aptamer sensors was 100 nM and the corresponding ESA value for it was 0.0335 ± 0.0033 cm^2. The optimum concentration for PGP + CHT + antibody sensors was 200 nM and the corresponding ESA value for it was 0.0305 ± 0.0035 cm^2.

Capture efficiency tests were performed on the chitosan to determine the optimum testing conditions for all of the EIS tests. The best testing condition was observed when the electrode was first placed in a pH 5 testing solution with bacteria and

then tested in a pH 7 solution. Since the chitosan is swollen at pH 5, this allowed for the aptamers to be fully exposed to the bacteria in the solution and enhanced the bacteria's attachment to the sensor. Then when the pH was changed to 7 the chitosan shrank and allowed for an extra layer of protection for the bacteria that has been captured.

The mean sensitivity towards *Listeria innocua* for the PGP + CHT + 100 nM aptamer was 12.14 ± 1.79 1/log(CFU/mL). The LOD for the PGP + CHT + 100 nM aptamer was 9.1 ± 1.1 CFU/mL. In addition to detecting a small number of cells the sensors were able to detect bacteria over a wide range of concentrations from $10 – 10^7$ CFU/mL. The sensitivity of the PGP + CHT + 100 nM aptamer sensor was also measured in the presence of two different bacteria suspensions. The suspension contained equally increasing concentrations of *L. innocua* and *S. aureus* and had a sensitivity value of 14.25 ± 1.69 1/log(CFU/mL) and an LOD of 9.4 ± 0.11 CFU/mL. When statistical analysis of the sensitivity values was conducted, the test showed no statistical significance between the two sensitivities. This means that this sensor will be very selective towards *Listeria spp.* and should only detect *Listeria* spp. when in a medium that contains other pathogens and bacteria.

The PGP + CHT biosensors were also tested in a real food sample, vegetable broth. The aptamers had a sensitivity of 3.76 ± 0.34 1/log(CFU/mL) and the antibodies had a value of 4.9 ± 0.4 1/log(CFU/mL). The LOD for the PGP + CHT + 100 nM aptamer was 31.12 ± 0.64 CFU/mL which was slightly higher than the PGP + CHT + 200 nM antibody at 23.9 ± 0.96 CFU/mL. When statistical analysis of the sensitivities and LODs were conducted it was determined that the two different treatments were not

statistically significant. Implying that other bio-recognition agents or even immunosensing agents could be adhered to the PGP + CHT platform and have similar detection capabilities. Even though the aptamers had a slightly higher LOD than the antibodies, due to specificity, the advantages of working with aptamers surpass this difference, in terms of cost, simplicity in attachment chemistry, durability, etc.

The PGP + 400 nM thiol aptamer and PGP + CHT + 100 nM aptamer sensors were comparable to each other and had significantly lower LOD values than the other two PGP platform sensors tested in PBS. However, when the PGP + CHT + 100 nM aptamer and PGP + CHT + 200 nM antibody sensors were tested in a real world sample, vegetable broth, the antibody sensor showed a lower LOD. The biosensors developed in this research for bacterial targets were shown to be viable concepts to expand upon for detection of other pathogens in complex food systems. The aptamer-based biosensors for the detection of *L. innocua* and *L. monocytogenes* could easily be changed to detect other bacteria simply by modifying the aptamer's specificity. In comparison to other biosensors in the literature the studied biosensors have competitive LOD and range of detection values. Along with that the biosensors created in this study all had an easy to follow impedance test procedure, low limit of detection and a short response time per test making these biosensors more feasible for everyday use and perhaps with more testing these sensors could one day replace the standard methods of detection that are currently being used by the food industry.

REFERENCES

Abdelhamid, HN, & Wu, H-F. (2013). Multifunctional graphene magnetic nanosheet decorated with chitosan for highly sensitive detection of pathogenic bacteria. *Journal of Materials Chemistry B, 1*(32), 3950-3961. doi: 10.1039/C3TB20413H

Abdollahi, M, Rezaei, M, & Farzi, G. (2014). Influence of chitosan/clay functional bionanocomposite activated with rosemary essential oil on the shelf life of fresh silver carp. *International journal of food science & technology, 49*(3), 811-818. doi: 10.1111/ijfs.12369

Abubakar, I, Irvine, L, Aldus, C, Wyatt, G, Fordham, R, Schelenz, S, . . . Hunter, P. (2007). A systematic review of the clinical, public health and cost-effectiveness of rapid diagnostic tests for the detection and identification of bacterial intestinal pathogens in faeces and food. *Health Technology Assessment, 11*(36), 1-185.

Ali, G, Oh, SH, Kim, SY, Kim, JY, Cho, BW, & Chung, KY. (2015). An open-framework iron fluoride and reduced graphene oxide nanocomposite as a high-capacity cathode material for Na-ion batteries. *Journal of Materials Chemistry A, 3*(19), 10258-10266. doi: 10.1039/c5ta00643k

AOAC. (1990b). Official method 990.12. Aerobic Plate Count in Foods. from International Association of Offical Analytical Chemists

Aptagen. (2015). Apta-Index: Internalin A of Listeria monocytogenes Retrieved 16 July 2014, from http://aptagen.com/aptamer-index/aptamer-details.aspx?id=404

Arora, P, Sindhu, A, Dilbaghi, N, & Chaudhury, A. (2011). Review: Biosensors as innovative tools for the detection of food borne pathogens. *Biosensors and Bioelectronics, 28*, 1-12. doi: 10.1016/j.bios.2011.06.002

Avetta, P, Nisticò, R, Calza, P, Fabbri, D, Magnacca, G, Faga, MG, . . . Martorana, S. (2014). Hernia-repair prosthetic devices functionalised with chitosan and ciprofloxacin coating: Controlled release and antibacterial activity. *Journal of Materials Chemistry B, 2*(32), 5287-5294. doi: 10.1039/c4tb00236a

Bai, S, Zhao, J, Zhang, Y, Huang, W, Xu, S, Chen, H, . . . Deng, XW. (2010). Rapid and reliable detection of 11 food-borne pathogens using thin-film biosensor chips. *Applied microbiology and biotechnology*.

Bajwa, A, Tan, ST, Bahreyni, B, & Mehta, R. (2013). Rapid detection of viable microorganisms based on a plate count technique using arrayed microelectrode. *Sensors (Switzerland), 13*(7), 8188-8198. doi: 10.3390/s130708188

Bakthavathsalam, P, Rajendran, VK, Saran, U, Chatterjee, S, & Jaffar Ali, BM. (2013). Immunomagnetic nanoparticle based quantitative PCR for rapid detection of Salmonella. *Microchimica Acta, 180*(13-14), 1241-1248. doi: 10.1007/s00604-013-1052-1

Balamurugan, S, Obubuafo, A, Soper, SA, & Spivak, DA. (2008). Surface immobilization methods for aptamer diagnostic applications. *Analytical and bioanalytical chemistry*.

Banica, F-G. (2012). *Chemical sensors and biosensors. [electronic resource] : fundamentals and applications*: West Sussex, United Kingdom : John Wiley & Sons, c2012.

Barsoukov, E, & Macdonald, JR. (2005). *Impedance spectroscopy. [electronic resource] : theory, experiment, and applications* (2nd ed. ed.). Hoboken, N.J: Wiley-Interscience.

Becker, C. (2003). Bloodless coup. Funded by the Army, Oregon researchers turn to the sea to develop a revolutionary bandage that stanches heavy bleeding. *Modern Healthcare, 33*(28), 30.

Belgacem, MN, & Gandini, A. (2008). *Monomers, polymers and composites from renewable resources* (1st ed.). Boston, MA: Elsevier.

Bin Mohd Yusoff, AR, Kim, D, Jang, J, Schneider, FK, & Da Silva, WJ. (2015). Au-doped single layer graphene nanoribbons for a record-high efficiency ITO-free tandem polymer solar cell. *Energy and Environmental Science, 8*(5), 1523-1537. doi: 10.1039/c5ee00749f

Binsi, PK, Ravishankar, CN, & Srinivasa Gopal, TK. (2013). Development and characterization of an edible composite film based on chitosan and virgin coconut oil with improved moisture sorption properties. *Journal Of Food Science, 78*(4), E526-E534. doi: 10.1111/1750-3841.12084

Braiek, M, Rokbani, K, Chrouda, A, Mrabet, B, Bakhrouf, A, Maaref, A, & Jaffrezic-Renault, N. (2012). An Electrochemical Immunosensor for Detection of Staphylococcus aureus Bacteria Based on Immobilization of Antibodies on Self-Assembled Monolayers-Functionalized Gold Electrode. *Biosensors (2079-6374), 2*(4), 417-426. doi: 10.3390/bios2040417

Burrs, SL, Vanegas, DC, Bhargava, M, Mechulan, N, Hendershot, P, Yamaguchi, H, . . . McLamore, ES. (2015). A comparative study of graphene-hydrogel hybrid bionanocomposites for biosensing. *Analyst, 140*(5), 1466-1476. doi: 10.1039/C4AN01788A

CDC. (2015). Listeria (Listeriosis). Retrieved 16 July 2014, from http://www.cdc.gov/listeria/

Chandy, T, Rao, GHR, Wilson, RF, & Das, GS. (2002). Delivery of LMW Heparin via Surface Coated Chitosan/peg-Alginate Microspheres Prevents Thrombosis. *Drug Delivery, 9*(2), 87-96. doi: 10.1080/10426500290095584

Chellat, F, Tabrizian, M, Yahia, L, Dumitriu, S, Chornet, E, & Rivard, CH. (2000). Study of biodegradation behavior of Chitosan-Xanthan microspheres in simulated physiological media. *Journal of Biomedical Materials Research, 53*(5), 592-599. doi: 10.1002/1097-4636(200009)53:5<592::AID-JBM20>3.0.CO;2-P

Chemburu, S, Wilkins, E, & Abdel-Hamid, I. (2005). Detection of pathogenic bacteria in food samples using highly-dispersed carbon particles. *Biosensors and Bioelectronics, 21*, 491-499. doi: 10.1016/j.bios.2004.11.025

Chen, A, & Holt-Hindle, P. (2010). Platinum-based nanostructured materials: Synthesis, properties, and applications. *Chemical Reviews, 110*(6), 3767-3804. doi: 10.1021/cr9003902

Chen, RH, Domard, A, Muzzarelli, RAA, Tokura, S, & Wang, DM. (2011). Advances in chitin/chitosan science and their applications. *Carbohydrate Polymers, 84*(2), 695. doi: 10.1016/j.carbpol.2010.11.049

Cheng, C, Gao, Z, Peng, Y, Bai, J, Liu, Y, Fan, X, . . . Zhang, X. (2014). Rapid detection of Listeria monocytogenes in milk by self-assembled electrochemical immunosensor. *Sensors and Actuators, B: Chemical, 190*, 900-906. doi: 10.1016/j.snb.2013.09.041

Chirkov, S. (2002). The antiviral activity of chitosan (review). *Applied Biochemistry And Microbiology, 38*(1), 1-8.

Choi, W, & Lee, J-w. (2012). *Graphene : synthesis and applications*: Boca Raton : CRC Press, 2012.

Claussen, JC, Kim, SS, Haque, AU, Artiles, MS, Porterfield, DM, & Fisher, TS. (2010). Electrochemical glucose biosensor of platinum nanospheres connected by carbon nanotubes. *Journal of Diabetes Science and Technology, 4*(2), 312-319.

Claussen, JC, Wickner, MM, Fisher, TS, & Porterfield, DM. (2011). Transforming the fabrication and biofunctionalization of gold nanoelectrode arrays into versatile electrochemical glucose biosensors. *ACS Applied Materials & Interfaces, 3*(5), 1765-1770. doi: 10.1021/am200299h

Cressingtion. (2015). Cressington 208HR High Resolution Sputter Coater. 2015, from http://cressington.com/

Cuero, RG, Duffus, E, Osuji, G, & Pettit, R. (1991). Aflatoxin control in preharvest maize: effects of chitosan and two microbial agents. *Journal of agricultural science*.

Cui, L, Jia, J, Guo, Y, Liu, Y, & Zhu, P. (2014). Preparation and characterization of IPN hydrogels composed of chitosan and gelatin cross-linked by genipin. *Carbohydrate Polymers, 99*, 31-38. doi: 10.1016/j.carbpol.2013.08.048

Cummins, M, Dogovski, C, Robert, R, Alderton, M, Chong, D, Proll, D, . . . Dolezal, O. (2014). Kinetic Characterization of a Panel of High-Affinity Monoclonal Antibodies Targeting Ricin and Recombinant Re-Formatting for Biosensor Applications. *Antibodies (2073-4468), 3*(2), 215-231. doi: 10.3390/antib3020215

Cunningham, AJ. (1998). *Introduction to bioanalytical sensors*. New York, NY: Wiley.

Daniels, J, & Pourmand, N. (2007). Label-free impedance biosensors: opportunities and challenges. *ELECTROANALYSIS, 19*(12), 1239-1257.

Darmadji, P, & Izumimoto, M. (1994). Effect of chitosan in meat preservation. *Meat science*.

De Vittorio, M, Martiradonna, L, & Assad, J. (2014). *Nanotechnology and Neuroscience: Nano-electronic, Photonic and Mechanical Neuronal Interfacing*. New York: Springer.

Devlieghere, F, Vermeulen, A, & Debevere, J. (2004). Chitosan: antimicrobial activity, interactions with food components and applicability as a coating on fruit and vegetables. *Food Microbiology, 21*, 703-714. doi: 10.1016/j.fm.2004.02.008

Doyle, MP, & Buchanan, R. (2013). *Food Microbiology. [electronic resource] : Fundamentals and Frontiers* (4th ed. ed.). Washington, DC: American Society for Microbiology Press.

Du, Y, Luo, X-L, Xu, J-J, & Chen, H-Y. (2007). A simple method to fabricate a chitosan-gold nanoparticles film and its application in glucose biosensor. *Bioelectrochemistry, 70*, 342-347. doi: 10.1016/j.bioelechem.2006.05.002

Duan, N, Wu, S, Dai, S, Miao, T, Chen, J, & Wang, Z. (2015). Simultaneous detection of pathogenic bacteria using an aptamer based biosensor and dual fluorescence resonance energy transfer from quantum dots to carbon nanoparticles. *Microchimica Acta, 182*(5/6), 917-923. doi: 10.1007/s00604-014-1406-3

Eun Jeong, HEO, Bo Ra, S, Hyun Jung, P, Young Jo, KIM, Jin San, M, Sung Hwan, WEE, . . . Yohan, Y. (2014). Rapid Detection of Listeria monocytogenes by Real-Time PCR in Processed Meat and Dairy Products. *Journal of Food Protection, 77*(3), 453-458. doi: 10.4315/0362-028X.JFP-13-318

Farber, JM, & Peterkin, PI. (1991). Listeria monocytogenes, a food-borne pathogen. *Microbiological Reviews, 55*(3), 476-511.

FDA. (2008). *Guidance for Industry: Control of Listeria monocytogenes in Refrigerated or Frozen Ready-To-Eat Foods; Draft Guidance*. Retrieved from http://www.fda.gov/Food/GuidanceRegulation/GuidanceDocumentsRegulatoryInformation/FoodProcessingHACCP/ucm073110.htm#monitor.

FDA. (2015). *Food Safety Modernization Act (FSMA)*. Retrieved from http://www.fda.gov/Food/GuidanceRegulation/FSMA/ucm256826.htm#prevention.

Fink, H-W, & Schonenberger, C. (1999). Electrical conduction through DNA molecules. *Nature, 398*(6726), 407.

FSIS, U. (2013). Media and Reagents. In L. Q. Staff (Ed.), Laboratory Guidebook. Athens, GA: United States Department of Agriculture.

Gao, J, Chen, Y, Liu, C, Miao, L, & Wang, X. (2015). Free-Standing Reduced Graphene Oxide Paper with High Electrical Conductivity. *Journal of Electronic Materials*, 6p. doi: 10.1007/s11664-015-4000-5

Genelink. (2004). Oligo Synthesis. Retrieved 1/20/2014, from http://www.genelink.com/Literature/ps/R26-6400-XXA.pdf

Georgakilas, V. (2014). *Functionalization of graphene*: Weinheim : Wiley-VCH, c2014.

Gibson, D, Coombs, P, & Pimbley, D. (1992). Automated Conductance Method for the Detection of Salmonella in Foods - Collaborative Study. *JOURNAL OF AOAC INTERNATIONAL, 75*(2), 293-302.

Hamann, CH, Hamnett, A, & Vielstich, W. (2007). *Electrochemistry* (2nd ed.). Weinheim: Wiley-VCH.

Hamula, CLA, Zhang, H, Li, F, Wang, Z, Chris Le, X, & Li, X-F. (2011). Selection and analytical applications of aptamers binding microbial pathogens. *In-Vivo and On-Site Analysis II, 30*(10), 1587-1597. doi: 10.1016/j.trac.2011.08.006

HEB. (2015). H‑E‑B Vegetable Broth. Retrieved 11/30/2015, 2015, from https://www.heb.com/product-detail/h-e-b-vegetable-broth/1605840

Hernández, R, Xavier Rius, F, Riu, J, Vallés, C, Benito, AM, & Maser, WK. (2014). Graphene-based potentiometric biosensor for the immediate detection of living bacteria. *Biosensors and Bioelectronics, 54*, 553-557. doi: 10.1016/j.bios.2013.11.053

Hirano, S, Itakura, C, Seino, H, Akiyama, Y, Nonaka, I, Kanbara, N, & Kawakami, T. (1990). Chitosan as an ingredient for domestic animal feeds. *Journal of agricultural and food chemistry (USA)*.

Howling, GI, Dettmar, PW, Goddard, PA, Hampson, FC, Dornish, M, & Wood, EJ. (2001). The effect of chitin and chitosan on the proliferation of human skin fibroblasts and keratinocytes in vitro. *Biomaterials, 22*, 2959-2966. doi: 10.1016/S0142-9612(01)00042-4

Huang, J, Yang, G, Meng, W, Wu, L, Zhu, A, & Jiao, Xa. (2010). An electrochemical impedimetric immunosensor for label-free detection of Campylobacter jejuni in diarrhea patients' stool based on O-carboxymethylchitosan surface modified Fe3O4 nanoparticles. *Biosensors and Bioelectronics, 25*, 1204-1211. doi: 10.1016/j.bios.2009.10.036

Hudson, S, & Smith, C. (1998). *Polysaccharides: Chitin and Chitosan: Chemistry and Technology of Their Use As Structural Materials*. Berlin: Springer.

Hughes, K. (2002). Chitosan and Dietary Fibers. *Prepared Foods, 171*(7), NS11.

Ito, M, Ban, A, & Ishihara, M. (2000). Anti-ulcer Effects of Chitin and Chitosan, Healthy Foods, in Rats. [Anti-ulcer Effects of Chitin and Chitosan, Healthy Foods, in Rats.]. *The Japanese Journal of Pharmacology, 82*(3), 218-225. doi: 10.1254/jjp.82.218

Jantra, J, Kanatharana, P, Asawatreratanakul, P, Thavarungkul, P, Hedstrom, M, & Mattiasson, B. (2011). Real-time label-free affinity biosensors for enumeration of total bacteria based on immobilized concanavalin A. *Journal of Environmental Science and Health - Part A Toxic/Hazardous Substances and Environmental Engineering, 46*(13), 1450-1460. doi: 10.1080/10934529.2011.609022

Jayasena, SD. (1999). Aptamers: An emerging class of molecules that rival antibodies in diagnostics. *Clinical Chemistry, 45*(9), 1628-1650.

Kamil, JYVA, Shahidi, F, & Jeon, YJ. (2002). Chitosan as an edible invisible film for quality preservation of herring and Atlantic cod. *Journal of Agricultural and Food Chemistry, 50*(18), 5167-5178. doi: 10.1021/jf011693l

Kärkkäinen, RM, Drasbek, MR, McDowall, I, Smith, CJ, Young, NWG, & Bonwick, GA. (2011). Aptamers for safety and quality assurance in the food industry: detection of pathogens. *International journal of food science & technology*(3).

Karteri, İ, Karataş, Ş, Al-Ghamdi, AA, & Yakuphanoğlu, F. (2015). The electrical characteristics of thin film transistors with graphene oxide and organic insulators. *Synthetic Metals, 199*, 241-245. doi: 10.1016/j.synthmet.2014.11.036

Kedzierski, S, Khoshnejad, M, & Caltagirone, GT. (2012). Synthetic Antibodies: The Emerging Field of Aptamers. *BioProcessing Journal, 11*(4), 46-49.

Keefe, AD, Pai, S, & Ellington, A. (2010). Aptamers as therapeutics. *Nat Rev Drug Discov, 9*(7), 537-550.

Kelland, L. (2007). The resurgence of platinum-based cancer chemotherapy. *Nature Reviews Cancer, 7*(8), 573-584. doi: 10.1038/nrc2167

Khezrian, S, Salimi, A, Teymourian, H, & Hallaj, R. (2013). Label-free electrochemical IgE aptasensor based on covalent attachment of aptamer onto multiwalled carbon nanotubes/ionic liquid/chitosan nanocomposite modified electrode. *Biosensors and Bioelectronics, 43*(0), 218-225. doi: 10.1016/j.bios.2012.12.006

Khoushab, F, & Yamabhai, M. (2010). Chitin Research Revisited. *Marine Drugs, 8*(7), 1988-2012. doi: 10.3390/md8071988

Kim, JH, Shin, JH, Lee, HJ, Lee, HJ, & Chung, IS. (1997). Effect of chitosan on indirubin production from suspension culture of Polygonum tinctorium. *Journal of Fermentation and Bioengineering, 83*(2), 206-208. doi: 10.1016/S0922-338X(97)83585-4

Kornacki, JL. (2005). Controlling listeria in the food processing environment. *Food technology*(11).

KPL. FAQs: Affinity Purified Antibodies and Conjugates.

KPL. ReserveAP Phosphatase-Labeled Antibody To Listeria. In I. KPL (Ed.). Gaithersburg, MD.

KPL. (2015). BacTrace Anti-Listeria Antibody, High Sensitivity. Retrieved 10/20/2013, 2013, from https://www.kpl.com/catalog/productdetail.cfm?catalog_id=17&Category_ID=535&Product_ID=1464

Kriegel, C, Arrechi, A, Kit, K, McClements, DJ, & Weiss, J. (2008). Fabrication, Functionalization, and Application of Electrospun Biopolymer Nanofibers. *Critical reviews in food science and nutrition, 48*(8), 775-797.

Lahiji, A, Sohrabi, A, Hungerford, DS, & Frondoza, CG. (2000). Chitosan supports the expression of extracellular matrix proteins in human osteoblasts and chondrocytes. *Journal of Biomedical Materials Research, 51*(4), 586-595. doi: 10.1002/1097-4636(20000915)51:4<586::AID-JBM6>3.0.CO;2-S

Lee, KY, Kwon, IC, Kim, YH, Jeong, SY, & Jo, WH. (1998). Preparation of chitosan self-aggregates as a gene delivery system. *Journal of Controlled Release, 51*(2-3), 213-220. doi: 10.1016/S0168-3659(97)00173-9

Lee, TC, Niederer, PF, & Reilly, RB. (2010). Biosensors. *Studies in Health Technology & Informatics, 152*, 109-118.

Li, S, Yan, Y, Zhong, L, Sang, Y, Cheng, W, Ding, S, & Liu, P. (2015). Electrochemical sandwich immunoassay for the peptide hormone prolactin using an electrode modified with graphene, single walled carbon nanotubes and antibody-coated gold nanoparticles. *Microchimica Acta*, 8p. doi: 10.1007/s00604-015-1528-2

Lin, C-W, Wei, K-C, Liao, S-s, Huang, C-Y, Sun, C-L, Wu, P-J, . . . Ma, C-CM. (2015). A reusable magnetic graphene oxide-modified biosensor for vascular endothelial growth factor detection in cancer diagnosis. *Biosensors & Bioelectronics, 67*, 431-437. doi: 10.1016/j.bios.2014.08.080

Lin, J, He, C, Zhao, Y, & Zhang, S. (2009). One-step synthesis of silver nanoparticles/carbon nanotubes/chitosan film and its application in glucose biosensor. *Sensors & Actuators: B. Chemical, 137*, 768-773. doi: 10.1016/j.snb.2009.01.033

Lipman, NS, Jackson, LR, Trudel, LJ, & Weis-Garcia, F. (2005). Monoclonal versus polyclonal antibodies: distinguishing characteristics, applications, and information resources. *ILAR journal*(3).

Liu, CP, Hui, YY, Tang, L, Lau, SP, Chen, ZH, Ren, JG, . . . Zapien, JA. (2013). Solution-processable graphene oxide as an insulator layer for metal-insulator-semiconductor silicon solar cells. *RSC Advances, 3*(39), 17918-17923. doi: 10.1039/c3ra42967a

Liu, JW. (2011). Oligonucleotide-functionalized hydrogels as stimuli responsive materials and biosensors. *Soft Matter, 7*(15), 6757-6767.

Liu, S, Puri, VM, & Demirci, A. (2009). Evaluation of Listeria innocua as a suitable indicator for replacing Listeria monocytogenes during ripening of Camembert cheese. *International journal of food science & technology*.

López-León, T, Carvalho, ELS, Seijo, B, Ortega-Vinuesa, JL, & Bastos-González, D. (2005). Physicochemical characterization of chitosan nanoparticles: electrokinetic and stability behavior. *Journal of Colloid and Interface Science, 283*(2), 344-351. doi: http://dx.doi.org/10.1016/j.jcis.2004.08.186

Lu, C-H, Yang, H-H, Zhu, C-L, Chen, X, & Chen, G-N. (2009). Graphene Platform for Sensing Biomolecules. *Angewandte Chemie*.

Luedtke, A. (2015). Applications of Graphene Oxide and Reduced Graphene Oxide. Retrieved 6/10/2015, 2015, from http://www.sigmaaldrich.com/technical-documents/articles/technology-spotlights/graphene-oxide.html#sthash.1vk90bJ5.dpuf

Lum, JD. (2014). *Impedance Biosensors for the Rapid Detection of Viral and Bacterial Pathogens Using Avian Influenza Virus Subtypes H5N1 and H7N2 and Escherichia coli O157:H7 as Model Targets.* (PhD Dissertation), University of Arkansas.

Luo, X-L, Xu, J-J, Du, Y, & Chen, H-Y. (2004). A glucose biosensor based on chitosan–glucose oxidase–gold nanoparticles biocomposite formed by one-step electrodeposition. *Analytical Biochemistry, 334*, 284-289. doi: 10.1016/j.ab.2004.07.005

Lvovich, VF. (2012). *Impedance spectroscopy. [electronic resource] : applications to electrochemical and dielectric phenomena*: Hoboken, N.J. : Wiley, c2012.

Ma, R, Pang, X, & Zhitomirsky, I. (2011). Electrodeposition of biopolymer films containing haemoglobin. *Surface Engineering, 27*(9), 693-697. doi: 10.1179/1743294411Y.0000000018

MacDonald, MA, & Andreas, HA. (2014). Method for equivalent circuit determination for electrochemical impedance spectroscopy data of protein adsorption on solid surfaces. *Electrochimica Acta, 129*, 290-299. doi: 10.1016/j.electacta.2014.02.046

Martinon Gaspar, M, & Moreira, RG. (2012). *Edible coating development for fresh-cut cantaloupe. [electronic resource]*: [College Station, Tex. : Texas A&M University, 2012].

McDonald, D, & Hunt, LB. (1982). *A History of Platinum and its allied metals*. England: Johnson Matthey.

McLamore, ES, Shi, J, Jaroch, D, Claussen, JC, Uchida, A, Jiang, Y, . . . Porterfield, DM. (2011). A self referencing platinum nanoparticle decorated enzyme-based microbiosensor for real time measurement of physiological glucose transport. *Biosensors and Bioelectronics, 26*, 2237-2245. doi: 10.1016/j.bios.2010.09.041

Meng, X, Yang, L, Kennedy, JF, & Tian, S. (2010). Effects of chitosan and oligochitosan on growth of two fungal pathogens and physiological properties in pear fruit. *Carbohydrate Polymers, 81*, 70-75. doi: 10.1016/j.carbpol.2010.01.057

Milner, ST. (1991). Polymer Brushes. *American Society for the Advancement of Science*, 905.

Minett, AI, Barisci, JN, & Wallace, GG. (2003). Coupling conducting polymers and mediated electrochemical responses for the detection of Listeria. *Analytica Chimica Acta, 475*, 37-45. doi: 10.1016/S0003-2670(02)01033-4

Mishra, SB, Mishra, AK, & Tiwari, A. (2011). Current Frontiers in Electrochemical Biosensors Using Chitosan Nanocomposites *Biosensor Nanomaterials* (pp. 237-246): Wiley-VCH Verlag GmbH & Co. KGaA.

Moreira, MdR, Roura, SI, & Ponce, A. (2011). Effectiveness of chitosan edible coatings to improve microbiological and sensory quality of fresh cut broccoli. *LWT - Food Science and Technology, 44*(10), 2335-2341. doi: http://dx.doi.org/10.1016/j.lwt.2011.04.009

Muzzarelli, R, Boudrant, J, Meyer, D, Manno, N, DeMarchis, M, & Paoletti, M. (2012). Review: Current views on fungal chitin/chitosan, human chitinases, food preservation, glucans, pectins and inulin: A tribute to Henri Braconnot, precursor of the carbohydrate polymers science, on the chitin bicentennial. *Carbohydrate Polymers, 87*, 995-1012. doi: 10.1016/j.carbpol.2011.09.063

Muzzarelli, RAA, Frega, N, Miliani, M, Muzzarelli, C, & Cartolari, M. (2000). Interactions of chitin, chitosan, N-lauryl chitosan and N-dimethylaminopropyl chitosan with olive oil. *Carbohydrate Polymers, 43*, 263-268. doi: 10.1016/S0144-8617(00)00170-3

Ni, X, Castanares, M, Mukherjee, A, & Lupold, SE. (2011). Nucleic acid aptamers: clinical applications and promising new horizons. *Current Medicinal Chemistry, 18*(27), 4206-4214.

Niaounakis, M. (2015). *Biopolymers : processing and products*: Oxford, U.K. ; Burlington, MA : William Andrew, [2015].

Oh, HI, Kim, YJ, Chang, EJ, & Kim, JY. (2001). Antimicrobial characteristics of chitosans against food spoilage microorganisms in liquid media and mayonnaise. *Bioscience, Biotechnology, and Biochemistry (Japan)*.

Ohk, SH, Koo, OK, Sen, T, Yamamoto, CM, & Bhunia, AK. (2010). Antibody–aptamer functionalized fibre-optic biosensor for specific detection of Listeria monocytogenes from food. *Journal of Applied Microbiology, 109*(3), 808-817. doi: 10.1111/j.1365-2672.2010.04709.x

Ottenbrite, RM, Huang, SJ, & Park, K. (1996). *Hydrogels and biodegradable polymers for bioapplications*: Washington, D.C. : American Chemical Society, 1996.

Ouattara, B, Simard, RE, Piette, G, Bégin, A, & Holley, RA. (2000). Inhibition of surface spoilage bacteria in processed meats by application of antimicrobial films prepared with chitosan. *International Journal of Food Microbiology, 62*, 139-148. doi: 10.1016/S0168-1605(00)00407-4

Park, H-C, Baig, I, Lee, S-C, Moon, J-Y, & Yoon, M-Y. (2014). Development of ssDNA Aptamers for the Sensitive Detection of Salmonella typhimurium and Salmonella enteritidis. *Applied Biochemistry & Biotechnology, 174*(2), 793-802. doi: 10.1007/s12010-014-1103-z

Pendergrast, PS, Marsh, HN, Grate, D, Healy, JM, & Stanton, M. (2005). Nucleic Acid Aptamers for Target Validation and Therapeutic Applications. *Journal of Biomolecular Techniques : JBT, 16*(3), 224-234.

Pospieszny, H. (1997). Antiviroid activity of chitosan. *Crop Protection, 16*(2), 105-106. doi: 10.1016/S0261-2194(96)00077-4

Radhakrishnan, R, Jahne, M, Rogers, S, & Suni, I. (2013). Detection of Listeria Monocytogenes by Electrochemical Impedance Spectroscopy. *ELECTROANALYSIS, 25*(9), 2231-2237.

Ravi Kumar, MNV. (2000). Review: A review of chitin and chitosan applications. *Reactive and Functional Polymers, 46*, 1-27. doi: 10.1016/S1381-5148(00)00038-9

Ren, J, Shi, W, Li, K, & Ma, Z. (2012). Ultrasensitive platinum nanocubes enhanced amperometric glucose biosensor based on chitosan and nafion film. *Sensors & Actuators: B. Chemical, 163*, 115-120. doi: 10.1016/j.snb.2012.01.017

Rinaudo, M. (2006). Chitin and chitosan: Properties and applications. *Progress in Polymer Science, 31*, 603-632. doi: 10.1016/j.progpolymsci.2006.06.001

Rodríguez-Núñez, JR, López-Cervantes, J, Sánchez-Machado, DI, Ramírez-Wong, B, Torres-Chavez, P, & Cortez-Rocha, MO. (2012). Antimicrobial activity of chitosan-based films against Salmonella typhimurium and Staphylococcus aureus. *International journal of food science & technology, 47*(10), 2127-2133. doi: 10.1111/j.1365-2621.2012.03079.x

Rong Huei, C, & Hwa, H-D. (1996). Effect of molecular weight of chitosan with the same degree of deacetylation on the thermal, mechanical, and permeability properties of the prepared membrane. *Carbohydrate Polymers, 29*(4), 353-358. doi: http://dx.doi.org/10.1016/S0144-8617(96)00007-0

Sankaranarayanan, S, Venkatraman, K, Sundar Raj, M, & Mohanraj, K. (2014). Graphene/cobalt oxide/polyaniline composites for super-capacitor application. *International Journal of ChemTech Research, 7*(5), 2176-2180.

Sanvicens, N, Pastells, C, Pascual, N, & Marco, MP. (2009). Nanoparticle-based biosensors for detection of pathogenic bacteria. *Trends in Analytical Chemistry, 28*, 1243-1252. doi: 10.1016/j.trac.2009.08.002

Sapsford, KE, Algar, WR, Berti, L, Gemmill, KB, Casey, BJ, Oh, E, . . . Medintz, IL. (2013). Functionalizing nanoparticles with biological molecules: developing chemistries that facilitate nanotechnology. *Chemical Reviews, 113*(3), 1904-2074. doi: 10.1021/cr300143v

Shahdost-fard, F, Salimi, A, Korani, A, & Sharifi, E. (2013). Fabrication of a highly sensitive adenosine aptasensor based on covalent attachment of aptamer onto chitosan-carbon nanotubes-ionic liquid nanocomposite. *Biosensors and Bioelectronics, 48*, 100-107. doi: 10.1016/j.bios.2013.03.060

Shahidi, F, & Abuzaytoun, R. (2005). Chitin, Chitosan, and Co-Products: Chemistry, Production, Applications, and Health Effects *Advances in Food and Nutrition Research* (Vol. Volume 49, pp. 93-135): Academic Press.

Shao, Y, Wang, J, Wu, H, Liu, J, Aksay, I, & Lin, Y. (2010). Graphene Based Electrochemical Sensors and Biosensors: A Review. *ELECTROANALYSIS, 22*(10), 1027-1036.

Shi, J, Marshall Porterfield, D, Zhang, H, Stanciu, LA, Snyder, A, Wang, MX, & Xie, J. (2012). An aqueous media based approach for the preparation of a biosensor platform composed of graphene oxide and Pt-black. *Biosensors and Bioelectronics, 38*(1), 314-320. doi: 10.1016/j.bios.2012.06.007

Simpson, BK, Gagne, N, Ashie, INA, & Noroozi, E. (1997). Utilization of chitosan for preservation of raw shrimp (Pandalus borealis). *Food biotechnology (New York, N.Y.) (USA)*.

Simpson, BK, Gagne, N, & Simpson, MV. (1994). Bioprocessing of chitin and chitosan. In A. M. Martin (Ed.), *Fisheries Processing* (pp. 155-173): Springer US.

Singh, G, Vajpayee, P, Rani, N, Jyoti, A, Gupta, KC, & Shanker, R. (2012). Bio-capture of S. Typhimurium from surface water by aptamer for culture-free quantification. *Ecotoxicology and Environmental Safety, 78*, 320-326. doi: 10.1016/j.ecoenv.2011.11.039

Siriviriyanun, A, Imae, T, & Nagatani, N. (2013). Electrochemical biosensors for biocontaminant detection consisting of carbon nanotubes, platinum nanoparticles, dendrimers, and enzymes. *Analytical Biochemistry, 443*(2), 169-171. doi: 10.1016/j.ab.2013.09.004

Song, S, Wang, L, Li, J, Fan, C, & Zhao, J. (2008). Aptamer-based biosensors. *Trends in Analytical Chemistry, 27*, 108-117. doi: 10.1016/j.trac.2007.12.004

Sugano, M, Fujikawa, T, Hiratsuji, Y, & Hasegawa, Y. (1978). Hypocholesterolemic effects of chitosan in cholesterol fed rats / Hypocholesterolemic effects of chitosan aminosugar in cholesterol fed rats. *Nutrition reports international*.

Taghdisi, SM, Danesh, NM, Lavaee, P, Sarreshtehdar Emrani, A, Ramezani, M, & Abnous, K. (2015). Aptamer Biosensor for Selective and Rapid Determination of Insulin. *Analytical Letters, 48*(4), 672-681. doi: 10.1080/00032719.2014.956216

Tanabe, Y, Yasuda, K, Azuma, C, Taniguro, H, Onodera, S, Suzuki, A, . . . Osada, Y. (2008). Biological responses of novel high-toughness double network hydrogels in muscle and the subcutaneous tissues. *Journal of Materials Science: Materials in Medicine, 19*(3), 1379-1387. doi: 10.1007/s10856-007-3255-7

ThermoFisher. (2014). Real-Time PCR Handbook (pp. 2-3): ThermoFisher Scientific Inc.

ThermoFisher. (2015). General Sandwich ELISA protocol. Retrieved 6/10/15, 2015

Tompkin, RB. (2002). Control of Listeria monocytogenes in the food-processing environment. *Journal of Food Protection, 65*(4), 709-725.

Torres-Chavolla, E, & Alocilja, EC. (2009). Aptasensors for detection of microbial and viral pathogens. *Biosensors and Bioelectronics, 24*(11), 3175-3182. doi: 10.1016/j.bios.2008.11.010

Tsai, Y-C, Chen, S-Y, & Liaw, H-W. (2007). Immobilization of lactate dehydrogenase within multiwalled carbon nanotube-chitosan nanocomposite for application to lactate biosensors. *Sensors & Actuators: B. Chemical, 125*, 474-481. doi: 10.1016/j.snb.2007.02.052

Tsaih, ML, & Chen, RH. (2003). The effect of reaction time and temperature during heterogenous alkali deacetylation on degree of deacetylation and molecular weight of resulting chitosan. *Journal of Applied Polymer Science, 88*(13), 2917-2923. doi: 10.1002/app.11986

USDA. (2012). *The bad bug book: foodborne pathogenic microorganisms and natural toxins handbook* (2 ed.). Washington, D.C.: U.S. Food & Drug Administration, Center for Food Safety & Applied Nutrition.

Vanegas, DC, Taguchi, M, Chaturvedi, P, Burrs, S, McLamore, ES, Tan, M, & Yamaguchi, H. (2014). A comparative study of carbon-platinum hybrid nanostructure architecture for amperometric biosensing. *Analyst, 139*(3), 660-667. doi: 10.1039/c3an01718d

Varshney, M, & Li, Y. (2007). Interdigitated array microelectrode based impedance biosensor coupled with magnetic nanoparticle–antibody conjugates for detection of Escherichia coli O157:H7 in food samples. *Biosensors and Bioelectronics, 22*, 2408-2414. doi: 10.1016/j.bios.2006.08.030

Velusamy, V, Arshak, K, Korostynska, O, Oliwa, K, & Adley, C. (2010). An overview of foodborne pathogen detection: In the perspective of biosensors. *Biotechnology Advances, 28*(2), 232-254. doi: 10.1016/j.biotechadv.2009.12.004

Vermeer, AWP, & Norde, W. (2000). The Thermal Stability of Immunoglobulin: Unfolding and Aggregation of a Multi-Domain Protein. *Biophysical Journal, 78*(1), 394-404. doi: 10.1016/S0006-3495(00)76602-1

Wagner, G, & Guilbault, GG. (1994). *Food biosensor analysis*: New York : M. Dekker, c1994.

Wang, C, Tan, X, Chen, S, Hu, F, Zhong, H, & Zhang, Y. (2012). The Construction of Glucose Biosensor Based on Platinum Nanoclusters-Multiwalled Carbon Nanotubes Nanocomposites. *Applied Biochemistry & Biotechnology, 166*(4), 889-902. doi: 10.1007/s12010-011-9478-6

Wang, J. (2005). Carbon-Nanotube Based Electrochemical Biosensors: A Review. *ELECTROANALYSIS, 17*(1), 7-14. doi: 10.1002/elan.200403113

Wang, J. (2007). Nanoparticle-based electrochemical bioassays of proteins. *ELECTROANALYSIS, 19*(7-8), 769-776. doi: 10.1002/elan.200603789

Wang, R, Ruan, C, Li, Y, Kanayeva, D, & Lassiter, K. (2008). TiO 2 nanowire bundle microelectrode based impedance immunosensor for rapid and sensitive detection of Listeria monocytogenes. *Nano Letters, 8*(9), 2625-2631. doi: 10.1021/nl080366q

Wang, Y, Ye, Z, & Ying, Y. (2012). New Trends in Impedimetric Biosensors for the Detection of Foodborne Pathogenic Bacteria. *Sensors & Actuators: B. Chemical, 12*(3), 3449-3471. doi: 10.3390/s120303449

Wang, YX, Ye, ZZ, & Ying, YB. (2014). Development of a Disposable Impedance Biosensor and its Application for Determination of Escherichia coli O157:H7. *TRANSACTIONS- ASABE, 57*(2), 585-592.

Wang, Z, Zhang, X, Yang, H, Nie, J, Ma, G, & Gu, J. (2014). Electrodeposition of alginate/chitosan layer-by-layer composite coatings on titanium substrates. *Carbohydrate Polymers, 103*(1), 38-45. doi: 10.1016/j.carbpol.2013.12.007

Wedmore, I, McManus, JG, Pusateri, AE, & Holcomb, JB. (2006). A special report on the chitosan-based hemostatic dressing: experience in current combat operations. *The Journal Of Trauma, 60*(3), 655-658.

Wong, E, & Giandornenico, CM. (1999). Current status of platinum-based antitumor drugs. *Chemical Reviews, 99*(9), 2451-2466.

WorldBook. (2014). Platinum: World Book, Inc.

Wu, WH, Li, M, Wang, Y, Ouyang, HX, Wang, L, Li, XC, . . . Lu, JX. (2012). Aptasensors for rapid detection of Escherichia coli O157: H7 and Salmonella typhimurium. *Nanoscale Research Letters, 7*. doi: 10.1186/1556-276X-7-658

Yang, L, & Li, Y. (2005). AFM and impedance spectroscopy characterization of the immobilization of antibodies on indium–tin oxide electrode through self-assembled monolayer of epoxysilane and their capture of Escherichia coli O157:H7. *Biosensors and Bioelectronics, 20*, 1407-1416. doi: 10.1016/j.bios.2004.06.024

Yao, K. (2012). *Chitosan-based hydrogels. [electronic resource] : functions and applications*: Boca Raton, FL : CRC Press, c2012.

Yao, KD, Yin, YJ, Xu, MX, & Wang, YF. (1995). Investigation of pH-sensitive drug delivery system of chitosan/gelatin hybrid polymer network. *Polymer International, 38*(1), 77-82.

Yi, HM, Wu, LQ, Bentley, WE, Ghodssi, R, Rubloff, GW, Culver, JN, & Payne, GF. (2005). Biofabrication with chitosan. *Biomacromolecules, 6*(6), 2881-2894.

Ylitalo, R, Lehtinen, S, Wuolijoki, E, Ylitalo, P, & Lehtimäki, T. (2002). Cholesterol-lowering properties and safety of chitosan. *Arzneimittel-Forschung, 52*(1), 1-7.

Yoon, J, & Kim, B. (2012). Lab-on-a-Chip Pathogen Sensors for Food Safety. *Sensors, 12*(8), 10713-10741.

Zelada-Guillén, GA, Bhosale, SV, Riu, J, & Rius, FX. (2010). Real-time potentiometric detection of bacteria in complex samples. *Analytical Chemistry, 82*(22), 9254-9260. doi: 10.1021/ac101739b

Zeng, Q, Cheng, J-S, Liu, X-F, Bai, H-T, & Jiang, J-H. (2011). Palladium nanoparticle/chitosan-grafted graphene nanocomposites for construction of a glucose biosensor. *Biosensors and Bioelectronics, 26*, 3456-3463. doi: 10.1016/j.bios.2011.01.024

Zhao, L, Wang, ZB, Li, JL, Zhang, JJ, Sui, XL, & Zhang, LM. (2015). A newly-designed sandwich-structured graphene-Pt-graphene catalyst with improved electrocatalytic performance for fuel cells. *Journal of Materials Chemistry A, 3*(10), 5313-5320. doi: 10.1039/c4ta06172a

Zhi, J, Cui, H, Chen, A, Xie, Y, & Huang, F. (2015). Efficient highly flexible dye sensitized solar cells of three dimensional graphene decorated titanium dioxide nanoparticles on plastic substrate. *Journal of Power Sources, 281*, 404-410. doi: 10.1016/j.jpowsour.2015.02.001

APPENDIX

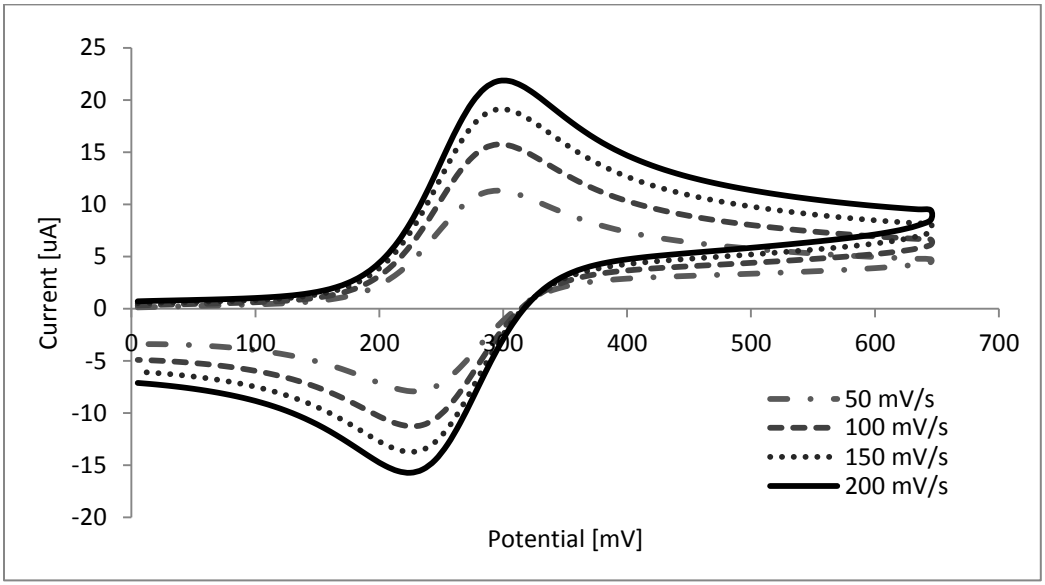

Figure A.1 – Representative cyclic voltammograms of bare electrodes in 4 mM $Fe(CN)_6$/1 M KNO_3 solution at 50, 100, 150 and 200 mV/s scan rates, each test was repeated three times.

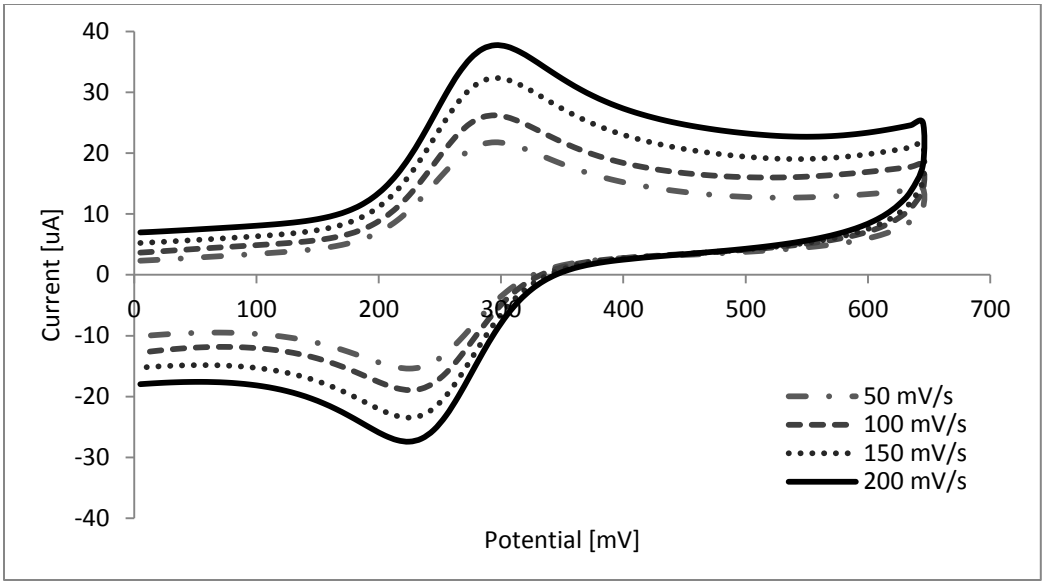

Figure A.2 – Representative cyclic voltammograms of PGP modified electrodes in 4 mM $Fe(CN)_6$/1 M KNO_3 solution at 50, 100, 150 and 200 mV/s scan rates, each test was repeated three times.

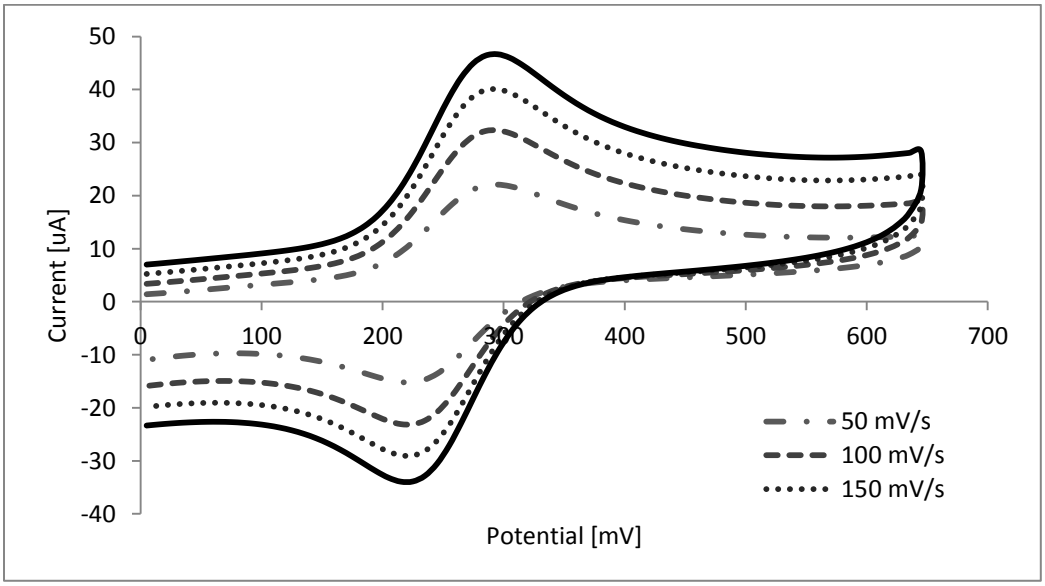

Figure A.3 – Representative cyclic voltammograms of PGP modified electrodes with 50 nM antibody bio-recognition agents in 4 mM $Fe(CN)_6$/1 M KNO_3 solution at 50, 100, 150, 200 mV/s scan rates, each test was repeated three times.

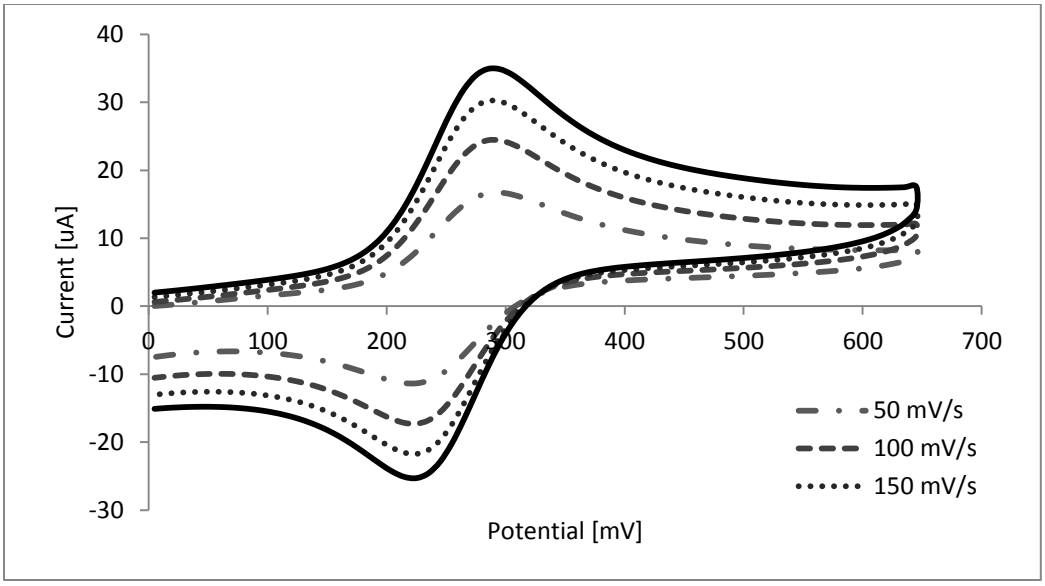

Figure A.4 – Representative cyclic voltammograms of PGP modified electrodes with 100 nM antibody bio-recognition agents in 4 mM $Fe(CN)_6$/1 M KNO_3 solution at 50, 100, 150, 200 mV/s scan rates, each test was repeated three times.

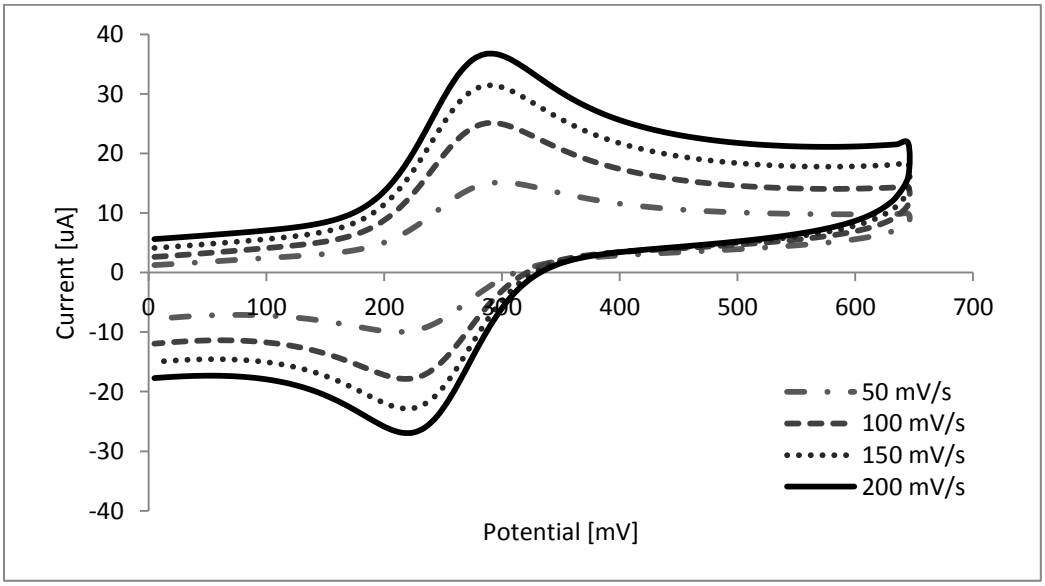

Figure A.5 – Representative cyclic voltammograms of PGP modified electrodes with 200 nM antibody bio-recognition agents in 4 mM $Fe(CN)_6$/1 M KNO_3 solution at 50, 100, 150, 200 mV/s scan rates, each test was repeated three times.

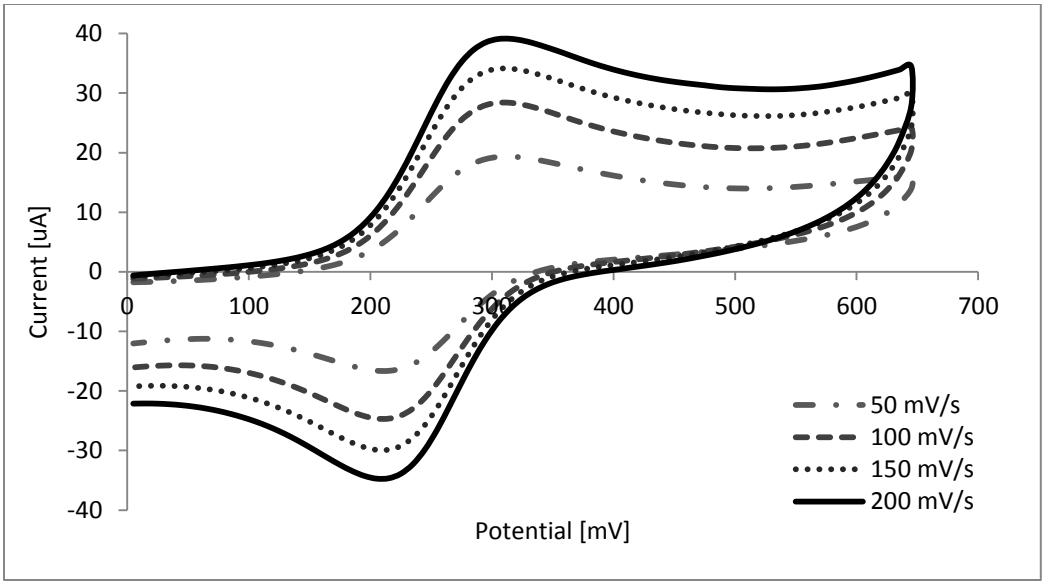

Figure A.6 – Representative cyclic voltammograms of PGP modified electrodes with 100 nM amine aptamer bio-recognition agents in 4 mM $Fe(CN)_6$/1 M KNO_3 solution at 50, 100, 150, 200 mV/s scan rates, each test was repeated three times.

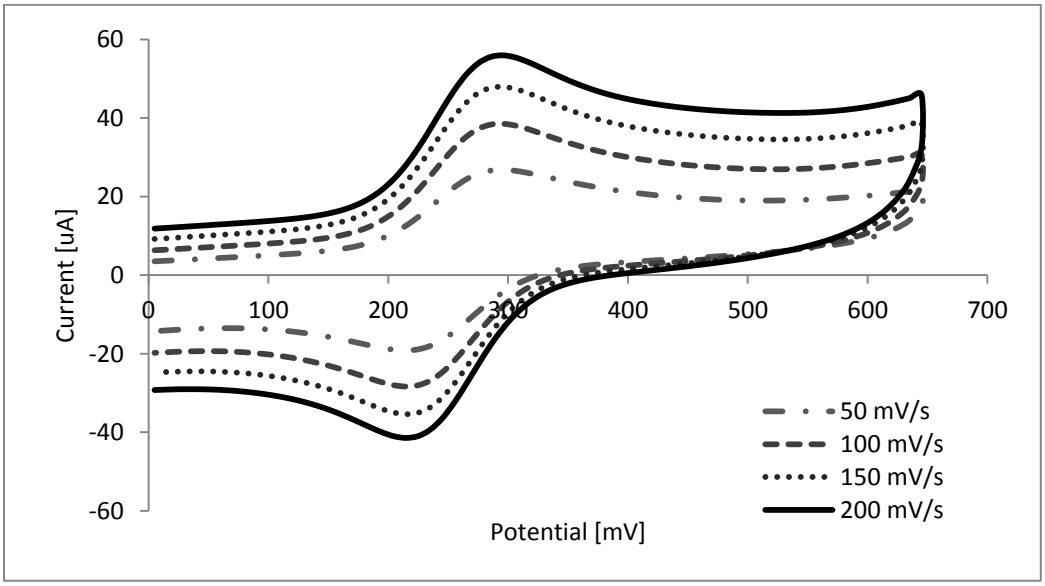

Figure A.7 – Representative cyclic voltammograms of PGP modified electrodes with 200 nM amine aptamer bio-recognition agents in 4 mM $Fe(CN)_6$/1 M KNO_3 solution at 50, 100, 150, 200 mV/s scan rates, each test was repeated three times.

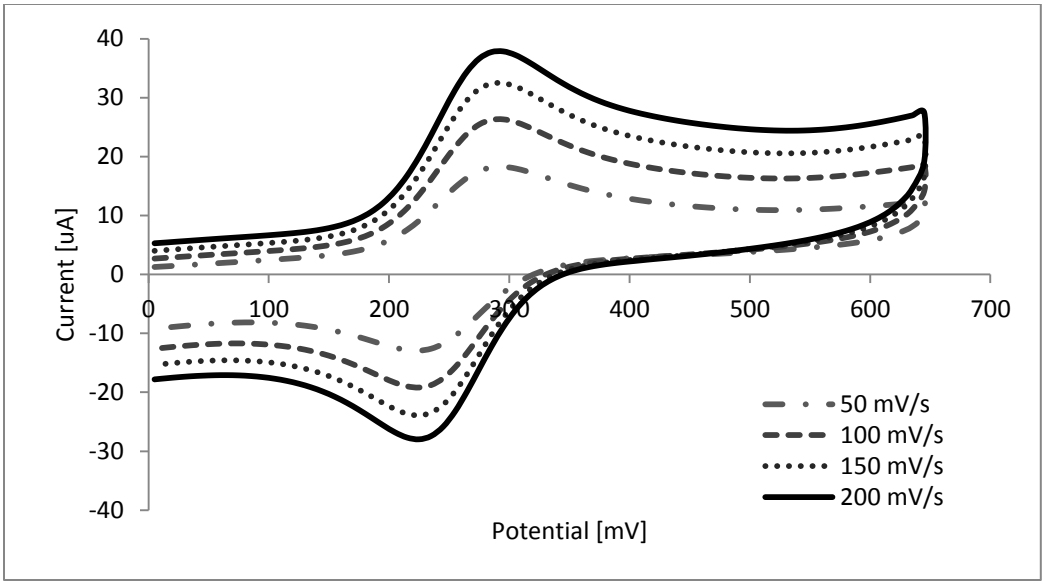

Figure A.8 – Representative cyclic voltammograms of PGP modified electrodes with 400 nM amine aptamer bio-recognition agents in 4 mM $Fe(CN)_6$/1 M KNO_3 solution at 50, 100, 150, 200 mV/s scan rates, each test was repeated three times.

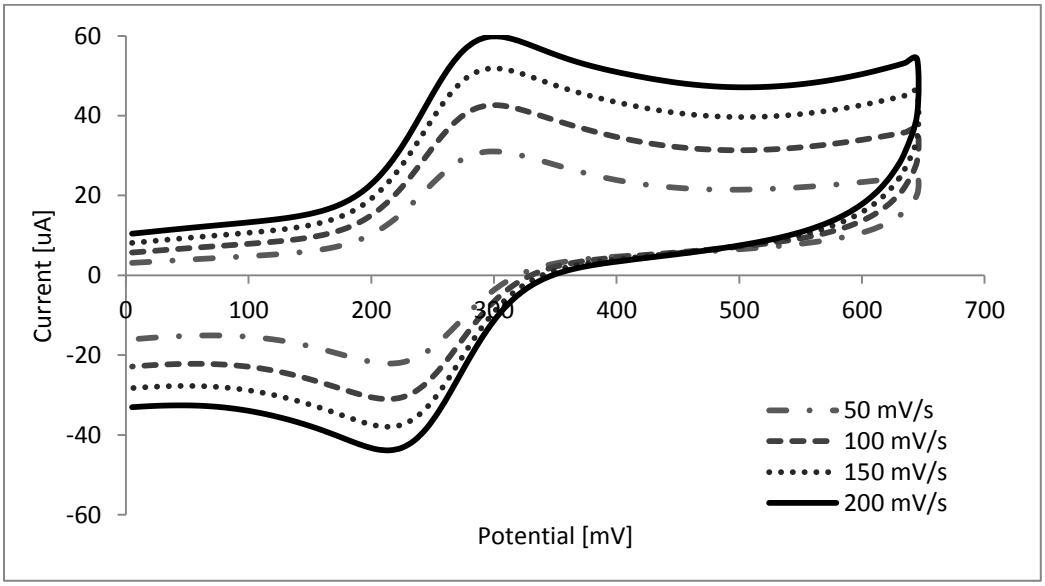

Figure A.9 – Representative cyclic voltammograms of PGP modified electrodes with 100 nM thiol aptamer bio-recognition agents in 4 mM $Fe(CN)_6$/1 M KNO_3 solution at 50, 100, 150, 200 mV/s scan rates, each test was repeated three times.

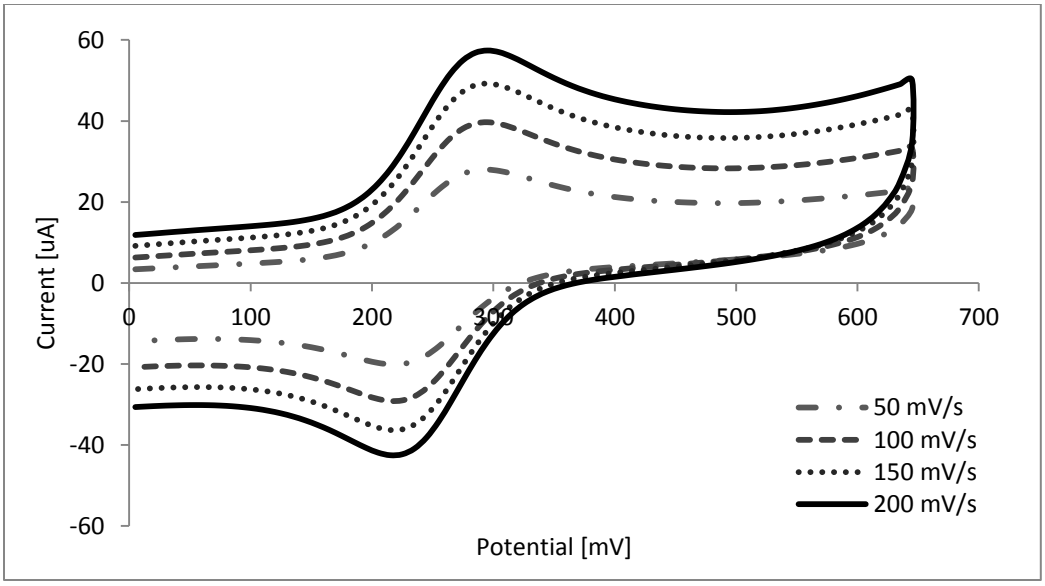

Figure A.10 – Representative cyclic voltammograms of PGP modified electrodes with 200 nM thiol aptamer bio-recognition agents in 4 mM $Fe(CN)_6$/1 M KNO_3 solution at 50, 100, 150, 200 mV/s scan rates, each test was repeated three times.

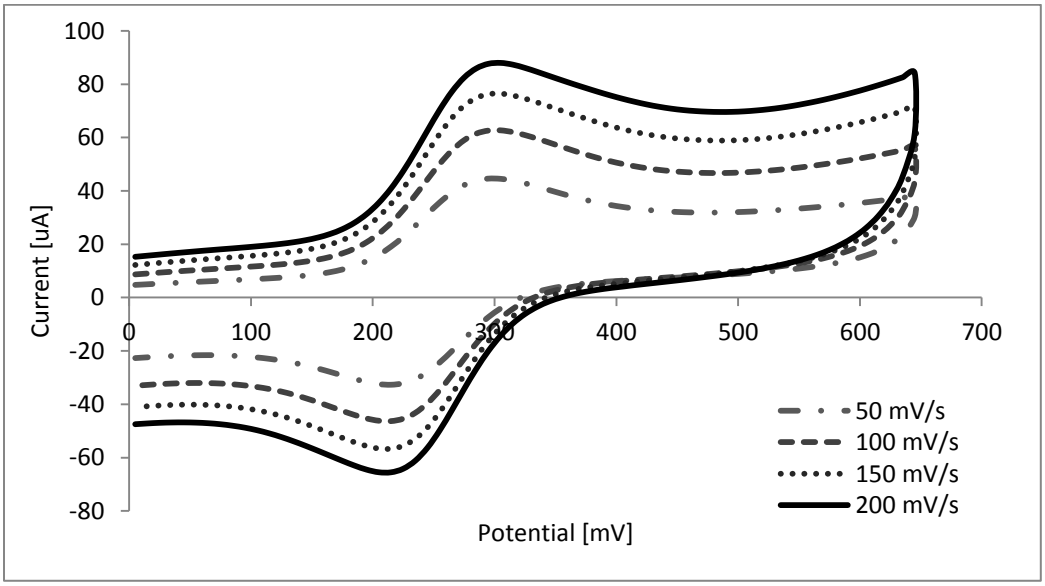

Figure A.11 – Representative cyclic voltammograms of PGP modified electrodes with 400 nM thiol aptamer bio-recognition agents in 4 mM $Fe(CN)_6$/1 M KNO_3 solution at 50, 100, 150, 200 mV/s scan rates, each test was repeated three times.

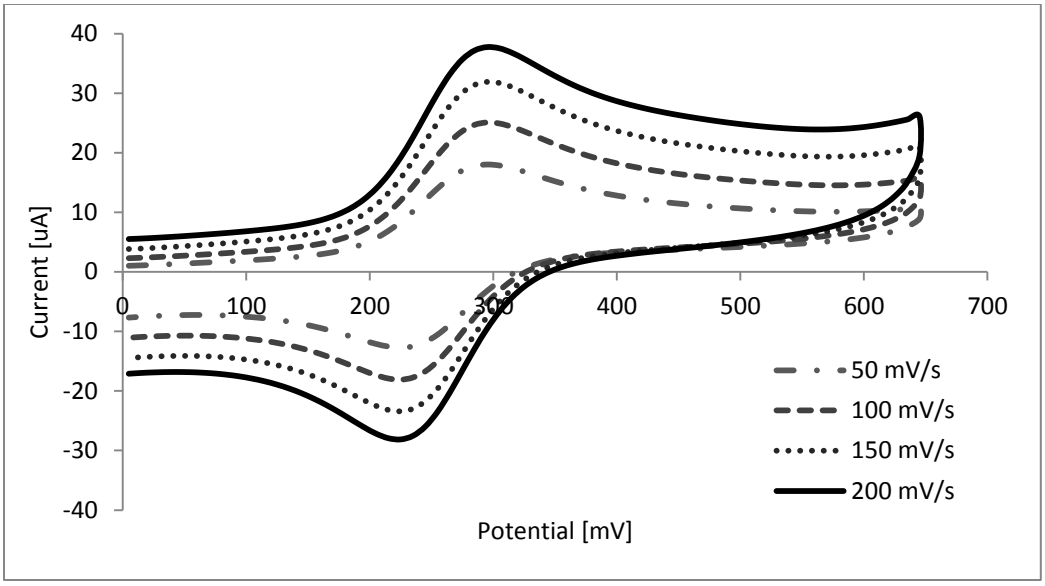

Figure A.12 – Representative cyclic voltammograms of PGP + CHT electrodes in 4 mM $Fe(CN)_6$/1 M KNO_3 solution at 50, 100, 150, 200 mV/s scan rates, each test was repeated three times.

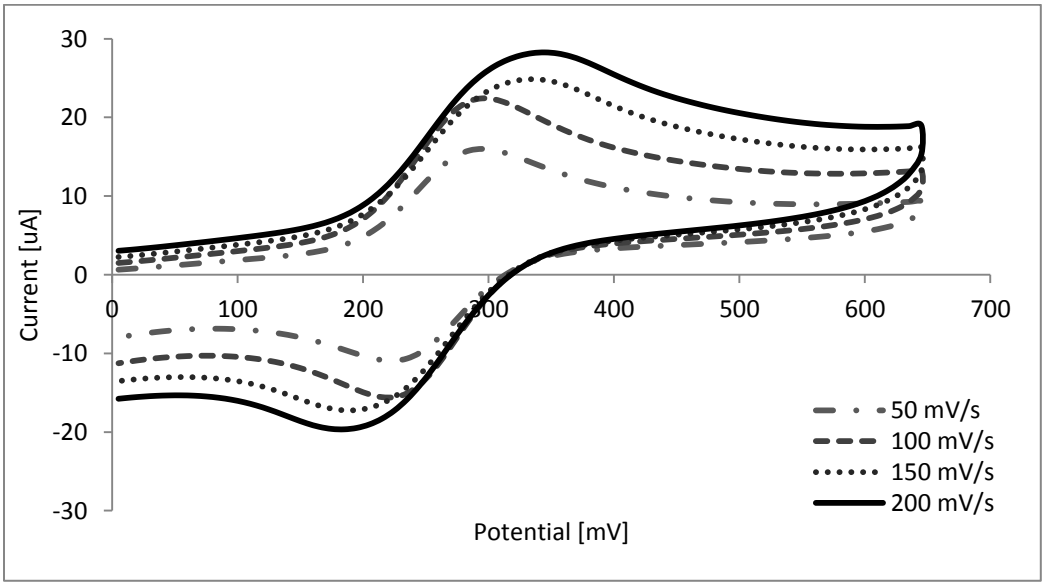

Figure A.13 – Representative cyclic voltammograms of PGP + CHT modified electrodes with 50 nM antibody bio-recognition agents in 4 mM $Fe(CN)_6$/1 M KNO_3 solution at 50, 100, 150, 200 mV/s scan rates, each test was repeated three times.

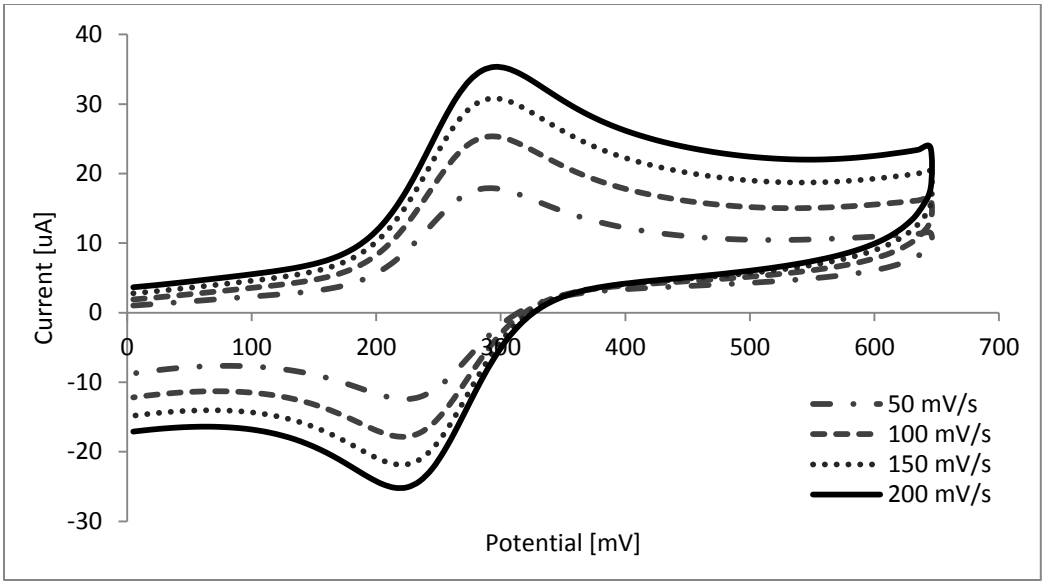

Figure A.14 – Representative cyclic voltammograms of PGP + CHT modified electrodes with 100 nM antibody bio-recognition agents in 4 mM $Fe(CN)_6$/1 M KNO_3 solution at 50, 100, 150, 200 mV/s scan rates, each test was repeated three times.

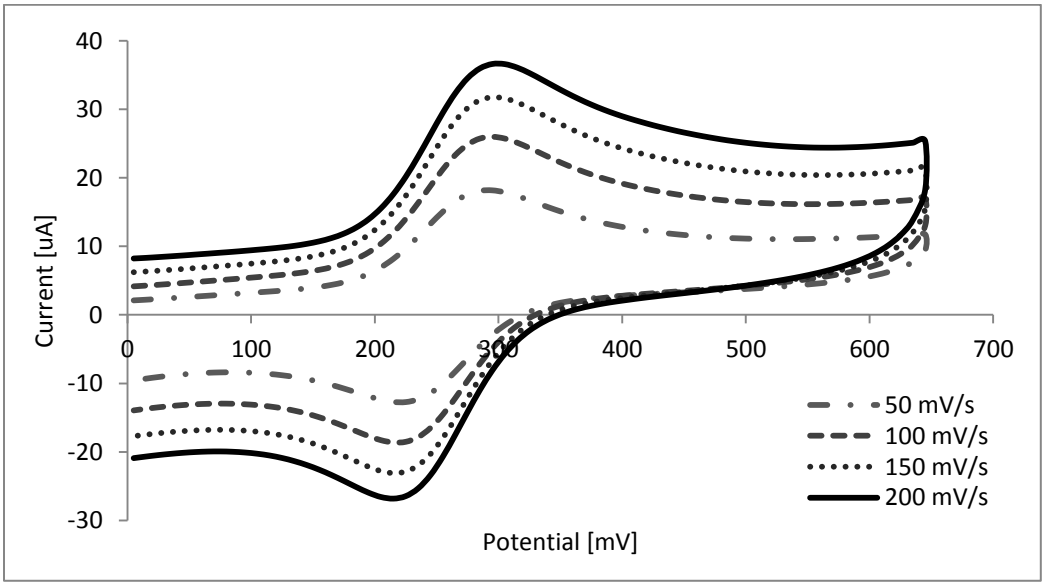

Figure A.15 – Representative cyclic voltammograms of PGP + CHT modified electrodes with 200 nM antibody bio-recognition agents in 4 mM $Fe(CN)_6$/1 M KNO_3 solution at 50, 100, 150, 200 mV/s scan rates, each test was repeated three times.

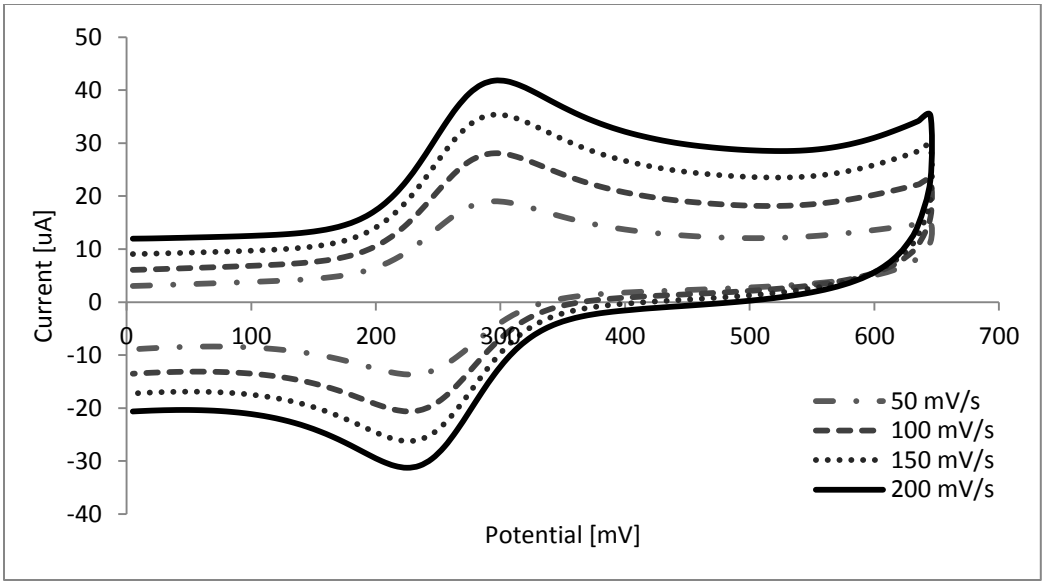

Figure A.16 – Representative cyclic voltammograms of PGP + CHT modified electrodes with 100 nM aptamer bio-recognition agents in 4 mM $Fe(CN)_6$/1 M KNO_3 solution at 50, 100, 150, 200 mV/s scan rates, each test was repeated three times.

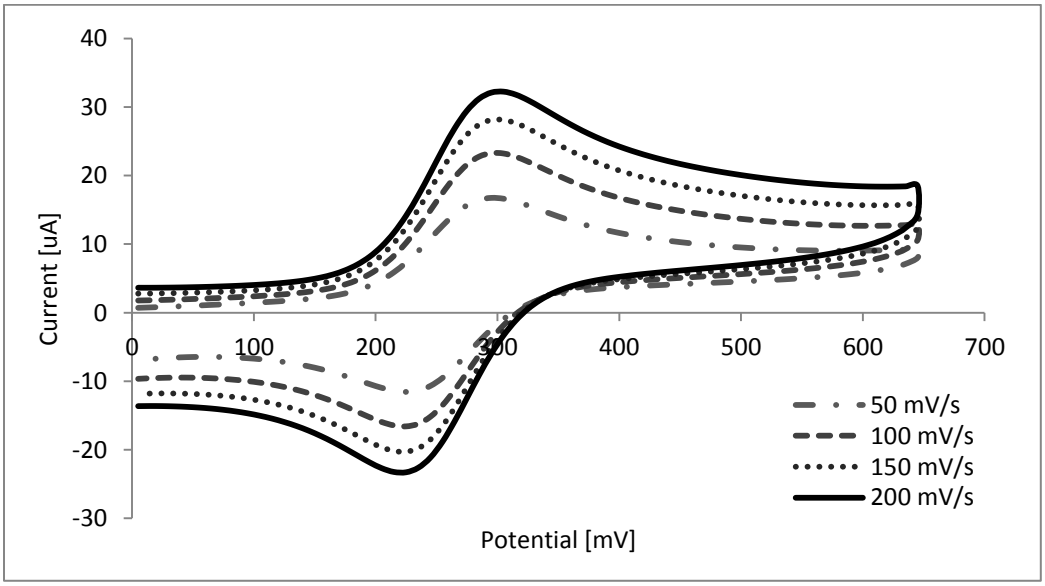

Figure A.17 – Representative cyclic voltammograms of PGP + CHT modified electrodes with 200 nM aptamer bio-recognition agents in 4 mM $Fe(CN)_6$/1 M KNO_3 solution at 50, 100, 150, 200 mV/s scan rates, each test was repeated three times.

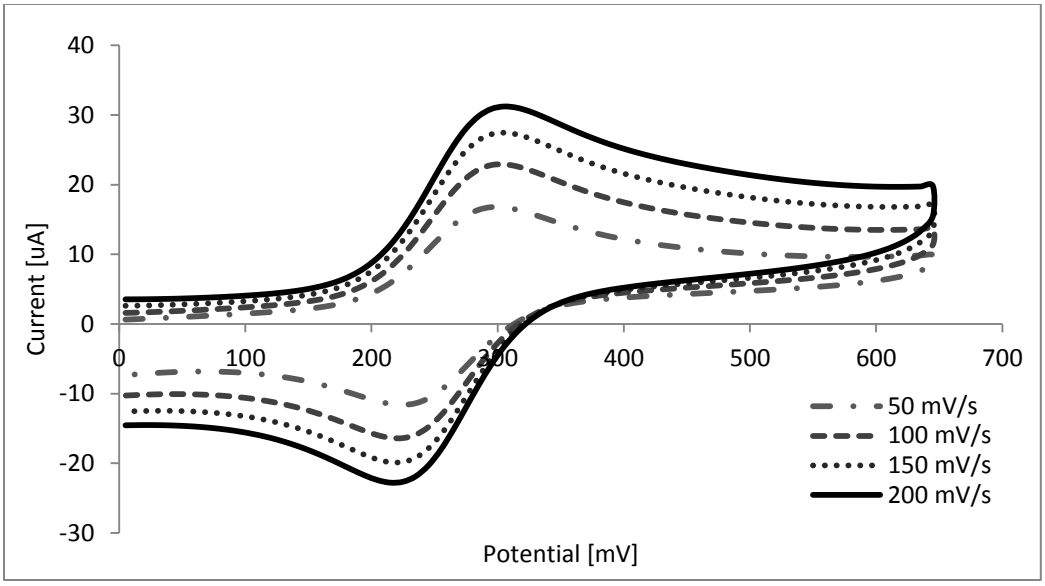

Figure A.18 – Representative cyclic voltammograms of PGP + CHT modified electrodes with 400 nM aptamer bio-recognition agents in 4 mM $Fe(CN)_6$/1 M KNO_3 solution at 50, 100, 150, 200 mV/s scan rates, each test was repeated three times.

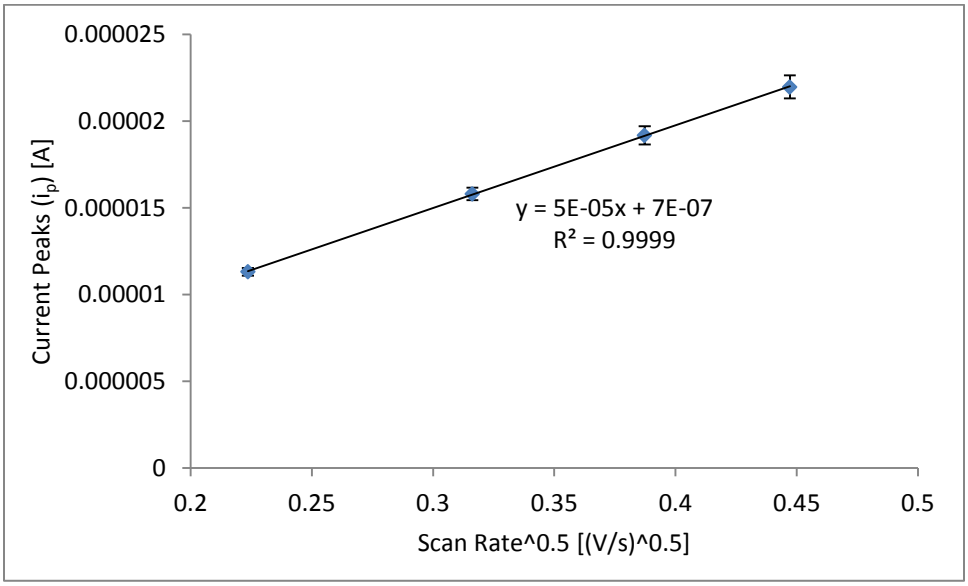

Figure A.19 - Characteristic Cottrell plot of bare modified electrodes, each test was repeated three times. Error bars represent standard deviation for each test condition.

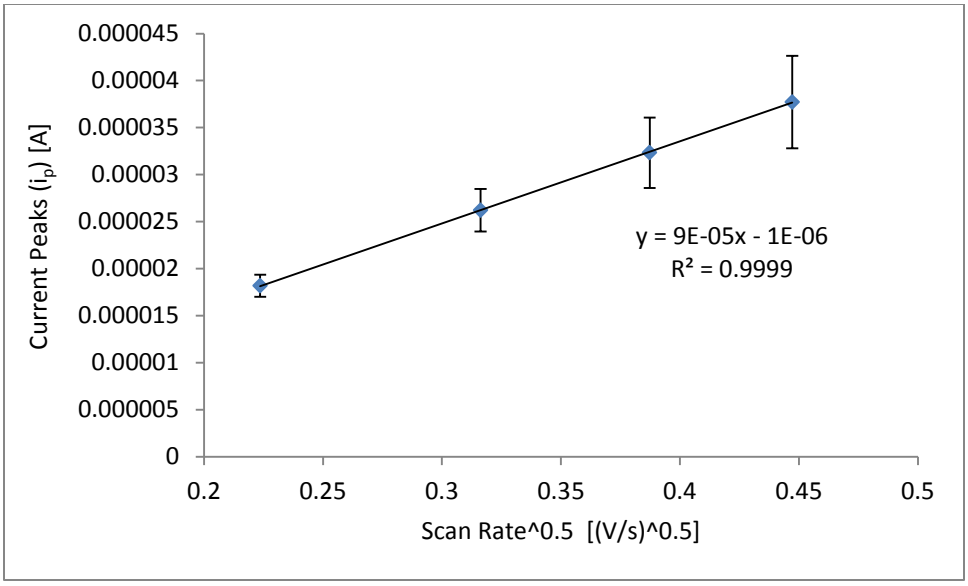

Figure A.20 - Characteristic Cottrell plot of PGP modified electrodes, each test was repeated three times. Error bars represent standard deviation for each test condition.

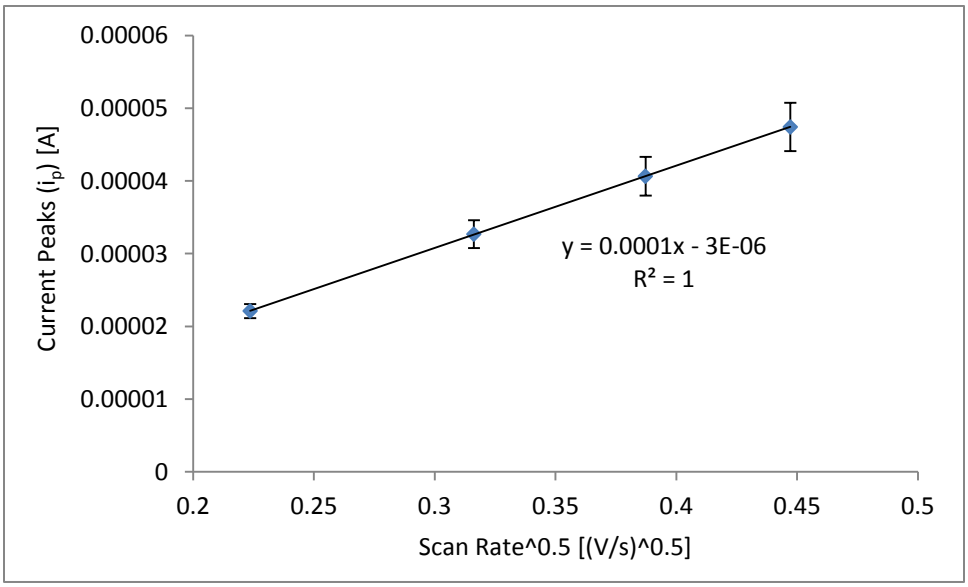

Figure A.21 - Characteristic Cottrell plot of a PGP modified electrode with 50 nM antibody bio-recognition agents, each test was repeated three times. Error bars represent standard deviation for each test condition.

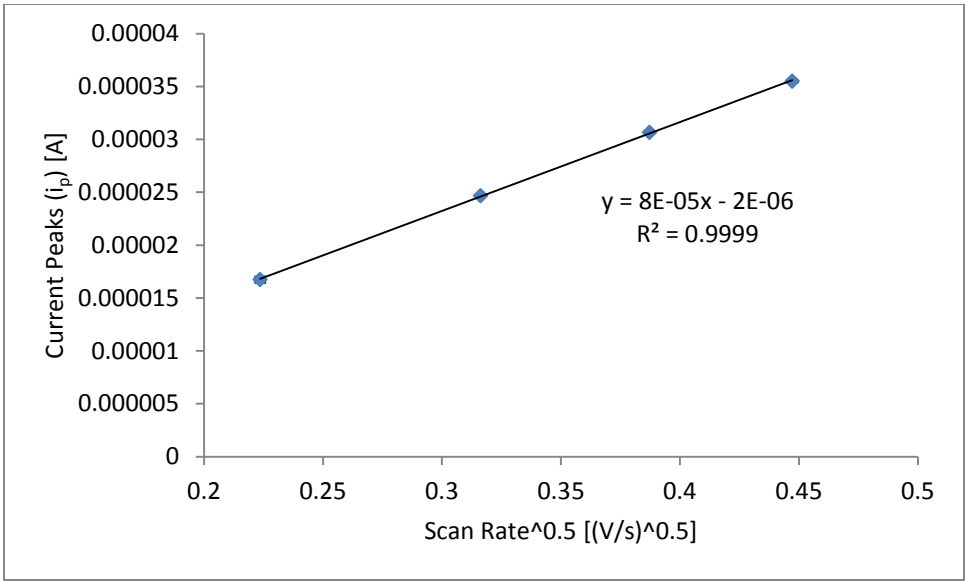

Figure A.22 - Characteristic Cottrell plot of a PGP modified electrode with 100 nM antibody bio-recognition agents, each test was repeated three times. Error bars represent standard deviation for each test condition.

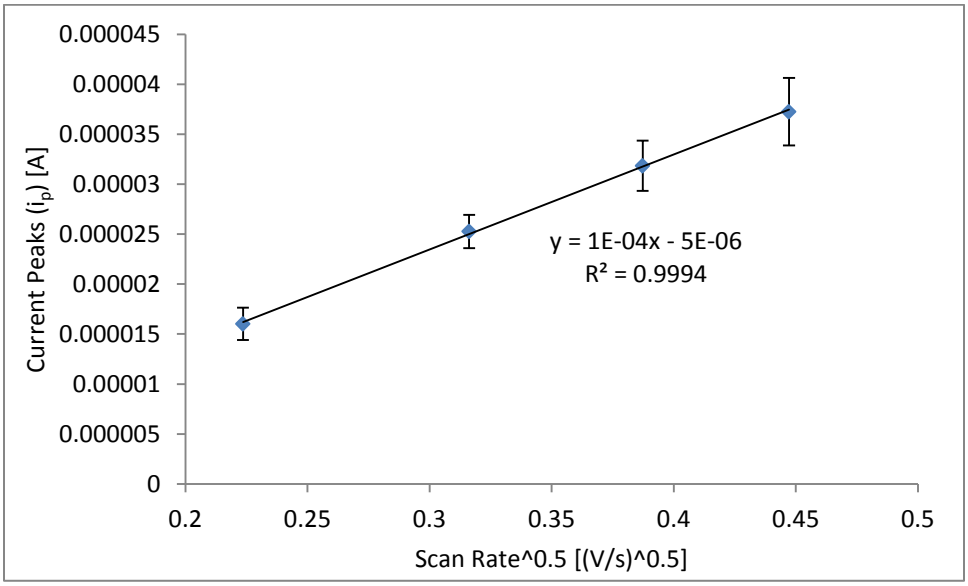

Figure A.23 - Characteristic Cottrell plot of a PGP modified electrode with 200 nM antibody bio-recognition agents, each test was repeated three times. Error bars represent standard deviation for each test condition.

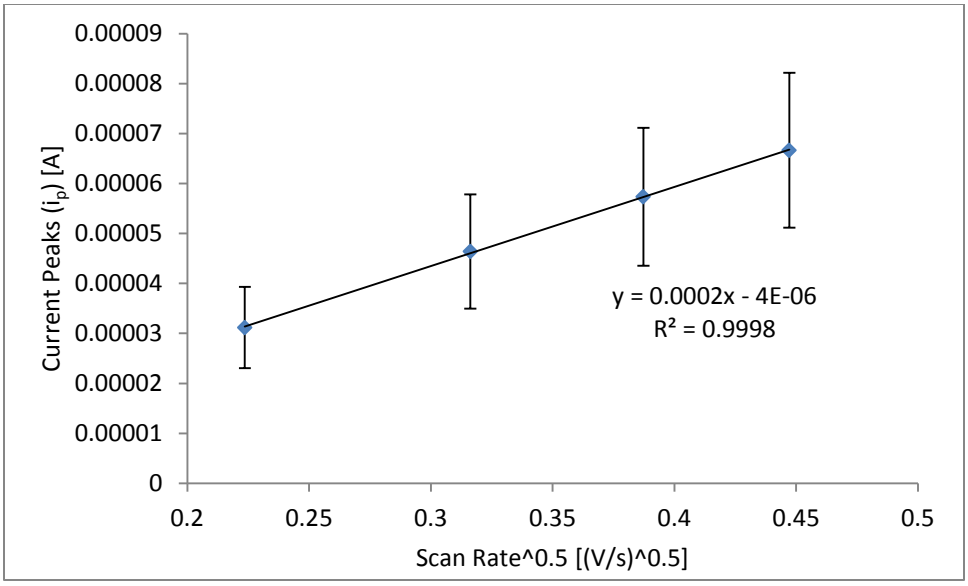

Figure A.24 - Characteristic Cottrell plot of a PGP modified electrode with 100 nM amine aptamer bio-recognition agents, each test was repeated three times. Error bars represent standard deviation for each test condition.

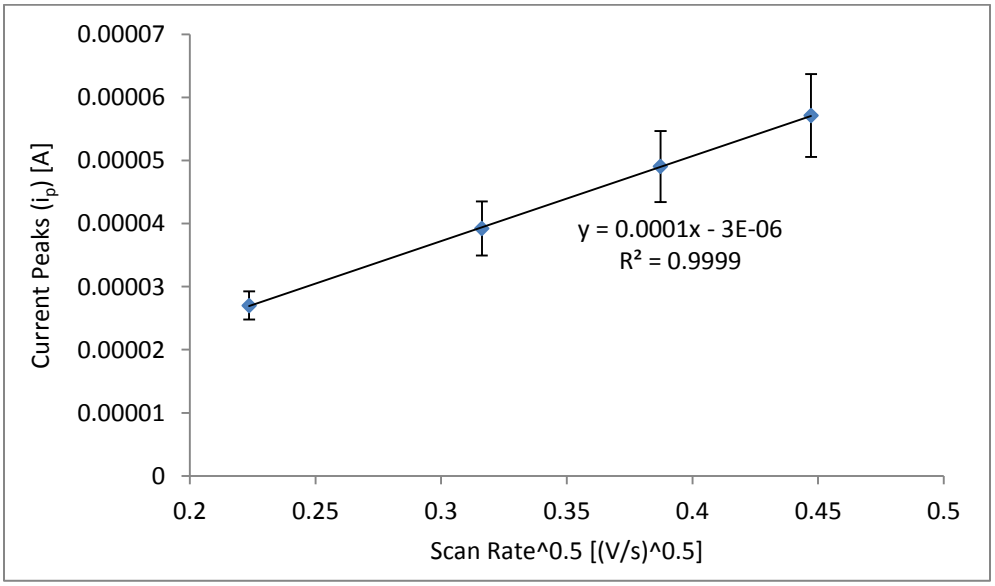

Figure A.25 - Characteristic Cottrell plot of a PGP modified electrode with 200 nM amine aptamer bio-recognition agents, each test was repeated three times. Error bars represent standard deviation for each test condition.

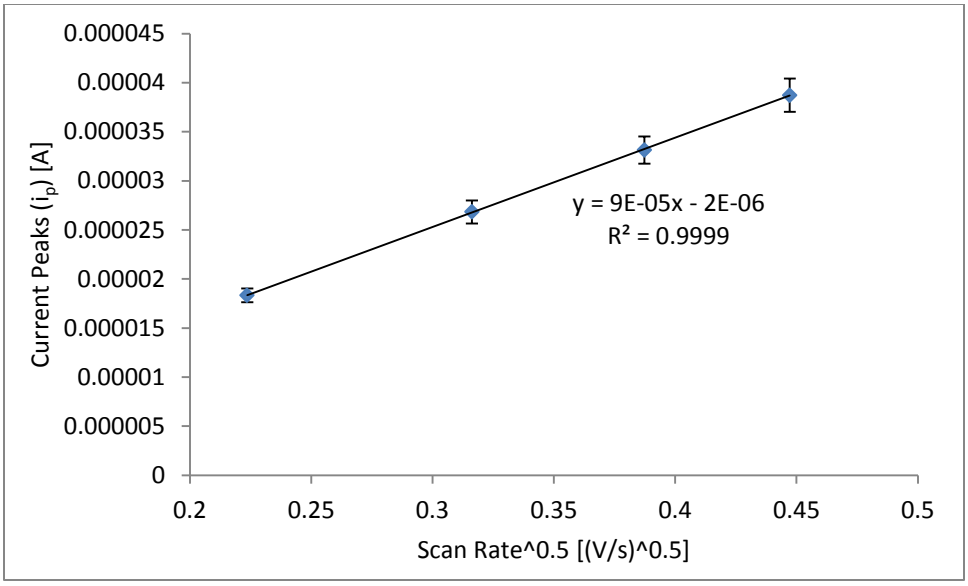

Figure A.26 - Characteristic Cottrell plot of a PGP modified electrode with 400 nM amine aptamer bio-recognition agents, each test was repeated three times. Error bars represent standard deviation for each test condition.

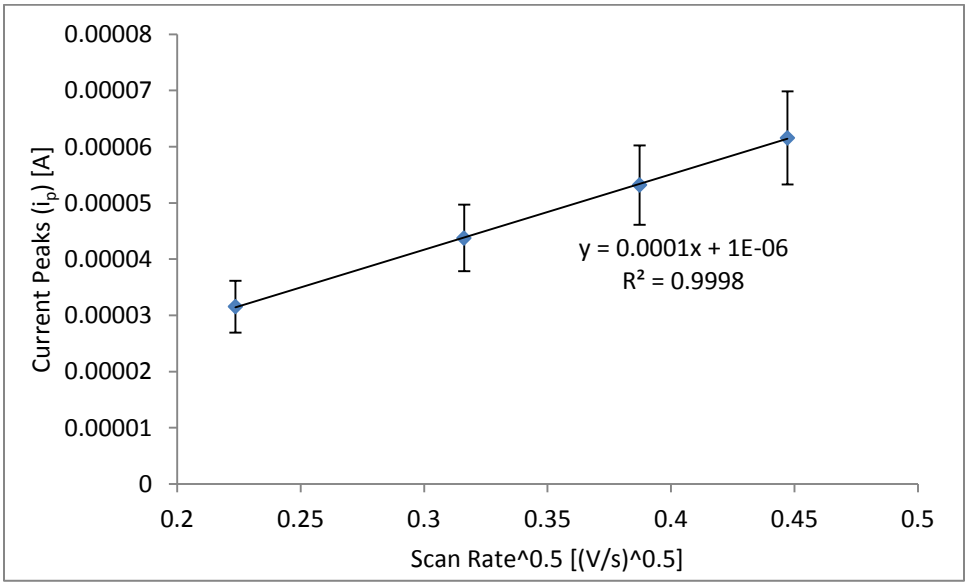

Figure A.27 - Characteristic Cottrell plot of a PGP modified electrode with 100 nM thiol aptamer bio-recognition agents, each test was repeated three times. Error bars represent standard deviation for each test condition.

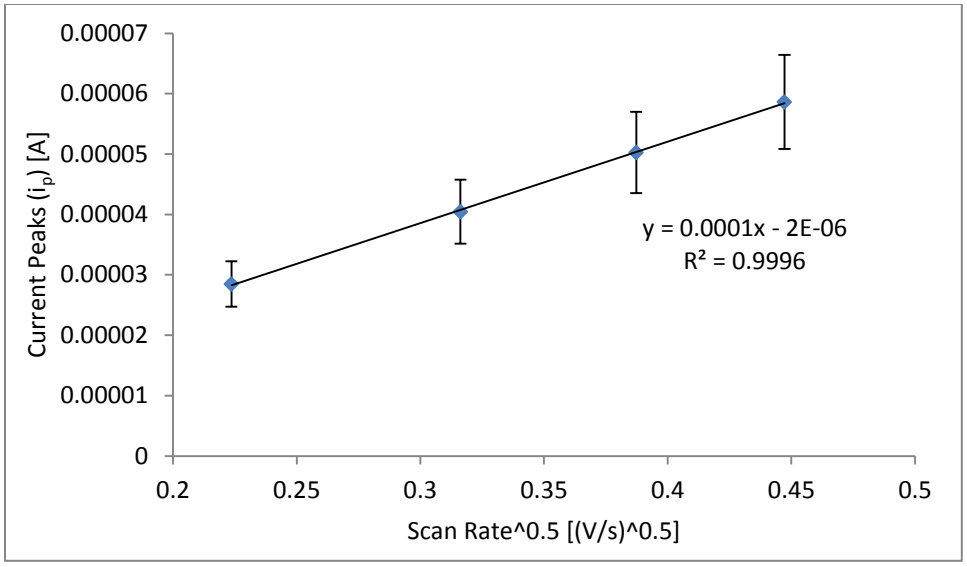

Figure A.28 - Characteristic Cottrell plot of a PGP modified electrode with 200 nM thiol aptamer bio-recognition agents, each test was repeated three times. Error bars represent standard deviation for each test condition.

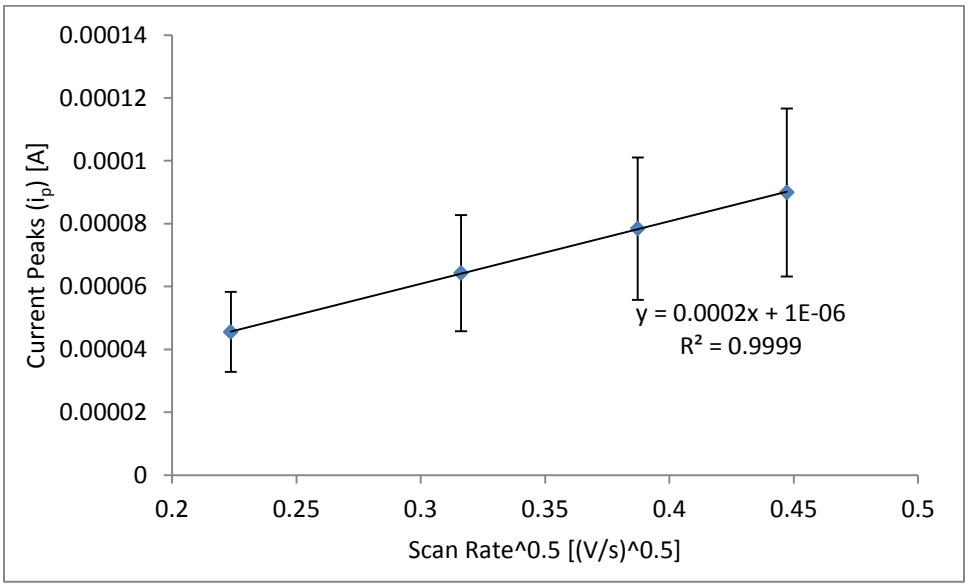

Figure A.29 - Characteristic Cottrell plot of a PGP modified electrode with 400 nM thiol aptamer bio-recognition agents, each test was repeated three times. Error bars represent standard deviation for each test condition.

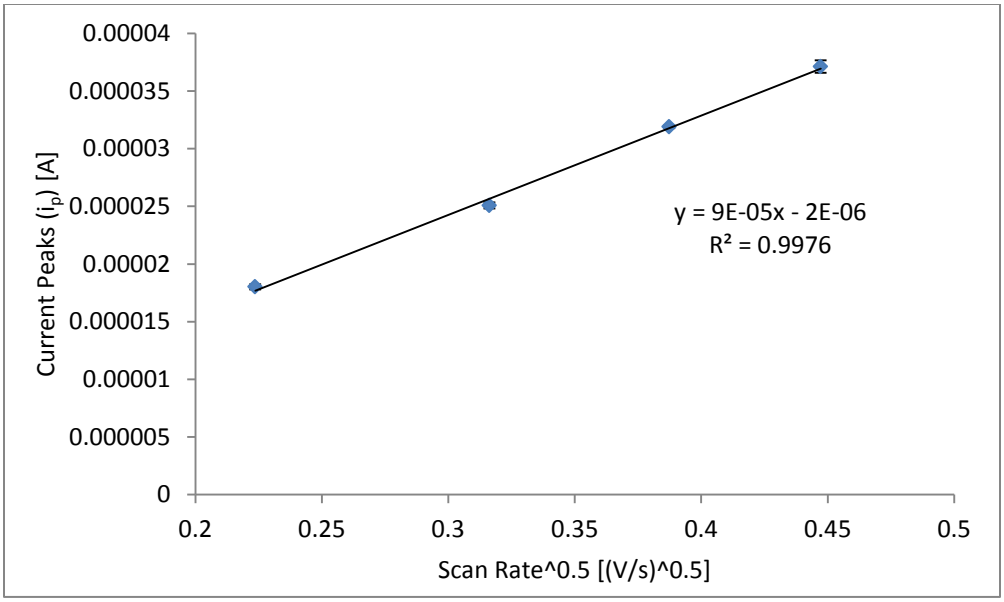

Figure A.30 - Characteristic Cottrell plot of a PGP + CHT modified electrode, each test was repeated three times. Error bars represent standard deviation for each test condition.

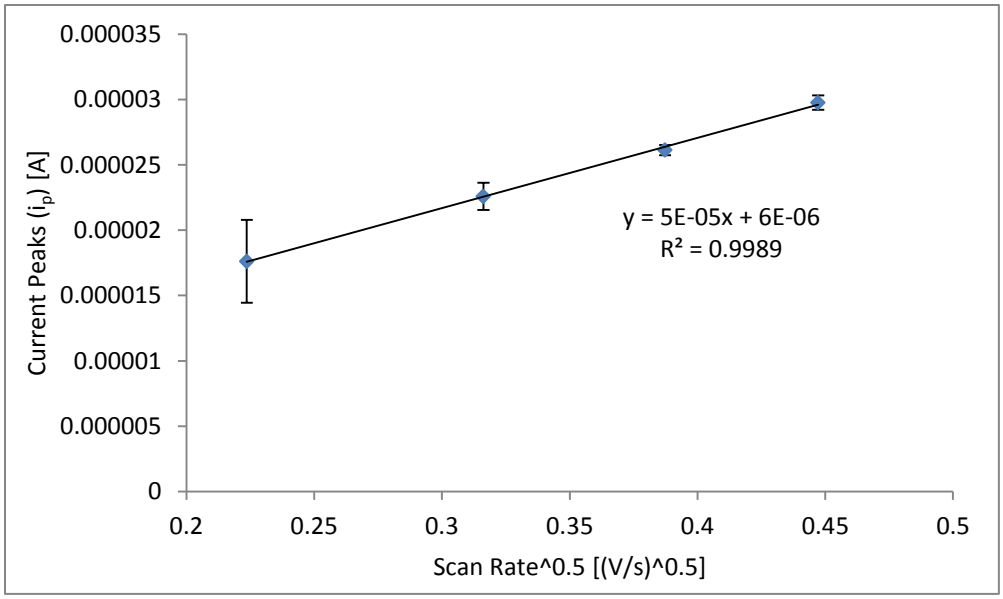

Figure A.31 - Characteristic Cottrell plot of a PGP + CHT modified electrode with 50 nM antibody bio-recognition agents, each test was repeated three times. Error bars represent standard deviation for each test condition.

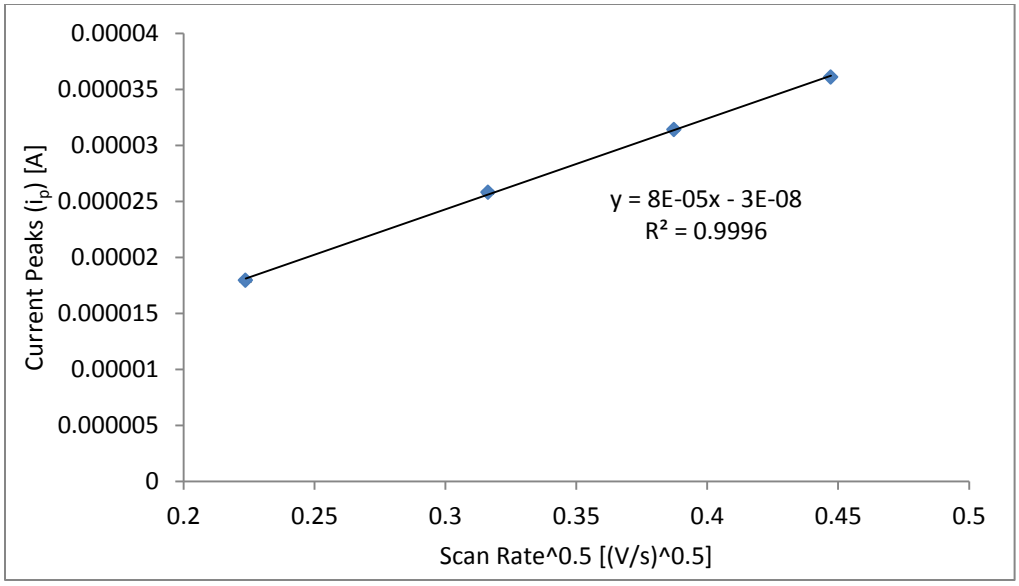

Figure A.32 - Characteristic Cottrell plot of a PGP + CHT modified electrode with 100 nM antibody bio-recognition agents, each test was repeated three times. Error bars represent standard deviation for each test condition.

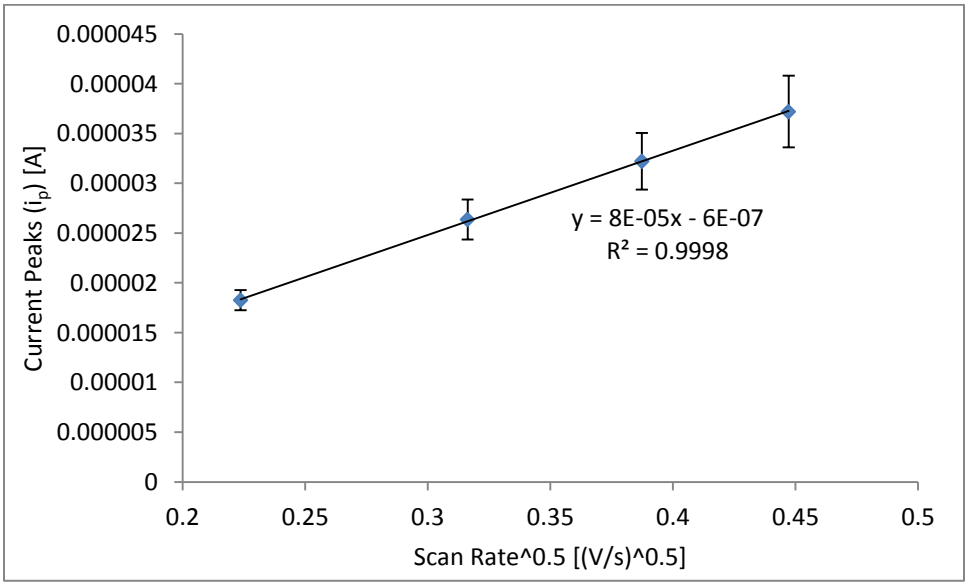

Figure A.33 - Characteristic Cottrell plot of a PGP + CHT modified electrode with 200 nM antibody bio-recognition agents, each test was repeated three times. Error bars represent standard deviation for each test condition.

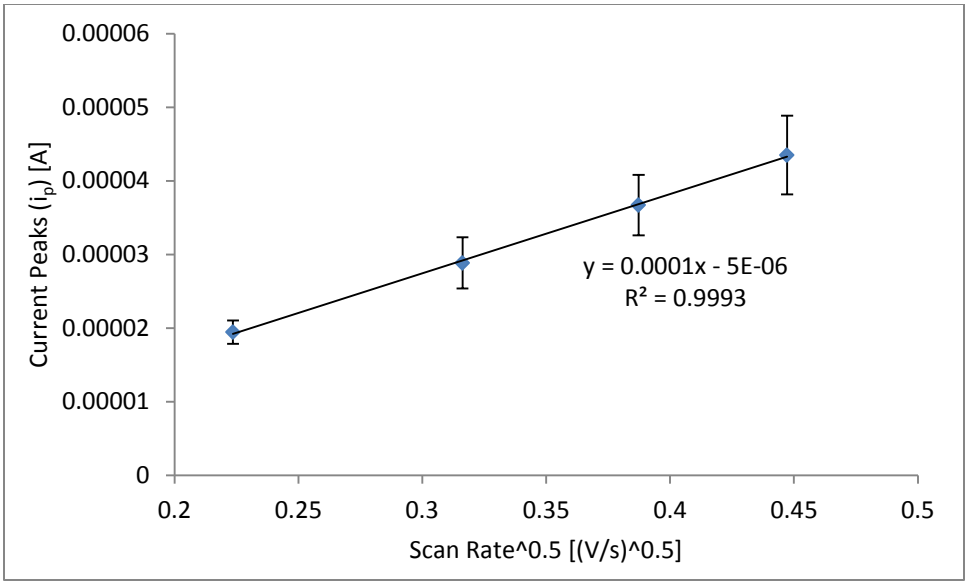

Figure A.34 - Characteristic Cottrell plot of a PGP + CHT modified electrode with 100 nM aptamer bio-recognition agents, each test was repeated three times. Error bars represent standard deviation for each test condition.

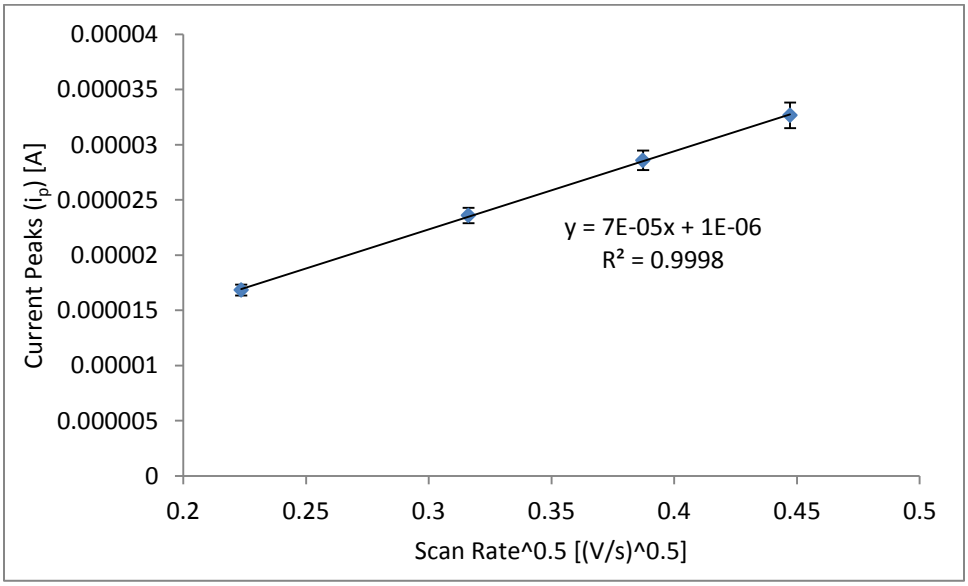

Figure A.35 - Characteristic Cottrell plot of a PGP + CHT modified electrode with 200 nM aptamer bio-recognition agents, each test was repeated three times. Error bars represent standard deviation for each test condition.

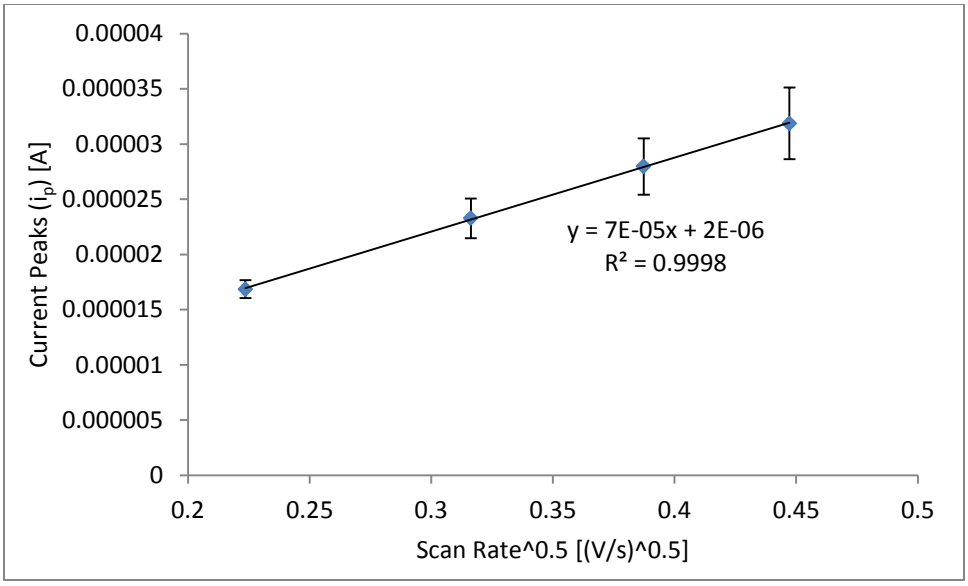

Figure A.36 - Characteristic Cottrell plot of a PGP + CHT modified electrode with 400 nM aptamer bio-recognition agents, each test was repeated three times. Error bars represent standard deviation for each test condition.